الجمهورية الجزائرية الديمقراطية الشعبية
وزارة التعليم العالي و البحث العلمي

university SAAD DAHLEB Blida
Institute of aeronautics and space studies

جامعة سعد دحلب البليدة
معهد علم الطيران والدراسات الفضائية

Dissertation Submitted in Partial Fulfillment
of the Requirements for the degree of

Master of Aeronautics in aircrafts propulsion

The Influence Of Splitter Blades Length In Centrifugal Compressor's Performance

Submitted by :

RAHMOUNI Aymen

Under the supervision of:

Mr LAAZAB Sebaa

Mr BEKHTI Ahmed

BLIDA 2023-2024

الملخص:

تبحث هذه الأطروحة في تأثير اختلافات طول الشفرة المقسمة على أداء ضاغط الطرد المركزي. باستخدام برنامج ديناميكيات السوائل الحسابية CFX ANSYS، يتم إجراء عمليات محاكاة على هندسة ضاغط الطرد المركزي المعدلة RADIVER التي وصفها في الأصل Kai U. Zeigler. تغير الدراسة بشكل منهجي طول شفرات التقسيم من 40٪ إلى 90٪ من نصف قطر الدافع وتفحص آثارها على مردود و أداء الضاغط. تتم عمليات المحاكاة في ظل ظروف تدفق لزجة وقابلة للانضغاط وثلاثية الأبعاد ومضطربة، باستخدام نموذج اضطراب SST k- ω لتمثيل دقيق للاضطراب. تشمل البيانات االأولية التي تم تحليلها التدفق الكتلي المصحح والمردود ونسبة الضغط ونسبة درجة الحرارة. يتم استخدام محاكاة الحالة الثابتة لالتقاط سلوك الضاغط بكفاءة في ظل ظروف تشغيل مختلفة لإثبات الظواهر الفيزيائية التي تظهر في Impeller وتأثيراتها على diffuser، وخاصة أداء مرحلة الضاغط.

الكلمات المفتاحية: سائل قابل لالنضغاط، لزج، سائل دوامي، الشفرات المقسمة، المحاكاة الرقمية.

Resumé:

Cette thèse étudie l'impact des variations de longueur d'aube sur les performances d'un compresseur centrifuge. En utilisant le logiciel de calcul de dynamique des fluides ANSYS CFX, des simulations sont menées sur une géométrie modifiée du compresseur centrifuge RADIVER décrite à l'origine par Kai U. Zeigler. L'étude modifie systématiquement la longueur des aubes intercalaire de 40% à 90% du rayon de la roue et examine leurs effets sur les mesures de performance du compresseur. Les simulations sontmenéesdans des conditions d'écoulement visqueux, compressibles, tridimensionnels et turbulents, enutilisant le modèle de turbulence k-ω SST pour une représentation précise de la turbulence. Les principaux paramètres de sortie analysés comprennent le débit massique corrigé, l'efficacité, le rapport de pressionet le rapport de température. Des simulations en régime permanent sontutilisées pour capturer efficacement le comportement du compresseur dans diverses conditions de fonctionnement afin de démontrer les phénomènes physiques qui apparaissent dans la turbine et leurs influences sur le diffuseur, enparticulier les performances de l'étage compresseur.

Mots clef : fluide compressible, visqueux, tourbillonnaire, les aubesintercalaires, simulation numerique.

Abstract:

This thesis investigates the impact of splitter blade length variations on the performance of a centrifugal compressor. Utilising ANSYS CFX computational fluid dynamics software, simulations are conducted on a modified RADIVER centrifugal compressor geometry originally described by Kai U. Zeigler. The study systematically alters the length of splitter blades from 40% to 90% of the impeller radius and examines their effects on compressor performance metrics. The simulations are conducted under viscous, compressible, three-dimensional, and turbulent flow conditions, using the k-ω SST turbulence model for accurate turbulence representation. The primary output parameters analysed include corrected mass flow, efficiency, pressure ratio, and temperature ratio. Steady-state simulations are employedto efficiently capture the compressor's behaviour under various operating conditions to demonstrate the physical phenomena that appear in the Impeller and their influences on the diffuser, particularly the performance of the compressor stage.

Keywords: compressible flow, viscous, vortex flow, impeller with splitter blades, numerical simulation.

Acknowledgements

After five years of higher education, beginning with the National Higher School of Hydraulics, which laid the foundation of my engineering knowledge,through the Department of Mechanical Engineering, where I received a bachelor's degree, and finally, the Institute of Aeronautics and Space Studies, where I achieved my dream of studying aeronautics and lived unforgettable moments, day and night, by the grace of God, I went through all this, sweet and bitter. And now, it is the end of my journey.

In this context, I would first like to express our gratitude to Almighty God, who allowed me to reach this academic level.

I want to give special thanks to my family and friends, whose moral and emotional support have been invaluable throughout this academic adventure. I cannot forget your support and all you have done for me. I give you all the love.

My Sincere thanks go to Mr. LAAZAB Sebaa for his expert guidance, constant encouragement, andunwavering dedication to me. His valuable teachings played a key role in the success of this thesis.

I would like to express my deep gratitude to Mr. REZOUG, the director of the Aeronautical Science Laboratory for numerical calculations. I sincerely thank him for all the facilities provided, which enabled us to accomplish this work successfully. His assistance has been invaluable in completing this thesis.

I would like to express my deep gratitude to all those whocontributed to completing this thesis. Their unwavering supportand their wise counsel greatly enriched this work.

We will never forget the best people we have met in our lives. We thank all our faithful friends, each by name, for all the positive attitudes and moments we shared together.

Of course, how do we forget the IBDAA Scientific Club, which occupies a special place in our hearts? Thank you to all the club members for your presence in my journey and for having lived the best university moments with me.

RAHMOUNI Aymen

Dedications

I dedicate these words to those whom God has commanded us to honor, to those who have given and offered so much, to you, my dear parents. My mother Saliha and my father Abdelkader, I dedicate this work to you; you have been my best support throughout my academic career. I dedicate this effort to you because you have always been my inspiration.

To my dear sister Khouloud and my dear brother Abderrahmane, I dedicate this work as a sign of my attachment, love, and affection for you and as a testimony of my gratitude for your efforts and support during my studies.

To my dear uncle Mohammed, who has been the cornerstone of my journey in the field of aeronautics. His unwavering support, inspiration, and guidance have been instrumental in achieving my dream to study in this field.

To Aya, Mohammed, Ahmed-Cherif, Chaima, and Ali. Patience, support, and understanding have been essential throughout this demanding period.

To all my friends, on difficult and easy roads, dark and bright, I dedicate this work to express my gratitude for having you in my life.

I dedicate this work to my loved ones who supported me. Your wishes for success, your support, and your encouragement have allowed me to reach this stage of my life.

Table of content

Chapter 03 : Simulation Workflow

Chapter 04 : Presentation and discussion of results

List of figures

Chapter 01: Introduction to Turbomachinery

Chapter 02 : Numerical model

Chapter 03 : Simulation Workflow

Chapter 04 : Presentation and discussion of results

Liste of tables

Chapter 02 : Numerical model

Chapter 03 : Simulation Workflow

Chapter 04 : Presentation and discussion of results

Nomenclature

P_s : Static pressure

P_t : total pressure

T : Static temperature

T_t : Total temperature

v : Specific volume

R : Gas constant

s : Entropy

h: Enthalpy

α_1 : Absolute inlet flow angle

α_2 : Absolute exit flow angle

β_1 : Relative inlet flow angle

β_2 : Relative exit flow angle

V : Absolute velocity

W : Relative velocity

U: Blade velocity

is: isentropic

Ec: kinetic energy

η : Efficiency

π : Pressure ratio

τ : Temperature ratio

F : External force

N,Ω :Rotation speed

PS: pressure side

SS: suction side

$u_{i,j,k}$: Velocity vector components

ρ : Density

R_{eL} : Reynolds number

RANS: Reynolds Averaged Navier-Stocks

LES: Large Eddy Simulation

DNS: Direct Numerical simulation

μ : Absolute viscosity

υ : Kinematic viscosity

k : Turbulence kinetic energy

ω : Turbulence frequency

ε : Turbulence dissipation rate

S.S.T: shear stress transport

y^{+} : Dimensionless number characterizing the Reynolds number value computed at the 'first-to-wall' mesh node

Δy : Boundary layer thickness

FVM: Finite Volume Method

$\dot{m}$: mass flow rate

Ma : Mach number

General introduction

Turbocompressors are essential in industries where fluid flow and rotating blade assemblies require energy transfer. In aerospace, they play a pivotal role in enhancing power augmentation. Among various turbocompressor types, radial compressors are particularly notable for their ability to achieve high-pressure ratios at low airflow rates, outpacing their axial counterparts.

The centrifugal compressor stage is a crucial component of turbocompressors and consists of two integral components: the dynamic rotor (centrifugal impeller) and the static stator (diffuser). The centrifugal impeller elevates fluid energy via a combination of heat and stagnation pressure increase, leading to heightened static pressure and kinetic energy. Conversely, the diffuser mitigates stagnation pressure losses and transforms the energy forms to increase static pressure while diminishing kinetic energy.

The complexity of flow analysis within compressor stages is characterised by its viscous, compressible, three-dimensional, and turbulent nature. Numerical methods are used to tackle this complexity.

In this thesis, we will modify the RADIVER centrifugal compressor geometry originally described by Kai U. Zeigler to create different splitter blade length variations. We will also perform several simulations using ANSYS CFX computational fluid dynamics software to analyze the key parameters, which will give us an idea ofa centrifugal compressor's overall performance and flow characteristics. We will compare this with the experimental data.

The query raisedis: what is the influence of splitter blade length on centrifugal compressor performance and efficiency, and what is its optimal configuration?

This thesis is divided into four chapters, each offering a stepping stone in exploring turbocompressors and answering our problem:

A literature review to explore previous studies and unravel the complexities of our subject.

- **Chapter 1: Generalities of Turbomachinery**

  This chapter provides a foundational understanding of turbomachinery, including comprehensive definitions and details specific to compressors, focusing on centrifugal compressors. It covers fundamental concepts such as types of compressors, operating principles, performance parameters, and typical applications.

- **Chapter 2: Analytical Equations and CFD Modeling**

  This chapter presents the analytical equations governing a stage of a centrifugal compressor, elucidating the fundamental principles underlying its operation. Additionally, it explores the governing equations for CFD modeling, emphasizing turbulence models such as the K-w SST model. The mathematical model used in CFD simulations is detailed, highlighting the finite volume method and numerical discretization techniques.

- **Chapter 3: Numerical Modeling and ANSYS CFX**

  This chapter delves into numerical modeling techniques and the usage of ANSYS CFX software for simulating centrifugal compressor geometries. It provides a comprehensive overview of modeling the impeller and diffuser geometries, detailing meshing procedures and conditions. The chapter also discusses the implementation of turbulence models, focusing on the K-w SST model, and describes the finite volume method for numerical discretisation.

- **Chapter 4: Results and Discussion**

  The final chapter presents the research findings and facilitates discussion on the results obtained from analytical equations, numerical simulations, and CFD modeling. It explores the implications of the study's outcomes on centrifugal compressor performance and efficiency, offering insights into potential improvements and future research directions.

Literature review:

Literature review:

Ziegler, K.U., Gallus, H.E., Niehuis, R. [1] [2] (2002a)

This study presents an experimental study of the effect of the wheel diffuser interaction on the configuration of unstable and time-averaged flow in the wheel and diffuser and the performance of these components. Part one deals with integrating integral flow losses and diffusion in the wheel, the diffuser, and the entire compressor. It has been shown that smaller radial spaces improve the recovery of the diffusive pressure, while the efficiency of the wheel is barely affected. The second part focuses on the reasons for this effect.

Yagnesh Sharma and Vasudeva Karanth [3] 2009

They studied the complex flow field within centrifugal fans, noting flow reversal on the impeller and diffuser vanes' suction sides. They proposed that introducing splitter vanes could enhance fan performance by improving the 'diffusion process, 'which is the gradual reduction in fluid velocity and increase in static pressure. Using computational fluid dynamics (CFD), they conducted a detailed numerical analysis of splitter vanes placed strategically at different locations along the impeller and diffuser. Their findings revealed that splitter vanes near the diffuser exit significantly improved static pressure recovery across the diffusing domain. Additionally, splitter vanes at the mid-span between blades showed marginal enhancements in static pressure recovery across the fan. However, splitter vanes placed near the suction side of the impeller trailing edge adversely affected static pressure recovery.

Jawad, Abdullah, Zulkifli, and Mahmood [4] 2013

A study was conductedto predict the performance of a modified centrifugal compressor used in turbochargers through numerical simulations. They aimed to enhance conventional turbocharger compressor performance by trimming the impeller. Using computational fluid dynamics (CFD), they simulated the flow inside the modified compressor geometries featuring double splitters. The study focused on understanding how impeller trimming affected compressor performance, particularly pressure ratio, efficiency, mass flow rate, and aerodynamic characteristics. Results showed that impeller modification significantly improved compressor performance, especiallywith the double splitter design, leading to increased pressure ratio and air mass flow rate.

Malik, Qureshi, Zheng, and Ikram [5] 2018

Conducted an aerodynamic study analysing a novel design of centrifugal compressor impellers featuring double splitter blades for performance enhancement. The study focused on investigating the effects of the splitter blade locations between two main blades. Results concluded that splitter blades positively impact compressor impeller performance, increasing the total pressure ratio and improving efficiency. A comprehensive comparison of the splitter blade locations identified that placing a larger splitter blade near the pressure surface and a smaller splitter blade near the suction surface of the primary blade resulted in uniform flow, reduced separation, and better efficiency compared to other configurations.

M. G. Khalafallah, H. S. Saleh, S. M. Ali & H. M. Abdelkhalek [6] 2021

The study analyses the impact of varying splitter vane positions in the diffuser on the performance of a high-speed centrifugal compressor in a small gas turbine. Using ANSYS 19 Workbench, simulations were conducted with two sets of vanes: one with splitter vanes and one without. Results show that positioning the splitter vanes closer to the pressure side of the primary vanes, precisely at 33% of the angular distance, significantly improves stage performance, increasing pressure recovery coefficient, pressure ratio, and stage efficiency compared to the original splitter position. Conversely, suboptimal positions decrease performance, highlighting the importance of optimal splitter vane placement for enhancing compressor performance.

KiryllKabalyk, WładysławKryłłowicz [7] 2016

A study investigated the performance of two centrifugal impellers with low inlet flow coefficients using computational fluid dynamics (CFD) modeling. One impeller featured nine main and nine splitter blades, while the other had only 18 main blades. Experimental measurements on a corresponding test rig verified the superior performance of the splitter-bladed impeller. The numerical simulations aimed to uncover the underlying reasons for the performance disparities between the impellers.

A. Malik, Q. Zheng, A. A. Zaidi, and H. Fawzy [8] 2018

Demonstrates a method to enhance pressure ratio and efficiency by incorporating multiple splitters into a centrifugal impeller with a vaneless diffuser. Using the DDA 404-III back-swept impeller of a centrifugal compressor as a case study, experimental modifications were made to include splitter blades. A sample impeller was designed and analysed with a configuration featuring a large splitter near the pressure surface and a small splitter near the suction surface of the primary blade. Results indicated that this configuration increased the total pressure ratio from 4.1 to 4.5, with a 2% improvement in efficiency. Additionally, the modified impeller exhibited a reduction in relative Mach number at the inlet.

S.A. MoussaviTorshizi, A. HajilouyBenisiand M. Durali [9] 2016

This study focuses on the multi-level optimisation of splitter blade profiles in a turbocharger compressor using a genetic algorithm to enhance performance. By iteratively adjusting the profiles at the hub, mid-span, and shroud of the splitter blades, the aim is to reduce incidence losses at the leading edge and optimise blade loading at the shroud. The impeller flow field analysis reveals improvements in reducing flow leakage at the shroud and losses at the leading edge. While numerical simulations predict a slight decrease in pressure ratio, a significant 2.2-point enhancement in isentropic efficiency is achieved. The optimisation results inform a new impeller's design, manufacturing, and testing, with experimental validation confirming the anticipated performance improvements.

Jun Ou, DonghaiJin&XingminGui [10] 2022

In their study, Jun Ou, DonghaiJin, and XingminGui investigate optimising load distribution between splitter blades and main blades in high-loading centrifugal compressors to enhance efficiency. Using CFD prediction, they analyse how different load ratios (CR) impact aerodynamic performance and internal vortices. Results show that reducing the load ratio improves flow uniformity and overall performance, with a 0.7% increase in stage isentropic efficiency observed. Their study highlights the importance of load distribution optimisation in enhancing high-loading centrifugal compressor performance.

Omidi, M., Liu, Y., Mohtaram, S. et al [11] 2022

This article addresses impeller design challenges in turbomachines, focusing on splitter blade designs. It uses CFD methods to adjust splitter blade positions at the hub and shroud to create different profiles from the main blades. Results show a 1.5% efficiency improvement in one case, indicating the potential for enhanced efficiency through CFD-driven modifications to splitter blade locations.

David C. Wilcox. [12] (1993)

Provides a comprehensive and detailed examination of turbulence models and their application in computational fluid dynamics (CFD). The book serves as both an introductory text and a reference guide, covering fundamental concepts of turbulence and various modeling approaches. Key topics include the statistical description of turbulent flows, the derivation and implementation of different turbulence models such as the k-ε model, the Reynolds stress model, and advanced models like the k-ω model. Wilcox's work is noted for its clear explanations, extensive theoretical background, and practical insights into the strengths and limitations of different models.

Chapter 01

Introduction to Turbomachinery

I.1. Generality of turbomachinery:

Turbomachinery is a dynamic and powerful engineering system that combines fluid mechanics and mechanical engineering. It consists of various devices manipulating fluid flow for multiple applications, including power generation and transportation. These machines, such as turbines, compressors, and pumps, play crucial roles in aviation, energy, and manufacturing, driving progress worldwide.

A turbomachine is a device that transfers energy between a continuously rotating machine component and a fluid in a continuous flow based on forces generated by the flow. The rotor, usually a bladed drum or wheel or a collection of bladed wheels, is responsible for the energy exchange. Energy can be transferred from the flow to the rotor or vice versa. When the energy is extracted from the flow, it drives the rotor, which drives a useful external load. This machine is generally referred to as power delivering or shaft power delivering, but regardless of the fluid used, it is commonly known as a turbine. The fluids used may include water, steam, air, gas produced by fuel combustion in pressurised air, or other fluids such as refrigerant in a cooling cycle.

If energy is supplied to the fluid by the rotor, an external motor is required to drive the machine, which is referred to as a shaft or power-receiving machine. The names used for these machines depend on the fluid and the energy component that is mainly increased. The energy exchanged between a rotor and a fluid is mechanical energy in a technical sense. In the machine, mechanical energy can only take two forms: velocity-associated energy (kinetic energy) and pressure-associated energy (pressure potential energy in the case of a constant-density fluid), ignoring the small effect of gravitational potential energy[20]. Some examples of power-receiving machines are:

1) Incompressible fluids such as water and oil, where there is dominantly a pressure increase
2) Compressible fluids such as air, gas, and vapor:
    a) with high-pressure increase(compressor)
    b) low-pressure increase(fan (puts air into motion))

I.1.1. Classification of turbomachinery:

Turbomachinery comes in many different shapes and serves a variety of purposes, which leads to its categorisation based on various standards:

- **The nature of the fluid:**

Machines behave differently with compressible and non-compressible fluids.

- **Energy transfer:**

According to the direction of energy transfer, there are two types of machines:

a) Generating machines: which increase the energy of the fluid by providing mechanical energy to the machine's shaft (such as compressors, pumps, etc.).

b) Driving machinesuse fluid energy on the machine's shaft (such as turbines).

- **According to the geometric shape of the wheel:**

There can be three types of machines:

- Centrifugal or radial machines feature fluid flow that exits in a radial plane.
- Axial machines exhibit fluid flow parallel to the machine's axis of rotation.
- Mixed machines showcase fluid flow with axial and radial components at the inlet or outlet.

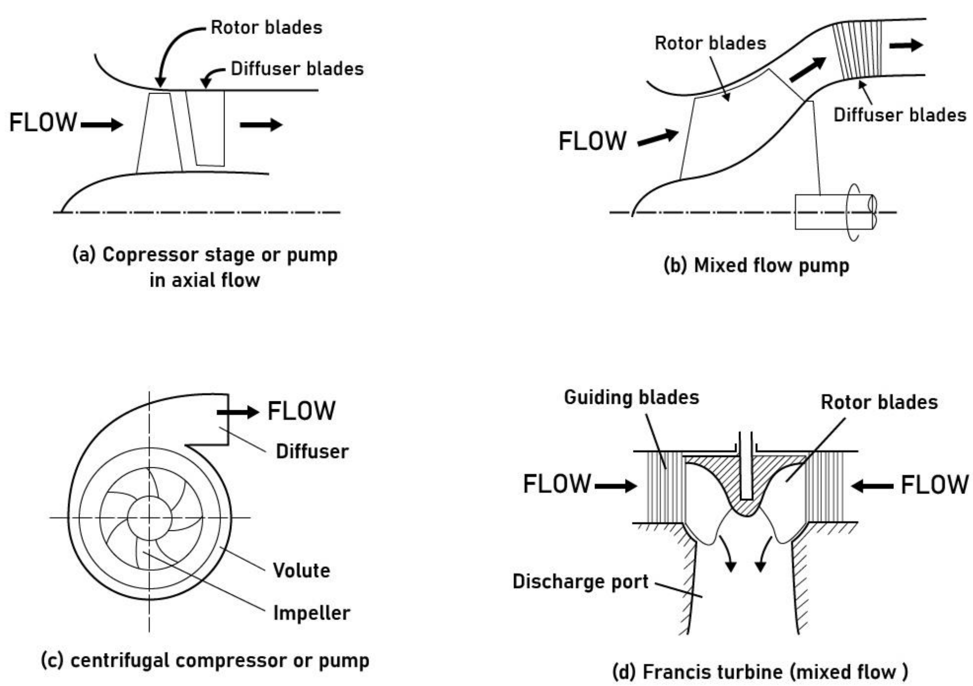

Figure I. 1: Different types of Turbomachines

I.1.2. Constitution of turbomachines:

Depending on whether a turbomachine has one or more rotors, it is classified as single-stage or multi-stage. A complete single-stage turbomachine consists of three distinct components through which the fluid passes successively, from the inlet to the outlet of the machine:

- Inlet Guide Vanes (IGV) The inlet guide vanes are the first components encountered by the fluid in its path. Their role is to guide the fluid from the machine's inlet section to the rotor's inlet, ensuring it attains suitable velocity and direction.
- Rotor (Impeller) In a turbomachine, the rotor is the most crucial element where energy exchange occurs. In a receiving machine, the energy provided by the driving motor is transferred to the fluid. In contrast, the rotor receives mechanical work in a driving machine as the fluid releases energy. The rotor also serves as the inlet for the diffuser.
- Diffuser: The diffuser, also known as the stator, collects the fluid at the rotor outlet and guides it to the outlet section of the machine at the desired velocity. It is also responsible for converting kinetic energy into pressure, which could serve as the outlet section of the machine.

I.1.3. Functioning and field of application:

a. Gas compression:

Gas compression is a vital function employed in a range of sectors, including the chemical industry for maintaining reaction pressure, the oil industry for extracting petroleum, and the production of compressed air. Compressors are also utilised alongside other components, such as turbines and combustion chambers, to generate mechanical energy or propulsion in aeronautics.

b. Ventilation:

"Air ventilation systems" are critical equipment that upholds air quality and manages indoor temperatures. These systems enable the seamless exchange of indoor and outdoor air, ensuring a supply of fresh air while aiding in the cooling process.

c. Energy recuperation from a fluid (turbines):

In the domain of fluid energy recuperation, turbines play a crucial role:

Turbines harness the hydraulic potential energy of liquids like water, which is commonly observed in dam installations.

Turbines have a wide array of applications in gases, from dental turbines to turbocompressors, turbo pumps, and intricate systems used in aeronautical propulsion. These turbines collaborate with components like compressors and combustion chambers to produce mechanical energy or propel aircraft.

I.2. Compressors:

I.2.1. Introduction :

Compressors are mechanical devices used tomove air, gas, or vapor and increase their pressure levels. The compressor pressure ratio (CR), which is the ratio of absolute discharge pressure to absolute suction pressure, is a crucial parameter in understanding compressor performance.

Due to compressors' mechanical limitations, multiple compression stages are often necessary to achieve higher pressures. This approach allows for a gradual increase in pressure while maintaining efficiency and effectiveness.

The principles governing compression theory, such as the ideal gas law and the laws of thermodynamics, play a vital role in understanding the behavior of gases during compression processes. The ideal gas law, in its original form, provides a fundamental framework for studying the properties of pure substances under varying pressure and temperature conditions:

$$Pv = RT \tag{I.1}$$

Where:

P = *Absolute* pressure

v = Specific volume

R = Gas constant

T = Absolute temperature

- **The first law of thermodynamics:**

The first law of thermodynamics asserts that energy is conserved; it cannot be created or destroyed, but it can be transformed from one form to another:

$$Q_h = \overline{W_w} + \Delta E \quad \text{(I.2)}$$

Where:

$Q_h =$ Heat into the system
$W_w =$ Work by the system
ΔE = Change in system energy

- **The second law of thermodynamics:**

The second law of thermodynamics states that the universe's entropy always increases. This is the same law that indicates that perpetual motion machines are impossible.

$$\Delta s \geq 0 \quad \text{(I.3)}$$

I.2.2. Compressor classification principles:

Compressors can be categorized according to several features:

➢ Functioning principle (volumetric, dynamic).

➢ Movement type of moving parts (linear, rotary).

➢ Types that compress air.

➢ Types that compress gas.

This classification helps distinguish the various compressor types and their specific characteristics.

I.2.3. The different types of air compressors:

In general, compressors are classified based on a kinematic scale into two primary types:

- **Volumetric compressors:** operate by isolating gas within a chamber whose volume changes. When the chamber's volume increases, it draws gas in from the intake side. Conversely, decreasing the chamber's volume compresses the gas, raising its pressure before it is released on the discharge side.

Within this category of compressors, there are further distinctions:

- Alternating volumetric compressors, which include pistons and membranes.
- Rotary volumetric compressors, such as vane, lobe, screw, and liquid annular types.

- **Flowmeter Compressors (continuous flow):**
- Dynamic compressors use a swiftly rotating impeller to accelerate the gas upon contact. The kinetic energy the gas gains as it speeds up is subsequently transformed into pressure whenthe gas decelerates.

This category of compressors includes:

  - Centrifugal compressors.
  - Axial compressors.
- Ejector compressor.

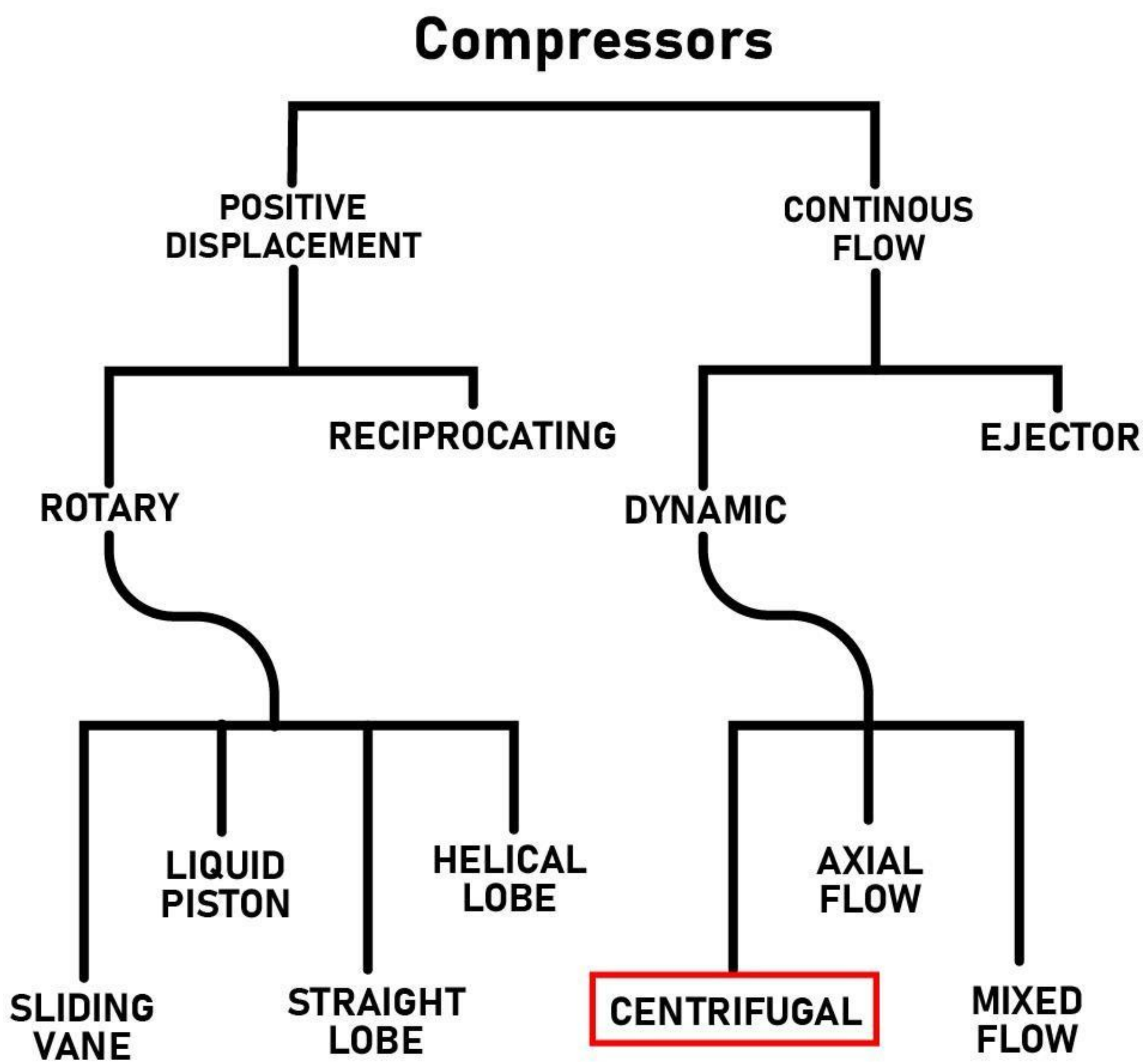

Figure I. 2: Compressors clasification

I.3. CENTRIFUGAL COMPRESSORS:

I.3.1. Introduction:

The centrifugal compressor is a type of dynamic machine that compresses gas by using the inertia from speeding up, slowing down, and changing the direction of the gas with rotating blades. The impeller has a back plate or disk with blades extending from the center to the edge. These blades can be open, semi-enclosed, or fully enclosed. In an open impeller, the blades are attached directly to the center hub and can be made from a single piece of material or attached separately. Enclosed impellers have blades between two disks, preventing gas leakage that occurs in open designs. However, making enclosed impellers is more complex and expensive.

It consists of one or more levels, each with a spinning part called an impeller and a stationary part known as a diffuser.

Impeller: The impeller is the rotating component of the compressor. It consists of a backing plate or disc with radial vanes attached from the hub to the outer rim. These vanes play a crucial role in accelerating the gas.

Diffuser: The diffuser, on the other hand, is the stationary element. Its purpose is to convert the high-velocity gas exiting the impeller into high-pressure gas. By slowing down the gas and increasing its pressure, the diffuser ensures efficient compression.

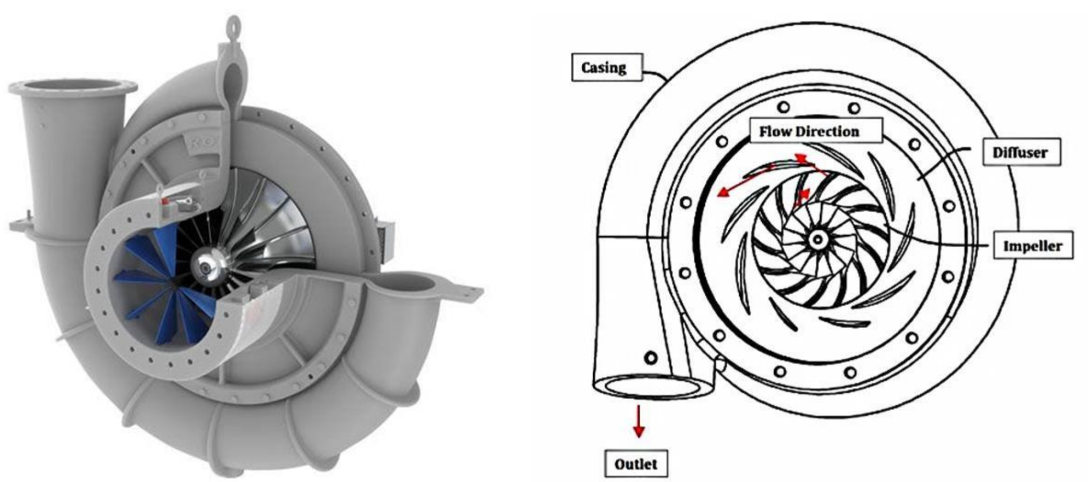

Figure I. 3 : Centrifugal compressor elements

I.3.2. Design Variations:

a) **In impeller:** there are many variation designs in impeller but mainly there is two concepts of impeller design :

- **Impeller geometry :**

- **Open Impeller:** In an open impeller design, the radial vanes are directly attached to the hub. However, this design has to contend with gas leakage between the moving vanes and the stationary diaphragm.

- **Semi-Enclosed Impeller:** This design sandwiches the vanes between two discs, reducing gas leakage compared to the open impeller.

- **Enclosed Impeller:** The enclosed design completely encases the vanes between two discs, eliminating gas leakage. However, it's more challenging and costly to manufacture.

Figure I. 4 : Impeller geometry types

- **Blade inclination at exit:**

There are three types of moving wheels, distinguished by the inclination of the blades at their exit:

- **Radial Blades**: In this type, the blades are positioned radially, meaning they are perpendicular to the axis of rotation at the exit.($\beta_2 = 90^\circ$)

- **Backward-Swept Blades:** Here, the blades are inclined backward relative to the direction of rotation. This design is often employed to improve efficiency and reduce the energy loss associated with the fluid flow.($\beta_2 \prec 90^\circ$)

- **Forward-Swept Blades:** In this configuration, the blades are inclined forward relative to the direction of rotation. This design can be used to achieve higher pressure ratios but may come with increased energy losses and mechanical stress.($\beta_2 \succ 90^\circ$)

Each type of blade inclination offers specific advantages and is selected based on the desired performance characteristics of the turbomachine.

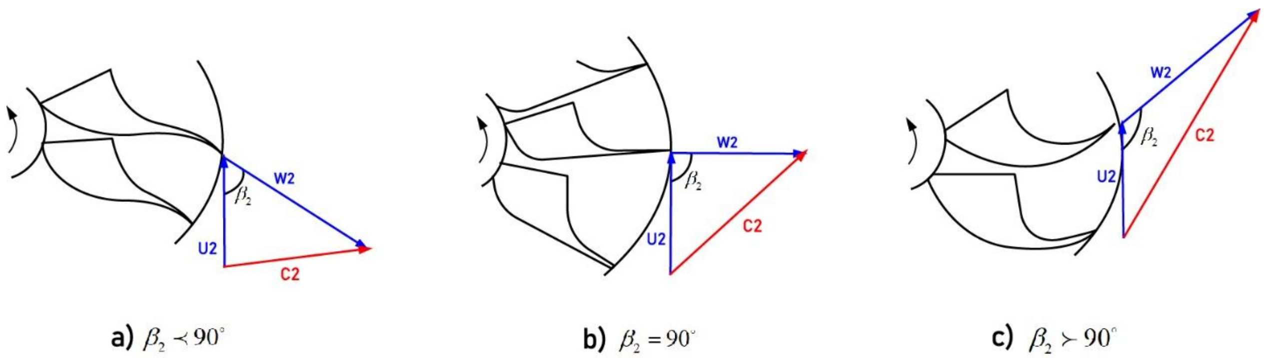

Figure I. 5 : Different blade inclinations at exit

b) Diffuser: The diffuser, on the other hand, is the stationary element. Its purpose is to convert the high-velocity gas exiting the impeller into high-pressure gas. By slowing down the gas and increasing its pressure, the diffuser ensures efficient compression.

The diffusers in centrifugal compressors can be divided into two primary categories: vaneless diffusers and vaned diffusers (see Figure I.6).

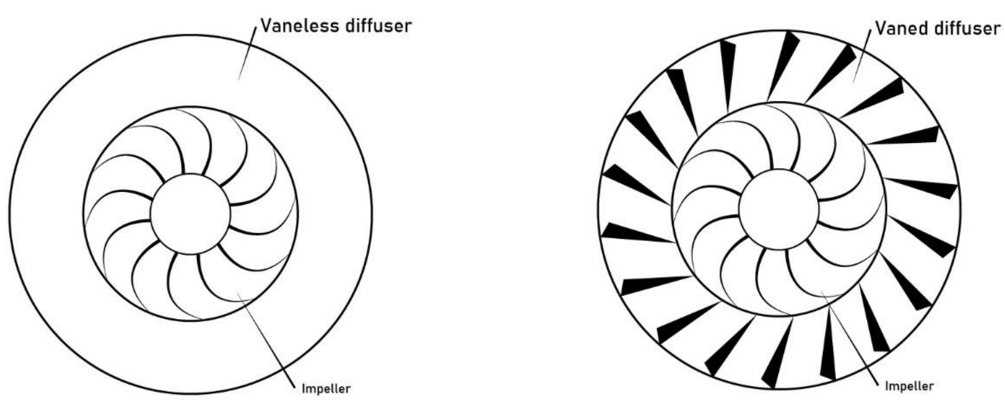

Figure I. 6 : Types of diffusers

- **The vaneless diffuser:**

The vaneless diffuser's design is straightforward, featuring parallel or nearly parallel walls that create a radial annular passage from the impeller outlet radius to a specific outlet radius of the diffuser. Following the diffuser is typically a volute or a collecting chamber that channels the flow to a single exit. To stabilize the flow entering the diffuser, a small pinch is commonly employed.

- **The vaned diffuser :**

Vaned diffusers have a more limited flow range, which can restrict their operational flexibility. This makes them less adaptable to changes in flow conditions compared to vaneless diffusers.

These diffusers are designed to achieve higher-pressure recovery and efficiency. The presence of vanes helps guide the flow better, enhancing aerodynamic performance and minimizing energy losses. This makes vaned diffusers particularly suitable in applications where high efficiency is more critical than flexibility. There are several types of vaned diffusers, as illustrated in Figure I.7

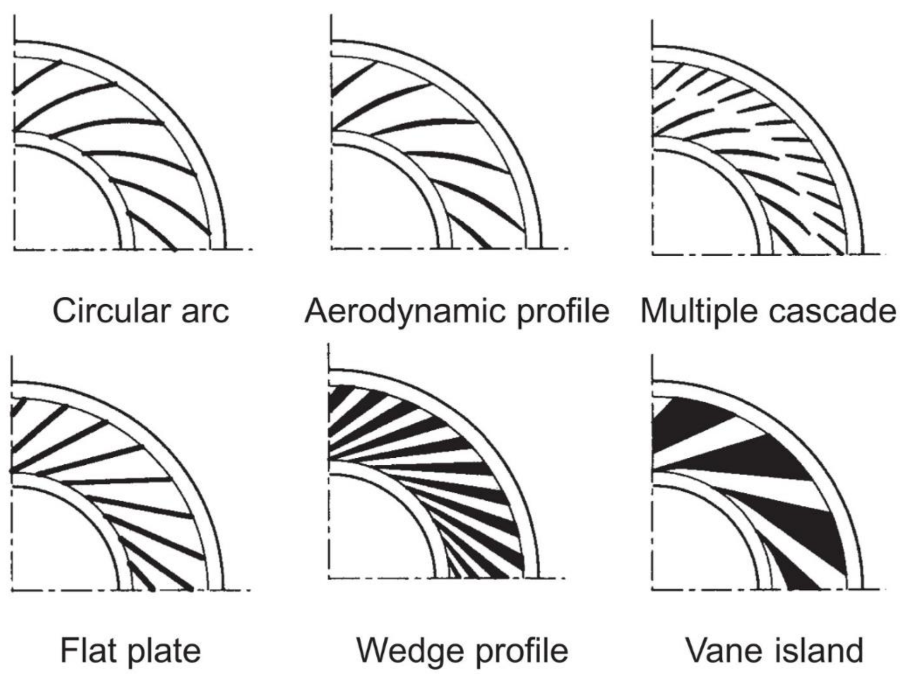

Figure I. 7: Types of Vaned Diffusers,
Source: Casey M, Robinson C. Diffuser Design. In: Radial Flow Turbocompressors: Design, Analysis, and Applications

In summary, centrifugal compressors efficiently compress gases using rotating impellers and stationary diffusers, with various design options to balance performance and manufacturing considerations.

I.3.3. Velocity triangles:

Velocity triangles are used in the analysis and design of centrifugal compressors. They provide a graphical representation of the relationships between the fluid's various velocity components as it moves through the impeller.

Velocity triangles in centrifugal compressors can be expressed as follows [12]:

$$V = W + U \tag{I.4}$$

Where V, W, and U are, respectively, the vectors of absolute velocity, relative velocity, and blade velocity. Figure I.8Shows the main projections of these vectors in the r, z, and θ directions. The angles α and β represent the absolute and relative flow angles, respectively.

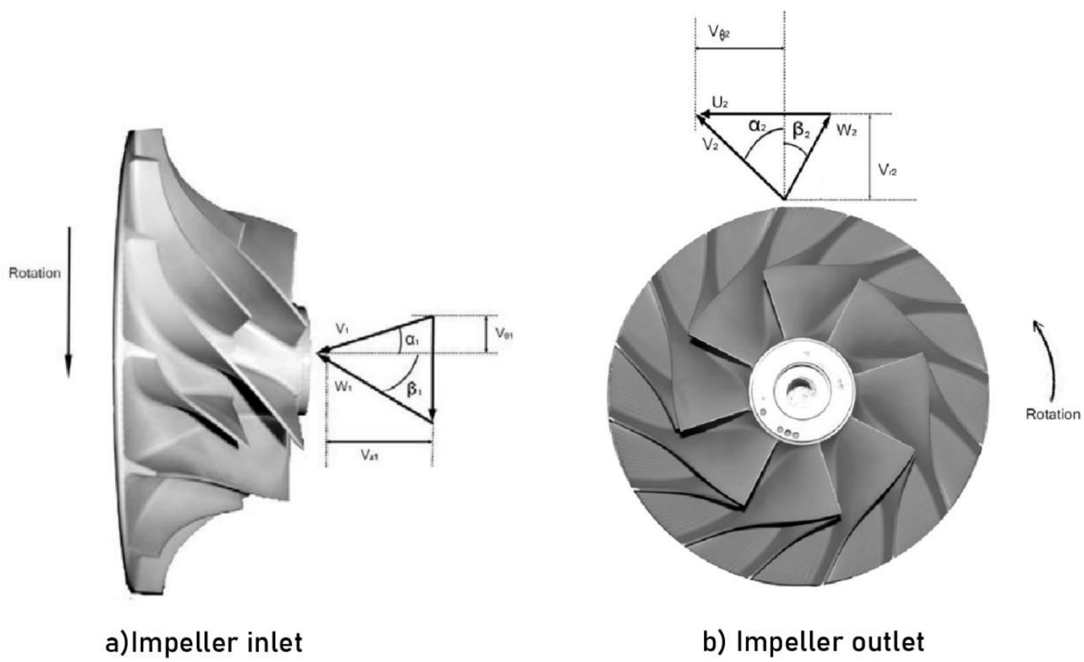

Figure I. 8 : Velocity triangle in centrifugal compressor [12]

I.3.4. Operating Principle of a Centrifugal Compressor Stage:

Centrifugal compressors operate by converting rotational kinetic energy into dynamic energy, and subsequently into pressure energy, of the working fluid. as illustrated in (figure I.9).

The process begins with the high-speed rotating impeller pulling in ambient air through the inlet. As the air enters the impeller, it encounters the rotating blades, which impart centrifugal force, causing the air to move radially outward. The air, now accelerated, travels around the casing of the compressor, facilitating a smooth and controlled flow to the next stage. Upon reaching the diffuser, the flow area increases, causing the high-velocity air to decelerate and, consequently, increasing its static pressure. Finally, the pressurized air is directed through the outlet pipe, ready for various applications such as powering pneumatic tools, driving turbines, or other industrial processes requiring compressed air. This sequence of air intake, centrifugal acceleration, controlled flow, deceleration in the diffuser, and final pressurization ensures the effective functioning of the centrifugal compressor.

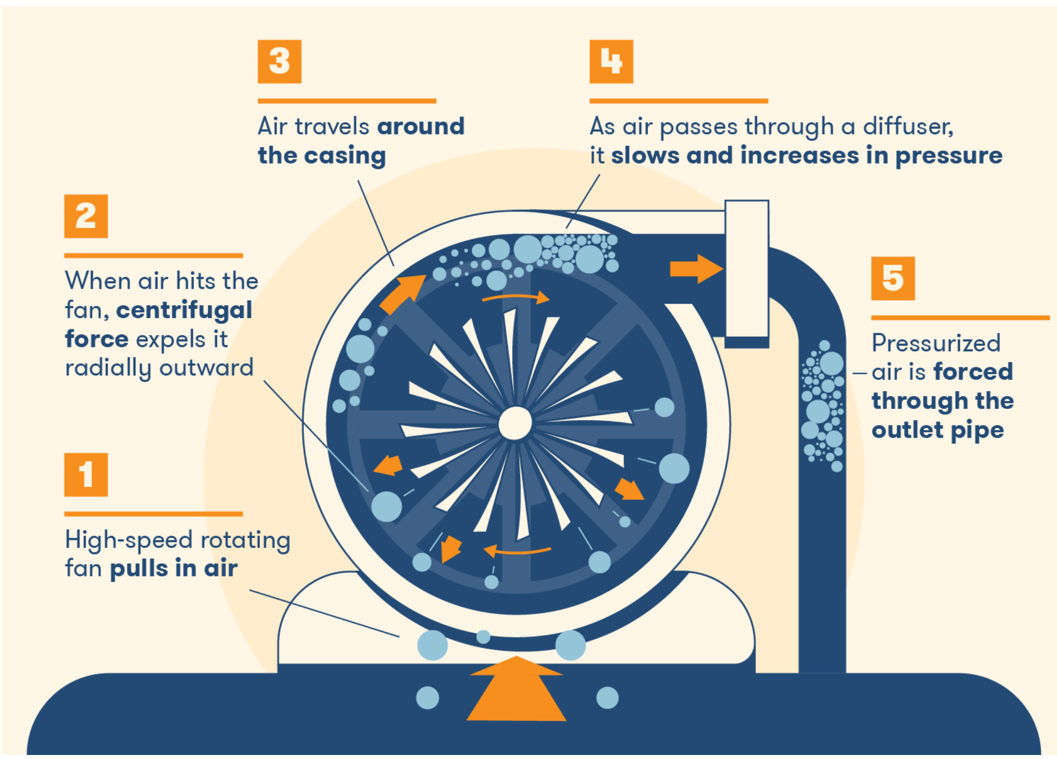

Figure I. 9 : Process of compression in centrifugal compressors.

Source: https://sollantcompressor.com/

To more deeply understand the functioning of a centrifugal compressor, we can use the T-S (Temperature-Entropy) diagram shown in (figure I.10). This diagram provides a detailed thermodynamic perspective on the processes occurring within the compressor.

Gas evolution in a compressor is typically adiabatic due to its small size and limited heat exchange with the surroundings. On the (T,S) diagramfeaturing two isobars $P1$ and $P2$, the initial state of the fluid at pressure $P1$ is marked as position "1". The reversible adiabatic compression is shown as the path from "1" to "2is". The actual adiabatic compression, accounting for internal losses converted into heat, is represented by the curve from "1" to "2".

During the "1" to "2" section, the compressor's rotor increases the fluid's energy in static pressure and heat. This total pressure rise comprises an increase in static pressure from $P1$ to $P2$ and an increase in kinetic energy from Eci1 to Eci2. In the "2" to "3" section (diffuser), there is no energy gain, but a total pressure decline due to losses. Energy transforms into an increase in static pressure from $P2$ to $P3$ and a decrease in kinetic energy from Eci2 to Eci3.

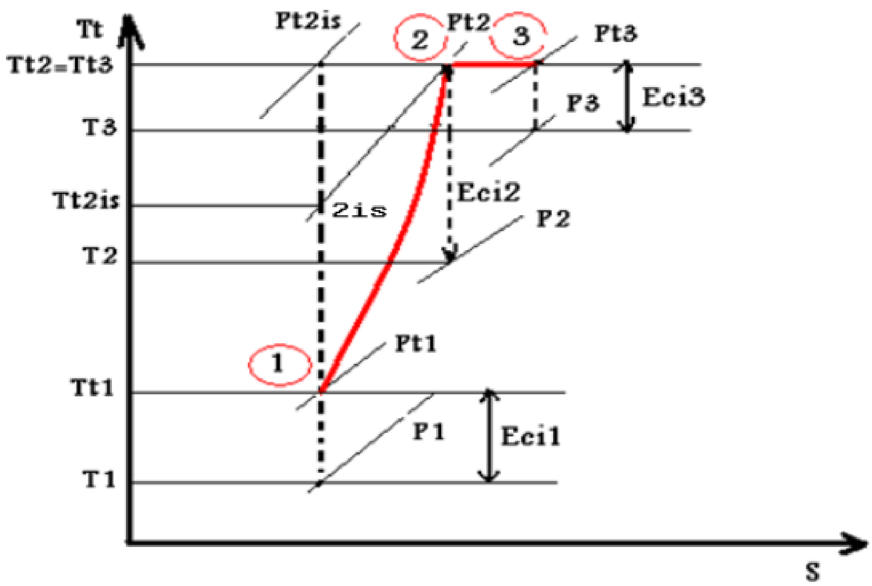

Figure I. 10 : T-S diagram for centrifugal compressor stage

I.3.5. Centrifugal Compressor characteristics :

To understand the performance of a centrifugal compressor, we can analyze its performance curve, which typically consists of three important curves:

- Differential Pressure (or sometimes Polytropic Head) vs. Inlet Flow Rate
- Brake Power vs. Inlet Flow Rate,
- Efficiency vs. Inlet Flow Rate

- **Differential Pressure vs. Inlet Flow Rate Curve:**

In the performance curve of a centrifugal compressor, the differential pressure (or head) is indicated on the vertical axis, while the inlet flow rate is shown on the horizontal axis. As the compressor inlet flow rate increases, the head developed by the compressor begins to decrease. The compressor achieves its maximum differential pressure at a point known as the surge point. The flow and pressure corresponding to this surge point are referred to as the surge flow and surge pressure.

The relationship between the inlet flow rate and the differential pressure (head) is such that any change in one parameter affects the other. Thus, the inlet flow rate and differential pressure are interdependent, and neither can be altered without influencing the other.

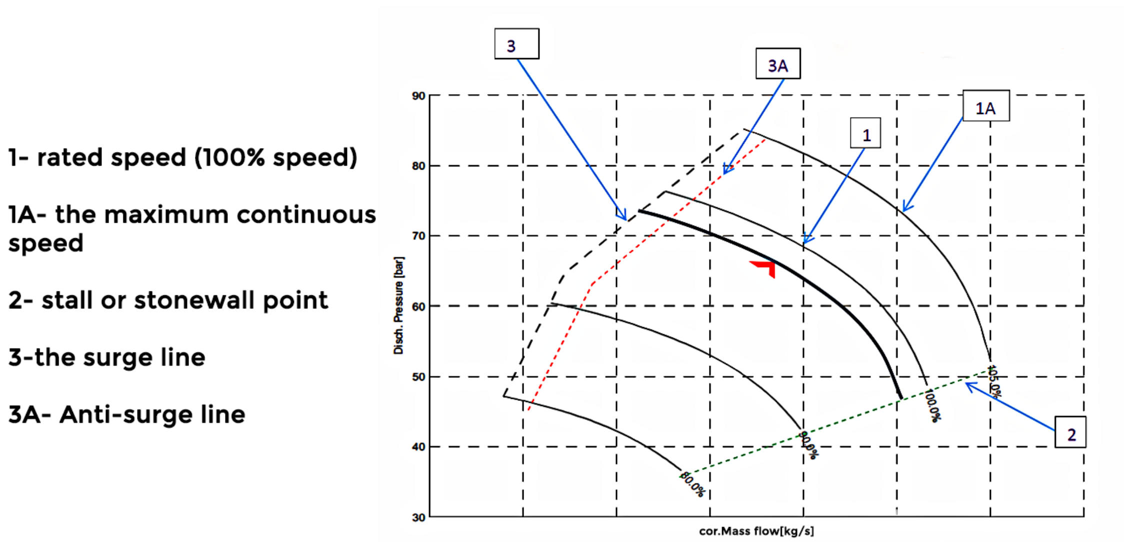

Figure I. 11 : centrifugal compressor performance curve

- **The operating point:**

The red mark on the performance curve indicates the operating point of a centrifugal compressor. The flow rate at this point is termed the "Operating Flow," while the associated discharge pressure is known as the "Operating Discharge Pressure."

- **Speed :**

As observed from the performance curve, the flow rate versus discharge pressure curves vary with different compressor speeds. In other words, the relationship between flow rate and discharge pressure changes according to the compressor's operating speed.

- **Stall or Stone Wall Point:**

The maximum flow developed by a centrifugal compressor is called Stall or Stonewall Point. Below this point, the compressor is aerodynamically unstable.

Physically, if the flow rate is increased, the angle of relative velocity will decrease until it reaches a minimum value. This corresponds to an obstruction of the channel in which the fluid reaches the speed of sound.

- **Surge:**

Surge is a complex unsteady phenomenon that occurs under certain operating conditions. It manifests when the airflow rate falls below a specific threshold for a given rotational speed, resulting in significant periodic fluctuations in pressure and flow rate at varying frequencies. This leads to a cyclic back-and-forth movement of airflow in the reverse direction. There are two types of surge:

Classical Surge: Characterized by oscillations in both pressure and flow rate.

Deep Surge: In this situation, the oscillations in flow are so large that a complete reversal of flow occurs within the pressure system.

- **Efficiency:**

The isentropic efficiency can be defined as the ratio of the total entropy change in an isentropic transformation to the total entropy change in a real transformation:

$$\eta_{is} = \frac{\Delta s_{is}}{\Delta s_{real}} \tag{I.5}$$

$$\eta_{is} = \frac{h_{t2is} - h_{t1}}{h_{t2} - h_{t1}} = \frac{h_{t3is} - h_{t1}}{h_{t3} - h_{t1}} = \frac{T_{2is} - T_{t1}}{T_{t2} - T_{t1}} = \frac{\pi_{c-t}^{\frac{\gamma-1}{\gamma}} - 1}{\tau_t - 1} \tag{I.6}$$

Where:

$$\begin{cases} \tau_t = \dfrac{T_{t2}}{T_{t1}} \\ \pi_t = \dfrac{p_{t2}}{p_{t1}} \end{cases}$$

- Isentropic transformation : $\tau_t = \pi_{c-t}^{\frac{\gamma-1}{\gamma}}$

I.3.6. Review of Impeller Flow:

Centrifugal compressors were initially designed with the assumption that there would be no flow separations within the impeller and that the impeller discharge flow would be axisymmetric. However, this assumption was challenged by Dean and Senoo's 1960 [13] paper on "jet-wake flow," which used experimental investigations to demonstrate that the flow actually consists of two distinct regions: a high relative velocity jet on the pressure side (jet) of the impeller blade and a low relative velocity wake on the suction side (wake). Despite acknowledging that actual flow would feature smoother velocity gradients between these regions, the authors proposed this simplified model to better predict losses instead of the then-prevailing assumption of a uniform exit flow field.

In addition to the jet-wake pattern, several other flow phenomena develop within impeller passages, further complicating the flow dynamics in centrifugal compressors. These include vortices at the impeller leading edge near both the hub and shroud, as well as potential shocks near the blade tip in high-speed machines. Tip leakage flow, which moves from the pressure side to the suction side through the gap between the blade and shroud, also plays a significant role. Additionally, the jet and wake regions can develop distinct secondary flow patterns. These interacting flow features collectively make the impeller flow field more complex, thereby challenging the accurate prediction of centrifugal compressor performance.

The following figure I.12 Illustrates the different flow phenomena that develop within the impeller passage:

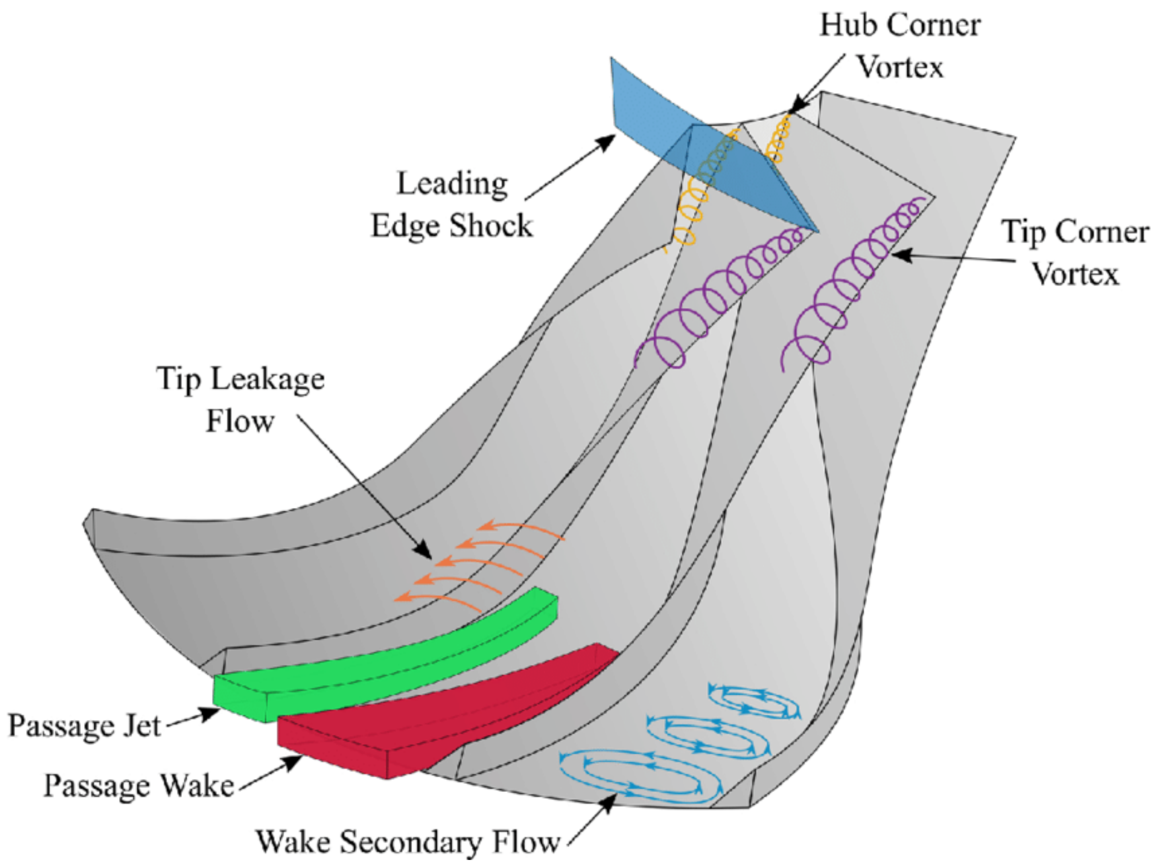

Figure I. 12: Different flow phenomena in centrifugal compressor impeller.

Source: Development and validation of a new method to model slip and work input

- **Slip :**

In centrifugal compressors, slip refers to the phenomenon where the actual flow velocity at the impeller exit is lower than the theoretical velocity predicted by basic momentum calculations. This difference occursbecause the fluid does not fully follow the impeller's rotating motion, influenced by factors like friction, flow separation, and secondary flows.

I.3.7. The different aerodynamicforces applied to fluid flow through a centrifugal compressor:

In a centrifugal compressor, the aerodynamic forces experienced by the fluid particles are very important to determine the machine's performance and efficiency. The main aerodynamic forces in a centrifugal compressor include [12]:

- **the inertial force**: due to changes in the particle's velocity along its path (expressed per unit volume):

$$F_{inertia} = -\rho W \frac{\partial W}{\partial s} u_s \tag{I.7}$$

- **Centrifugal Force:**The rotating impeller generates a centrifugal force that drives the air or gas outward from the center:

$$F_{centrifugal} = -\rho \Omega^2 r.u_r \tag{I.8}$$

Where

$\Omega = \Omega.u_z$: the rotation vector .

u_r :radial direction vector.

- **The Coriolis force:** due to the rotation of the wheel is given by:

$$F_{Coriolis} = -2\rho \Omega \times W \tag{I.9}$$

The Coriolis force is determined by a cross-product involving the relative velocity; its direction directly depends on the particle's trajectory in the wheel's reference frame (see Figure 2.12 for a representation in a blade-to-blade plane).

- **The Centrifugal force due to curvature:**since the trajectory in the relative reference frame is curved, we introduce the centrifugal force due to these curvatures. Its expression is essentially analogous to the centrifugal force arising from rotation.

$$F_{centrifugal-curvature} = \rho \frac{W^2}{R_c} u_n \tag{I.10}$$

Where

R_c: curvature radius

- **The deceleration force:** in a centrifugal compressor, The deceleration force refers to the force acting against the motion of the fluid as it passes through the compressor. This force is primarily caused by converting kinetic energy into pressure energy during the compression process.

The projection of these forces in a Blade to blade plane is illustrated in Figure I.13 :

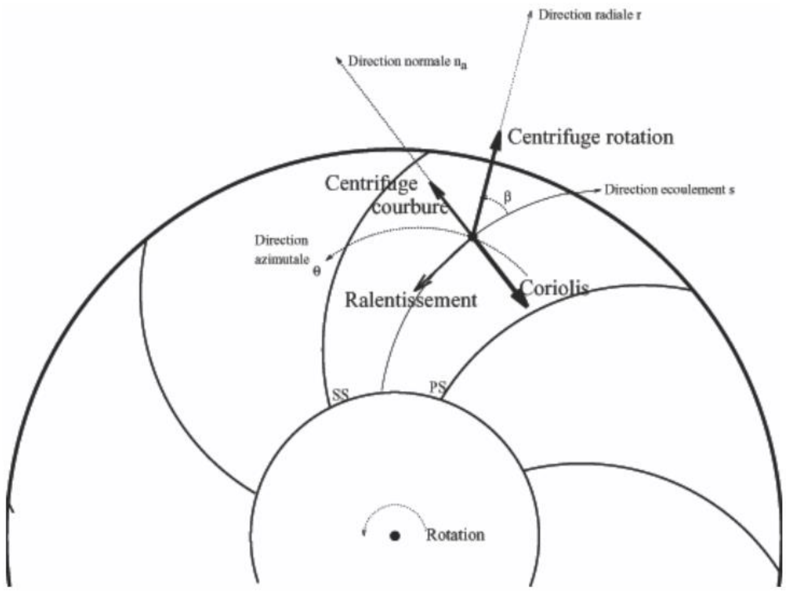

Figure I. 13 : representation of acting forces in Blade To Blade plane [12]

I.3.8. Different reference views in centrifugal compressor:

Flows in a centrifugal compressor are generally three-dimensional, viscous, turbulent, and involve compressible fluids. To simplify the study and analysis of the internal flow, it is decomposed into three types of reference surfaces, as shown in Figure (1.9). This decomposition leads to three types of flows:

- **Meridional Flow:** This type of flow is analyzed along the meridional plane, a cross-sectional plane passing through the axis of rotation. It helps understand the fluid's movement in the radial and axial directions within the compressor.
- **Blade-to-Blade Flow:** This type of flow is examined on a plane between two adjacent impeller blades. It is crucial for analyzing the flow behavior and interactions between the blades, including the effects of blade geometry on the flow patterns.
- **Orthogonal Plane Flow:** This type of flow is observed on a plane orthogonal to the meridional plane. It provides insights into the flow patterns perpendicular to the primary flow direction, aiding in understanding secondary flows and cross-sectional velocity profiles.

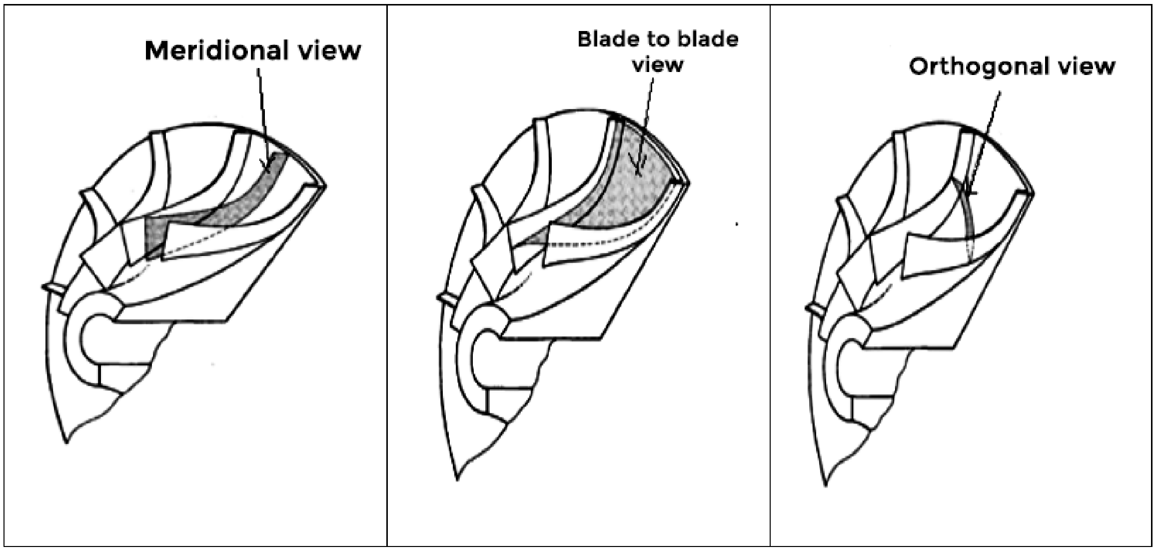

Figure I. 14 : Reference views in centrifugal compressor

- **Field of application :**

Centrifugal compressors have a wide range of applications across various industries due to their ability to handle large volumes of gases at high pressures efficiently. These are some of the primary fields where centrifugal compressors are commonly used:

a) Oil and Gas Industry:

Natural Gas Processing: Used in gas gathering, boosting, and transmission pipelines.

Refineries: Employed in processes like fluid catalytic cracking and hydrocracking.

Petrochemical Plants: Utilized for processes requiring high-pressure gas compression.

b) Chemical Industry:

Production of Chemicals: Used in producing ammonia, urea, and other chemical processes requiring compressed gases.

Polymerization Processes: Essential in the production of various polymers.

c) Power Generation:

Gas Turbines: Serve as an integral part of gas turbines for power generation.

Combined Cycle Plants: These are used in the gas compression stages of combined cycle power plants.

d) **Aerospace Industry:**

Aircraft Engines: Integral to the operation of jet engines and auxiliary power units.

Automotive Industry:

Turbochargers: These are used in turbocharging systems to increase internal combustion engines' efficiency and power output.

e) **Manufacturing and Industrial Processes**

f) **Mining Industry:**

Ventilation Systems: Provide compressed air for ventilation in underground mines.

Pneumatic Equipment: Power pneumatic tools and equipment used in mining operations.

Chapter 02

Numerical model

II.1. Introduction:

Mathematical modelling is the foundation of computational fluid dynamics (CFD), providing the essential framework for simulating and understanding fluid behaviour. Three three-dimensional differential equations encompassing all possible fluid flow scenarios describe fluid mechanics phenomena. However, analytical solutions to these equations are not yet available. Appropriate hypotheses can be simplified into solvable one-dimensional forms to facilitate preliminary design processes.

The fundamental equations governing mass, momentum, and energy conservation allow us to represent complex fluid interactions accurately. This chapter focuses on these critical equations and key concepts in turbulence modeling, boundary conditions, and numerical methods.

II.2. Governing Equations of Fluid Flow:

Fluid flow behavioris governed by fundamental equations describingmass, momentum, and energy conservation. The primary governing equations include the continuity equation, the Navier-Stokes equations, and the energy equation.

In general, the conservation equations for an unsteady, compressible Newtonian fluid are expressed as follows [15]:

- **Continuity Equation:**

The continuity equation represents the conservation of mass in a fluid flow:

$$\frac{\partial(\rho)}{\partial t}+\frac{\partial(\rho.u_i)}{\partial x_i}=0 \qquad \text{(II.1)}$$

- **The Momentum Conservation Equation:**

$$\frac{\partial(\rho.u_i)}{\partial t}+\frac{\partial(\rho.u_i.u_j)}{\partial x_j}=-\frac{\partial p}{\partial x_i}+\frac{\partial\tau_{ij}}{\partial x_j}+S_i \qquad \text{(II.2)}$$

Where:

S_i : In fluid dynamics, the source term encompasses all volumetric forces acting on the fluid, including gravity, centrifugal, and Coriolis forces.

$$S_i = S_{i,cor} + S_{i,cent} = -2.\varepsilon_{ijk}.\rho.\omega_j.u_k - \varepsilon_{ijk}.\varepsilon_{klm}.\rho.\omega_j.\omega_l.r_m \tag{II.3}$$

τ_{ij} : The viscous stress tensor for a Newtonian fluid is given by:

$$\tau_{ij} = \delta_{ij}.\lambda.\frac{\partial u_k}{\partial x_k} + \mu.\left(\frac{\partial u_i}{\partial x_j} + \frac{\partial u_j}{\partial x_i}\right) = \delta_{ij}.\lambda.\frac{\partial u_k}{\partial x_k} + 2.\mu.\delta_{ij} \tag{II.4}$$

Where:

δ_{ij} :*The Kronecker symbol and is defined as follows*: $\begin{cases} \delta_{ij} = 1 \text{si } i = j \\ \delta_{ij} = 0 \text{si } i \neq j \end{cases}$

- **Energy Conservation equation:**

$$\frac{\partial(\rho.h_t)}{\partial t} + \frac{\partial(\rho.h_t.u_j)}{\partial x_j} = \frac{\partial p}{\partial t} + \frac{\partial}{\partial x_j}.\left(K.\frac{\partial T}{\partial x_j}\right) + \frac{\partial}{\partial x_j}(\tau_{ij}.u_j) + S_E \tag{II.5}$$

Where:

h_t :The total energy (the sum of internal energy and kinetic energy)

S_E :Energy source term.

μ:The molecular viscosity depends on the temperature, according to Sutherland's law:

$$\mu = \mu(\frac{T}{T_0})^{3/2}.\frac{T_0 + S_0}{T + S_0} \tag{II.6}$$

II.3. Turbulence Modeling:

Turbulence is a condition of fluid motion characterised by apparently random and chaotic three-dimensional vorticity. When turbulence is present, it dominates all other flow phenomena and increases energy dissipation, mixing, heat transfer, and drag.

Three methods of simulating turbulent flows are distinguished for solving equations of high Reynolds number flows (see Figure II.1).

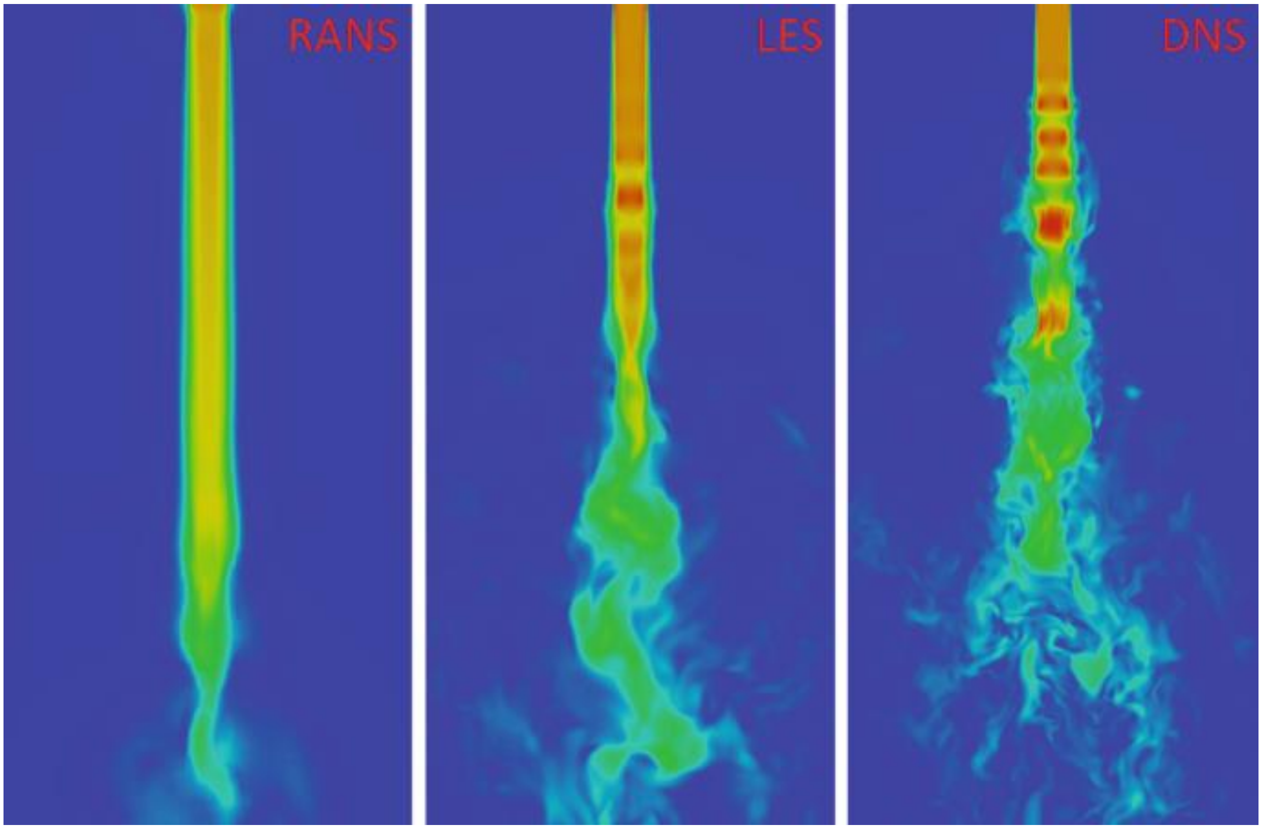

Figure II. 1 : difference between DNS, LES and RANS in turbulence modelling.

Source: Rodriguez, S. (2019). LES and DNS Turbulence Modeling

II.3.1. Direct Numerical Simulation (DNS):

Direct Numerical Simulation (DNS) directly solves fluid mechanics problems using the three-dimensional, unsteady Navier-Stokes equations. It captures the average flow and the turbulent fluctuations without relying on any turbulence model. The mesh used in DNS must be thin enough to capture the smallest turbulence eddies, necessitating a sufficiently small vortex. Although DNS is the most accurate method for simulating turbulent flows and is faster than other methods, it requires powerful computing machines and significant computational time. Despite being impractical for most engineering problems due to the massive computational resources required, DNS is crucial for our fundamental understanding of the physics of turbulence. The most advanced DNS simulations have achieved spatial resolution with several nodes on the order of magnitude needed to capture the entire turbulence spectrum.

II.3.2. Large Eddy Simulation (LES):

Large Eddy Simulation (LES) is a computational technique utilised for modeling turbulent flows, particularly when resolving all turbulent scales is impractical. It involves explicitly separating large-scale turbulent structures while modeling the effects of smaller scales through subgrid-scale models. LES relies on spatial filtering to differentiate resolved large-scale motions from unresolved small-scale turbulence. This approach effectively captures the large vortices while addressing dissipative processes caused by viscosity, thermal conductivity, and diffusivity at scales smaller than those explicitly solved by the mesh. While LES provides precise simulations of turbulent features, it is computationally demanding in terms of time due to the requirement of resolving complex turbulent phenomena.

II.3.3. Reynolds-Averaged Navier-Stokes (RANS):

The Navier-Stokes equations can be averaged to derive the mean equations of fluid flows known as Reynolds Averaged Navier-Stokes (RANS) equations. These equations closely resemble the original equations but include extra terms in the momentum equations called Reynolds stress terms, which are unknown and must be modeled.

Turbulence models are designed to capture the impact of turbulence by addressing the unknown Reynolds stress terms. These models are usually classified according to the following categories: additional equations are needed to model the turbulence effect on the flow. The models range from basic algebraic relations and become more intricate and detailed as the number of equations utilised increases. RANS modeling is the most commonly used approach in industrial applications.

When the flow is turbulent, any vector quantity or scalar can be decomposed into an average and fluctuating part. For example, the instantaneous velocity field for incompressible turbulent flow can be decomposed into a time-averaged velocity and its corresponding fluctuation:

$$u_i = \overline{u}_i + u_i' \qquad \text{(II.7)}$$

Where

u_i : Instantaneous velocity.

$\overline{u}_i = \dfrac{1}{\Delta t}\displaystyle\int_t^{t+\Delta t} u_i \, dt$: time-averaged velocity

u_i' : Velocity fluctuation.

The direct solution of the governing equations is generally not feasible for the majority of engineering scenarios. These equations yield highly disordered turbulent solutions at the Reynolds numbers commonly encountered in practical situations, necessitating modellingthe impact of the smallest scales. Most turbulence models rely on a one-point averaging of the governing equations. The following sections will outline the averaging procedure.

Let ϕ be any dependent variable. It is convenient to define two different types of averaging of ϕ:

- Reynolds averaging (Classical time averaging) :

$$\begin{aligned} &\bar{\Phi} \equiv \frac{1}{T}\int_T \Phi(t)\,dt \\ &\Phi' \equiv \Phi - \bar{\Phi} \end{aligned} \tag{II.8}$$

- Favre averaging (Density weighted time averaging):

$$\begin{aligned} &\tilde{\Phi} \equiv \frac{\overline{\rho\Phi}}{\bar{\rho}} \\ &\Phi'' \equiv \Phi - \tilde{\Phi} \end{aligned} \tag{II.9}$$

Where:

$$\begin{cases} \overline{\Phi'} = 0 \\ \overline{\Phi''} \neq 0 \end{cases}$$

The continuity, momentum, and energy equations are time-averaged to derive an averaged form of the governing equations. The following exact open equations are obtained by introducing a density-weighted time average decomposition (II.9) of u_i and h_t and a standard time average decomposition (II.8) of ρ and p :

$$\frac{\partial\bar{\rho}}{\partial t} + \frac{\partial(\bar{\rho}.u_i)}{\partial x_i} = 0 \tag{II.10}$$

$$\frac{\partial(\bar{\rho}.u_i)}{\partial t} + \frac{\partial(\bar{\rho}.u_i.u_j)}{\partial x_j} = -\frac{\partial\bar{p}}{\partial x_j} + \frac{\partial(\overline{\tau_{ij}} + \overline{\rho.u_i^{\backslash\backslash}.u_j^{\backslash\backslash}})}{\partial x_j} + \overline{S_i} \tag{II.11}$$

$$\begin{aligned} &\frac{\partial(\bar{\rho}.h_t)}{\partial t} + \frac{\partial(\bar{\rho}.h_t.u_j)}{\partial x_j} = \frac{\partial\bar{p}}{\partial t} + \frac{\partial}{\partial x_j}(-\overline{q_j} - \overline{\rho.h_t^{\backslash\backslash}.u_j^{\backslash\backslash}} + \overline{t_{ij}.u_{ij}^{\backslash\backslash}} \\ &-\frac{1}{2}.\overline{\rho.u_i^{\backslash\backslash}.u_j^{\backslash\backslash}} + (\overline{t_{ij}} + \bar{\rho}.\tau_{ij}).u_j) + \overline{S_E} \end{aligned} \tag{II.12}$$

Equation(II.10), (II.11) and (II.12)are referred to as the Favre averaged Navier-Stokes equations. The stress tensor of Reynolds corresponds to a diffusion term in the majority of flows. Since the RANS model only provides access to averaged quantities, the fluctuation U'U′ is not known and is required to complete the system of equations. In most scenarios, the Boussinesq hypothesis is utilised, which aligns with the Reynolds stress tensor and the mean deformation tensor, as described by the following equation:

$$\overline{-\rho.u_i^{\backslash\backslash}.u_i^{\backslash\backslash}} = \mu_T.\left[\frac{\partial\overline{u_i}}{\partial x_j}+\frac{\partial\overline{u_j}}{\partial x_i}-\frac{2}{3}.\frac{\partial\overline{u_k}}{\partial x_k}\right]-\frac{2}{3}.\bar{\rho}.k.\delta_{ij} \tag{II.13}$$

Where:

$k=\frac{1}{2}.\overline{u_i^{\backslash\backslash}.u_j^{\backslash\backslash}}$: Is the turbulent energy.

μ_T : Turbulent viscosity.

$-\frac{2}{3}.\bar{\rho}.k.\delta_{ij}$, It can be likened to an additional pressure force; in practice, it is negligible compared to the pressure force.

Hence, the averaged Navier-Stokes equations can be expressed in a manner resembling the form of the Navier-Stokes equations:

- **Continuity equation:**

$$\frac{\partial\bar{\rho}}{\partial t}+\frac{\partial(\bar{\rho}.u_i)}{\partial x_i}=0 \tag{II.14}$$

- **The Momentum Conservation Equation:**

$$\frac{\partial(\bar{\rho}.u_i)}{\partial t}+\frac{\partial(\bar{\rho}.u_i.u_j)}{\partial x_j}=-\frac{\partial\overline{p}}{\partial x_j}+\frac{\partial}{\partial x_j}\left[(\mu+\mu_T)\left(\frac{\partial u_i}{\partial x_j}+\frac{\partial u_j}{\partial x_i}-\frac{2}{3}\delta_{ij}\frac{\partial u_k}{\partial x_k}\right)\right]-\frac{2}{3}\bar{\rho}k+\overline{S_i} \tag{II.15}$$

- **Energy Conservation equation:**

$$\frac{\partial(\bar{\rho}.h_t)}{\partial t}+\frac{\partial(\bar{\rho}.h_t.u_j)}{\partial x_j}=\frac{\partial\overline{p}}{\partial t}+\frac{\partial}{\partial x_j}\left[k.\frac{\partial\tilde{T}}{\partial x_j}-\frac{\mu_T}{P_{rT}}.\frac{\partial h_t}{\partial x_j}+(\overline{t_{ij}}+\bar{\rho}.\tau_{ij})u_i\right] \tag{II.16}$$

- **Perfect gas law :**

$$\bar{P}=\bar{\rho}.R.\bar{T} \tag{II.17}$$

These are an open set of partial differential equations with unknown correlation terms called Reynolds Stresses. They introduce six additional unknowns without adding any extra equations to the system, resulting in four equations for 10 unknowns, which need to be modelledto obtain solvable closed-form equations.

In the process of modelling the Reynolds stress term following a turbulence model based on the Boussinesq hypothesis, two new variables are introduced:

Turbulent Viscosity (μ_t): This property measures the effective viscosity due to turbulence, which is analogous to the molecular viscosity but much more significant in magnitude.

Kinetic Energy (k): This represents the kinetic energy per unit mass due to turbulent fluctuations.

The RANS equation system requires two more pieces of information to be completed. Specifically, we need to understand how turbulence changes over time and space. This requires two additional equations to describe the fluctuations' characteristic velocity, length, and time.

II.3.4.Two equations turbulence models :

Two-equation turbulence models are more frequently utilised in Computational Fluid Dynamics (CFD) to replicate turbulent flows and belong to a category of turbulence models. These models balance computational efficiency and accuracy, unlike simpler models that rely on a single equation (e.g., zero-equation models) or more complex models like Reynolds Stress Models (RSM) [14].

The most popular two-equation turbulence models are :

- $k-\omega$ (k-omega) turbulence model.
- $k-\varepsilon$ (k-epsilon) turbulence model.
- $S.S.T$ (shear stress transport) model.

➢ $k-\varepsilon$ **(k-epsilon) turbulence standard model:**

The $k-\varepsilon$ (k-epsilon) turbulence model is one of the most widely used models in Computational Fluid Dynamics (CFD) for simulating turbulent flows. It is economical and provides reasonable accuracy for a wide range of flows. A two-equation model gives a general description of turbulence using two transport equations: the turbulent kinetic energy (k) and its rate of dissipation (ε) [14].

- **the turbulent kinetic energy (k):**

$$\frac{\partial(\bar{\rho}.k)}{\partial t}+\frac{\partial}{\partial x_j}\left[(\mu+\frac{\mu_T}{\sigma_k})\frac{\partial k}{\partial x_j}\right]+P_k-\bar{\rho}.\varepsilon \qquad \text{(II.18)}$$

- **the rate of dissipation (ε):**

$$\frac{\partial(\bar{\rho}.\varepsilon)}{\partial t}+\frac{\partial}{\partial x_j}(\bar{\rho}.u_j.\varepsilon)=\frac{\partial}{\partial x_j}\left[(\mu+\frac{\mu_T}{\sigma_\varepsilon})\frac{\partial \varepsilon}{\partial x_j}\right]+\frac{\varepsilon}{k}(C_{\varepsilon 1}.P_k-C_{\varepsilon 2}.\bar{\rho}.\varepsilon) \qquad \text{(II.19)}$$

Where:

P_k : The production of turbulence due to viscous forces and buoyancy.

$$P_k=\mu_T.\frac{\partial}{\partial x_j}\left(\frac{\partial u_j}{\partial x_j}+\frac{\partial u_j}{\partial x_i}\right)-\frac{2}{3}\frac{\partial u_i}{\partial x_j}.\left(3.\mu_T.\frac{\partial u_k}{\partial x_k}+\bar{\rho}.k\right) \qquad \text{(II.20)}$$

In the case where the full buoyancy mode is used, the production term P_{kb} will be modeled as follows:

$$P_{kb}=\frac{\mu_t}{\rho.\sigma_\rho}.g.\frac{\partial \rho}{\partial x_j} \qquad \text{(II.21)}$$

In case the Boussinesq buoyancy model is used, the modeling is the following:

$$P_{kb}=\frac{\mu_t}{\rho.\sigma_\rho}.\beta.g.\frac{\partial T}{\partial x_j} \qquad \text{(II.22)}$$

The $k-\varepsilon$ Model expressed the turbulent viscosity as follows:

$$\mu_t=C_\mu\rho\frac{k^2}{\varepsilon} \qquad \text{(II.23)}$$

The $k-\varepsilon$ model uses empirically derived constants, which are in ANSYS CFX [15]:

Table II. 1 : constants [15]

Constant	C_μ	$C_{\varepsilon 1}$	$C_{\varepsilon 2}$	σ_k	σ_ε
Value	0.09	1.44	1.92	1.0	1.3

Advantages

- The model is relatively straightforward to implement and computationally efficient.
- It performs reasonably well for many types of turbulent flows, making it a popular default choice.
- Suitable for both free shear flows (like jets and wakes) and wall-bounded flows (like boundary layers).

Note:

The $k-\varepsilon$ turbulence model is simple, robust, and economical. It applies the wall law for $y^{+} \succ 30$, which inadequately accounts for boundary layer separation phenomena.

➢ $k-\omega$ **(k-omega) turbulence model:**

The turbulence model known as k-omega ($k-\omega$), first developed by Wilcox [14], is widely used for simulating turbulent flow conditions. The k-omega model is a two-equation model that, in addition to the conservation equations, solves two transport equations (PDEs) to account for history effects such as the convection and diffusion of turbulent energy. These transport equations deal with turbulent kinetic energy (k), representing the energy in turbulence, and specific turbulent dissipation rate (ω), which signifies the turbulence frequency. $\omega$is also known as the scale of turbulence [14].

- Turbulent Kinetic Energy (k):

$$\frac{\partial(\bar{\rho}k)}{\partial t}+\frac{\partial}{\partial x_j}(\bar{\rho}.u_j.k)=\frac{\partial}{\partial x_j}\left[\left(\mu+\frac{\mu_T}{\sigma_{k1}}\right).\frac{\partial k}{\partial x_j}\right]+P_k-\beta.\bar{\rho}.k.\omega \qquad \text{(II.24)}$$

- The turbulence frequency (ω):

$$\frac{\partial(\bar{\rho}.\omega)}{\partial t}+\frac{\partial}{\partial x_j}(\bar{\rho}.u_j.\omega)=\frac{\partial}{\partial x_j}\left[\left(\mu+\frac{\mu_T}{\sigma_{\omega1}}\right)\frac{\partial \omega}{\partial x_j}\right]+\alpha_1.\frac{\omega}{k}.P_k-\beta_1.\bar{\rho}.\omega^2 \qquad \text{(II.25)}$$

The ($k-\omega$) model expressed the turbulent viscosity as follows:

$$\mu_t=\rho.\frac{k}{\omega} \qquad \text{(II.26)}$$

According to SimScale documentation [17],the real difference between ($k-\varepsilon$)and ($k-\omega$) models is the empirical coefficients appearing in the equations ($\sigma_k, \sigma_\varepsilon, \beta$...)

The relation between dissipation rate (ε) and specific dissipation rate (ω)is given by:

$$\varepsilon = C_{\mu}.k.\omega \tag{II.27}$$

The $k-\omega$ model uses empirically derived constants, which are in ANSYS CFX[15] :

Table II. 2 : $k-\omega$ model constansts [15]

Constant	C_{μ}	α_1	β_1	σ_k	σ_{ω}
Value	0.09	5/9	0.075	2.0	2.0

Various versions of the k-omega model are available, including Standard k-omega, k-omega BSL, k-omega SST, and others. Each incorporates specific adjustments to enhance performance in particular fluid flow scenarios.

Since the k-omega BSL is used to get the shear stress transport model, we are going to do a brief presentation of it :

$k-\omega$ **BSL (baseline) model:**

This turbulence model combines linearly the equations of the two previous modelssuchas:

Wilcox model [14]:

$$\frac{\partial(\bar{\rho}k)}{\partial t} + \frac{\partial}{\partial x_j}(\bar{\rho}.u_j.k) = \frac{\partial}{\partial x_j}\left[\left(\mu + \frac{\mu_T}{\sigma_{k1}}\right).\frac{\partial k}{\partial x_j}\right] + P_k - \beta.\bar{\rho}.k \tag{II.28}$$

$$\frac{\partial(\bar{\rho}.\omega)}{\partial t} + \frac{\partial}{\partial x_j}(\bar{\rho}.u_j.\omega) = \frac{\partial}{\partial x_j}\left[\left(\mu + \frac{\mu_T}{\sigma_{\omega 1}}\right)\frac{\partial \omega}{\partial x_j}\right] + \alpha_1.\frac{\omega}{k}.P_k - \beta_1.\bar{\rho}.\omega^2 \tag{II.29}$$

The BSL (Baseline) turbulence model combines the advantages of both models but still fails to correctly predict the start and quantity separation of smooth surface flow. and to get this model, the part of $k-\omega$ is multiplied by F_1 and the part of $k-\varepsilon$ is multiplied by $(1-F_1)$:

$$\frac{\partial(\bar{\rho}.k)}{\partial t} + \frac{\partial}{\partial x_j}(\bar{\rho}.u_j.k) = \frac{\partial}{\partial x_j}\left[\left(\mu + \frac{\mu_T}{\sigma_{k3}}\right).\frac{\partial k}{\partial x_j}\right] + P_k - \beta^{\backslash}.\bar{\rho}.k.\omega \tag{II.30}$$

$$\frac{\partial(\bar{\rho}.\omega)}{\partial t} + \frac{\partial}{\partial x_j}(\bar{\rho}.u_j.\omega) = \frac{\partial}{\partial x_j}\left[\left(\mu + \frac{\mu_T}{\sigma_{\omega 3}}\right).\frac{\partial k}{\partial x_j}\right] + (1-F_1).2\,.\frac{\bar{\rho}}{\sigma_{\omega 2}.\omega}.\frac{\partial k \partial \omega}{\partial x_j^{\,2}} + \alpha_3.\frac{\omega}{k}.P_k - \beta_3\,.\bar{\rho}.\omega^2 \tag{II.31}$$

Where:

F_1 Is the mixing function :

$$F_1 = \tanh(\arg_1^4) \quad \text{(II.32)}$$

$$\arg_1 = \min\left[\max\left(\frac{\sqrt{k}}{\beta^{\backslash}.\omega.y};\frac{500.v}{\omega.y^2}\right);\frac{4.\rho.k}{CD_{k\omega}.\sigma_{\omega 2}.y^2}\right] \quad \text{(II.33)}$$

$$CD_{k\omega} = \max\left(2.\rho.\frac{1}{\sigma_{\omega 2}.\omega}.\frac{\partial k \partial \omega}{\partial x_j^{\ 2}}.10^{-10}\right) \quad \text{(II.34)}$$

The model uses empirically derived constants, which are in ANSYS CFX[15] :

Table II. 3 :BSL model constants [15]

Constant	$\beta^{\backslash}$	α_1	β_1	σ_{k2}	$\sigma_{\omega 2}$	σ_{k1}	$\sigma_{\omega 1}$	α_2	β_2
Value	0.09	5/9	0.075	1	1/0.856	2.0	2.0	0.44	0.828

Advantages:

- The $k-\omega$ model performs well in the near-wall region without requiring additional damping functions. Making it suitable for flows with complex boundary layers.
- It handles adverse pressure gradients more accurately than the $k-\varepsilon$

Note:

The model provides a good prediction of boundary layer separation and reattachment. Indeed, it uses the near-wall law, which requires a very fine mesh size near the wall with $y^+ \prec 2$.

- $k-\omega$ **SST (Shear Stress Transport) model:**

The two models of turbulence Baseline ($k-\omega$) BSL and SST are identical, but themodelSST proposes a new expression of the kinematic viscosity of turbulenceto better predict the detachment.

The SST turbulence model, derived from the Baseline (BSL) model, was developed by Menter in 1994[18] by combining the advantages of the $k-\omega$ and $k-\varepsilon$ models. This hybrid version, the SST model, is more versatile as it utilises the $k-\omega$ formulation in the boundary layer and wake and the $k-\varepsilon$ formulation in free-stream regions away from the wall.

The two functions are combined through the blending function. F_2 given by[17] :

$$S.S.T = F_2(k-\omega)+(1-F_2)(k-\varepsilon) \tag{II.35}$$

Where:

Near the wall, $F_2 = 1$ ($k-\omega$ model)

Away from the wall, $F_2 = 0$ ($k-\varepsilon$ model)

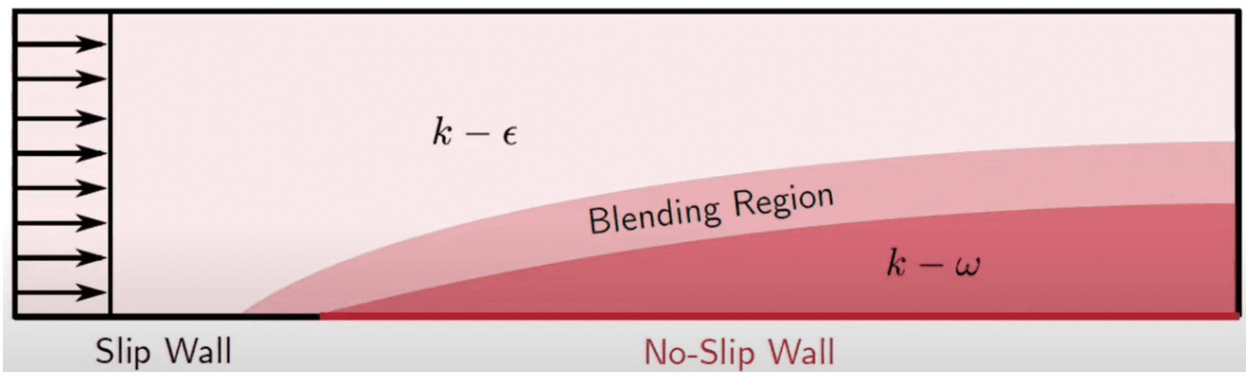

Figure II. 2: presentation scheme of SST model [17]

The transport equations:

- Turbulent kinetic energy:

$$\frac{\partial(\bar{\rho}.k)}{\partial t}+\frac{\partial}{\partial x_j}(\bar{\rho}.u_j.k)=\frac{\partial}{\partial x_j}\left[\left(\mu+\frac{\mu_T}{\sigma_{k3}}\right).\frac{\partial k}{\partial x_j}\right]+P_k-\beta^{\backslash}.\bar{\rho}.k.\omega \tag{II.36}$$

- Turbulence frequency :

$$\frac{\partial(\bar{\rho}.\omega)}{\partial t}+\frac{\partial}{\partial x_j}(\bar{\rho}.u_j.\omega)=\frac{\partial}{\partial x_j}\left[\left(\mu+\frac{\mu_T}{\sigma_{\omega 3}}\right).\frac{\partial k}{\partial x_j}\right]+(1-F_2).2\,.\frac{\bar{\rho}}{\sigma_{\omega 2}.\omega}.\frac{\partial k\partial\omega}{\partial x_j{}^2}$$
$$+\alpha_3.\frac{\omega}{k}.P_k-\beta_3\,.\bar{\rho}.\omega^2 \tag{II.37}$$

Note:

The constants used by the SST model are determined in the same way as those in the BSL model (see table II.3).

The model SST uses a limitation of the maximum turbulent viscosity value given by:

$$v_t=\frac{\mu_t}{\rho}=\frac{a_1.k}{\max(a_1.\omega\ ,\ S.F_2)} \tag{II.38}$$

$$F_2=\tanh(\arg_2^2) \tag{II.39}$$

$$arg_2 = \max\left(2.\frac{\sqrt{k}}{0.09.\omega.y}, \frac{500}{y^2.\omega}\right) \tag{II.40}$$

Where:

S: It is a function of the level of stress.

$$S = \sqrt{2.S_{ij}.S_{ji}} \tag{II.41}$$

II.3.5. The criteria for selecting a turbulence model:

- Flow characteristics.
- Accuracy requirements.
- Computational resources.
- Simulation objectives.
- Software capabilities.

II.4. Boundry layer thickness estimation and y+ :

In computational fluid dynamics (CFD), accurately resolving the boundary layer is crucial for predicting the behavior of turbulent flows near walls. The boundary layer is the thin region adjacent to the wall where viscous effects are significant, and its accurate simulation is essential for predicting drag, heat transfer, and other phenomena.

II.4.1. Boundry layer thickness estimation:

The boundary layer thickness (δ)can be estimated using various methods, depending on the flow conditions and the desired accuracy. For turbulent flows, the empirical correlation for a flat plate is often used:

$$\delta = \frac{0.37x}{\mathrm{Re}_x^{1/5}} \tag{II.42}$$

Where

x : The distance from the leading edge.

II.4.2. y+ estimation:

Based on the ANSYS CFX software, the estimates will be derived from correlations for a plate with a given Reynolds number:

$$R_{eL} = \frac{\rho.u_\infty.L}{\mu} \tag{II.43}$$

Where

$u_\infty = caracteristic\, velocity\, of\ the\ flow.$

The definition of (y+)for this estimation is:

$$\Delta y^+ = \frac{\Delta y.\mu_\tau}{\nu} \tag{II.44}$$

Where

Δy : is the distance between the wall and the first node of the mesh

The shear stress is defined by:

$$c_f = 2.\left(\frac{u_\tau}{u_\infty}\right)^2 \tag{II.45}$$

The equation (II.44)can be written as follows:

$$\Delta y = L.\Delta y^+.\sqrt{80}.R_{ex}^{1/14}.\frac{1}{R_{eL}} \tag{II.46}$$

To simplify the equation, we have :

$$R_{ex} = C.R_{eL}\text{, and } C^{1/14} \approx 1$$

So the equation (II.46) becomes:

$$\Delta y = L.\Delta y^+.\sqrt{80}.R_{eL}^{-13/14} \tag{II.47}$$

II.5. Boundary conditions :

There are several types of boundary conditions; the conditions we are going to use in this study are :

- Total pressure at the Inlet:

$$P_t = P_s.(1+\frac{\gamma-1}{2}.M^2)^{\gamma/\gamma-1} \tag{II.48}$$

- Total temperature at the inlet:

$$T_t = T_s.(1+\frac{\gamma-1}{2}M^2) \tag{II.49}$$

- Turbulence model (k –ε ; k –ω ,SST).
- Rotation speed N.
- Static pressure at the outlet.

II.6. Numerical approach :

The Finite Volume Method (FVM) is a powerful numerical approach used to solve partial differential equations, particularly those governing fluid dynamics, such as the Navier-Stokes equations. This method is widely used in computational fluid dynamics (CFD) because it is flexible in handling complex geometries and ensuring the conservation of physical quantities.

We will do a brief presentation about the Finite Volume Method and the detailed process is explained in the Finite Volume Method book [19].

II.6.1. Governing Equations:

The FVM starts by deriving governing equations in conservative form, using density-weighted averaging coupled with time averaging of RANS (Reynolds-averaged Navier-Stokes equations)[19]

The conservative form of the Navier-Stokes equations in the Finite Volume Method (FVM) is expressed by integrating the governing equations over a control volume and applying the divergence theorem to convert volume integrals into surface integrals. This approach ensures the conservation of mass, momentum, and energy within each control volume. The conservative form emphasises fluxes of conserved quantities across the boundaries of control volumes.

- **The continuity equation:**

$$\frac{\partial(\rho)}{\partial t}+\frac{\partial(\rho.u_j)}{\partial x_j}=0 \tag{II.50}$$

- **The Momentum Conservation Equation:**

$$\frac{\partial(\rho.u_i)}{\partial t}+\frac{\partial(\rho.u_i.u_j)}{\partial x_j}=-\frac{\partial p}{\partial x_i}+\frac{\partial \tau_{ij}}{\partial x_j}+S_u \tag{II.51}$$

- **The global equation:**

$$\underbrace{\frac{\partial(\rho.\phi_i)}{\partial t}}_{1}+\underbrace{\frac{\partial(\rho.u_j.\phi_i)}{\partial x_j}}_{2}=\underbrace{-\frac{\partial}{\partial x_j}(\Gamma_{eff}.(\frac{\partial \phi_i}{\partial x_j}))}_{3}+\underbrace{S_\phi}_{4} \tag{II.52}$$

Where:

1: the transient term

2: the convective term

3: the diffusive term

4: the source term

ϕ : Any scalar quantity (variable).

Γ_{eff} :Diffusion coefficient of the quantity ϕ to be transported.

These equations are integrated over each control volume. To transform some volume integrals into surface integrals, Gauss's divergence theorem is applied as follows:

$$\int_V \frac{\partial B_j}{\partial x_j} dV = \int_A B_j . n_j . dA \tag{II.53}$$

Where:

B_j : *an arbitrary vector*.

n_j : It's a unit vector on the surface A surrounding the control volume V

This theorem converts the volume integrals of divergence terms into surface integrals of fluxes across the control volume boundaries.

Now our governing equations will be as follows:

- **The continuity equation:**

$$\frac{d}{dt}\int_V \rho.dv + \int_A \rho.u_j.n_j.dA = 0 \tag{II.54}$$

- **The Momentum Conservation Equation:**

$$\frac{d}{dt}\int_V \rho.u_i.dv + \int_A \rho.u_j.u_i.n_j.dA = \int_A p.n_j.dA + \int_A \mu_{eff}.\left(\frac{\partial u_j}{\partial x_i} + \frac{\partial u_i}{\partial x_j}\right).n_j.dA + \int_V S_{ui}.dv \tag{II.55}$$

- **The global equation:**

$$\frac{d}{dt}\int_V \rho.\phi.dv + \int_A \rho.u_j.\phi.n_j.dA = \int_A \Gamma_{eff}.\left(\frac{\partial \phi}{\partial x_j}\right).n_j.dA + \int_V S_\phi.dv \tag{II.56}$$

Where :

V and A are control volume and the specific surfaces where integration is performed to measure various physical properties.

II.6.2. Discretized Form:

- **The continuity equation:**

$$\frac{V}{\Delta t}(\rho-\rho^{0})+\sum_{ip}(\rho.u_{j}.n_{j}.A)_{ip}=0 \tag{II.57}$$

- **The Momentum Conservation Equation:**

$$\frac{V}{\Delta t}(\rho.u_{i}-\rho^{0}.u_{i})+\sum_{ip}(\rho.u_{j}.u_{i}.n_{j}.A)_{ip}=\sum_{ip}(p.n_{j}.A)_{ip}+\sum_{ip}\left(\mu_{eff}\cdot\left(\frac{\partial u_{i}}{\partial x_{j}}+\frac{\partial u_{j}}{\partial x_{i}}\right).n_{j}.\right)_{ip}+\overline{S_{ui}}V \tag{II.58}$$

- **The global equation:**

$$\frac{V}{\Delta t}(\rho.\phi-\rho^{0}.\phi^{0})+\sum_{ip}(\rho.u_{j}.\phi.n_{j}.A)_{ip}=\sum_{ip}(\Gamma_{eff}\cdot\left(\frac{\partial \phi}{\partial x_{j}}\right).n_{j}.A)_{ip}+\overline{S_{\phi}}V \tag{II.59}$$

Where:

Δt :is the time step.

ip: indicates the evolution in an integration point, as shown in Figure II.3.

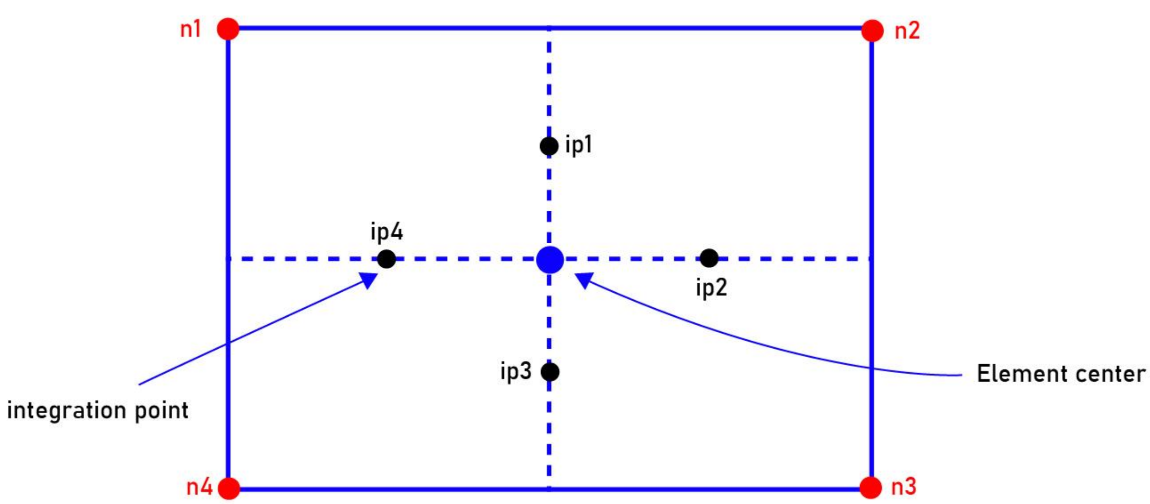

Figure II. 3: The integration points in control volume element

Chapter 03

Simulation Workflow

III.1. Introduction:

With the rapid evolution of numerical simulation tools and computational power, many codes like ANSYS CFX, GAMBIT, FLUENT, SIMSCALE, and NUMECA have emerged, revolutionizing the resolution of intricate fluid mechanics problems. These advancements, coupled with the recent strides in computational capabilities and numerical methods, have paved the way for detailed three-dimensional simulations. As a result, Computational Fluid Dynamics (CFD) has become an indispensable tool for industrial development and optimization, underscoring the significance of understanding the CFD simulation process.

This chapter covers simulation steps from geometry creation and mesh generation to simulation setup.The CFD solver employed in this study is ANSYS CFX integrated within the ANSYS software package, which is used to solve theunsteady, compressible, Reynolds-averaged, Navier-Stokes equations on structured grids by a finite volume approach. The flow governing equations are enclosed with Shear Stress Transport (SST), a two-equation turbulence model.

III.2. CFD simulation process:

Every Computational Fluid Dynamics (CFD) simulation involves three basic steps to analyse and predict the behaviour of fluid flows:

- Pre-processing
- Processing
- Post-processing

III.2.1. Pre-processing:

Pre-processing within the CFD software workflow encompasses several essential tasks. It begins with modelling the geometry and the flow domain, followed by mesh generation that discretises the geometry into computational elements. Pre-processing also involves specifying the material properties relevant to the fluid being simulated, then defining boundary conditions to constrain the flow behaviour within the computational domain and the initial conditions to start the simulation.

III.2.2. Processing:

The processing step involves defining the numerical parameters, such as configuring solver settings, reference state, physical model inputs, and discretisation methods. Each simulation type presents its distinct framework. Typically, a single problem can be tackled using various solvers and different solver parameters. Nonetheless, ensuring the accurate specification of solver parameters and numerical schemes is crucial for effectively resolving the problem.

III.2.3. Post-processing:

Interpreting the results is crucial in any numerical simulation, whichis accomplished during post-processing. Various tools, such as streamline and contour plots, are employed to examine the flow fields. Post-processing represents the CFD workflow's concluding phase, allowing the opportunity to visualise simulation results comprehensively and derive insights crucial for design optimisation decisions.

III.2.4. Simulation assumptions:

In this study of the flow through a centrifugal compressor, we assume that the flow regime is steady and compressible, occurring in a three-dimensional space. The fluid's thermodynamic propertiesshould align with an ideal gas's. Furthermore, the heat source term is considered zero, and external body forces are negligible.

III.3. Compressor Geometry and Specifications:

The experimental investigations were carried out on a radial compressor with a "backward curved" blade impeller followed downstream by a "channel" slatted diffuser, for which a test case is available, named Radiver (see Figure III.1), described by Ziegler et al. [1], [2].

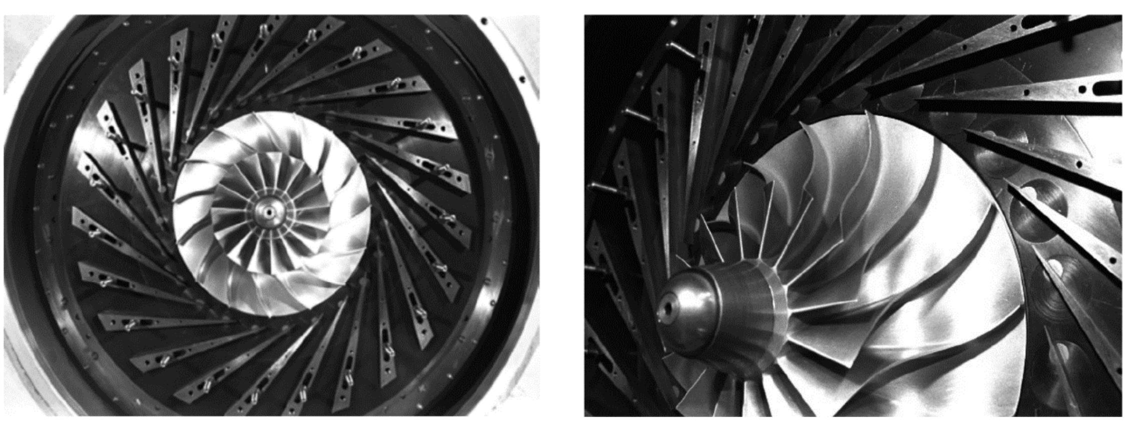

Figure III. 1 : Centrifugal compressor stage - front wall removed [1]

III.3.1. Dimensional specifications:

The stage features an unshrouded impeller with 15 backswept blades (angled at 38 degrees from the radial direction) and a diffuser with 23 wedge vanes. The suction pipe design and inlet contour, along with the absence of inlet guide vanes, ensure axial flow at the impeller inlet. The aerodynamic design of the wedge vaned diffuser is based on the characteristic parameters for flat diffusers (Runstadler et al., 1975). The diffuser's construction allows for independent continuous adjustment of the diffuser vane angle, indicated by the vane suction side angle (α_{SS}), and the radial gap between the impeller outlet and the diffuser vane inlet, shown by the radius ratio (r4/r2) (Figure III.2).The dimensional specifications for the stage at nominal speed and with the reference diffuser geometry are given in Table III.1. [1]

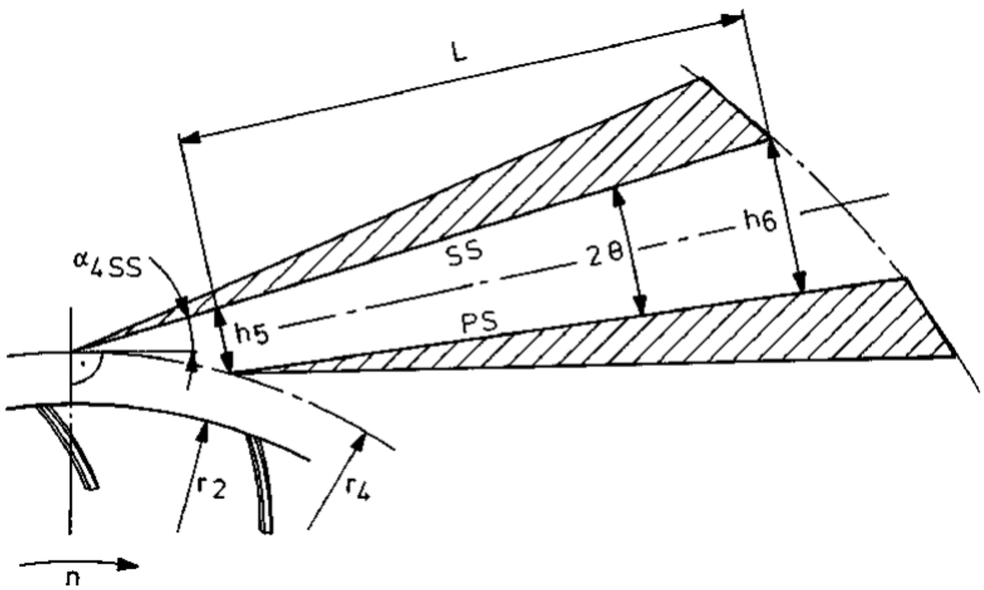

Figure III. 2 : Geometric parameters α4SS and r4/r2

Table III. 1 : Technical data of the basic configuration

Compressor:
- Rotation speed $N_0 = 35200 \;\; 1/\min$
- Impeller tip speed $u_2 = 498 \;\; m/s$
- Relative tip mach number impeller inlet $Ma_{W1} = 0.95$
- Absolute Mach number impeller exit $Ma_2 = 0.94$
- Maximum total pressure ratio $\pi_{t,\max} = 4.07$
- Maximum corrected mass flow $\dot{m}_{red,\max} = 2.50 \;\; kg/s$
- Maximum isentropic efficiency $\eta_{is,\max} = 83.4\%$
- Specific speed $N_s = 89 \;\; \mathrm{rpm}(\mathrm{ft}^3/s)^{1/2}/\mathrm{ft}^{3/4}$
Impeller:
- Tip radius $r_2 = 135 \;\; mm$
- Number of blades $Z_I = 15$
- Blade backsweep angle at impeller exit $\beta_b = 38^\circ$
Diffuser:
- Constant meridional diffuser height b=11.1 mm
- Number of vanes $z_D = 23$
- Vane angle $\alpha_{4SS} = 16.5°$
- Radial gap $r_4/r_2 = 1.10$
- Thickness of angular leading edge $AS = b/h_5 = 0.68$
- Vane wedge angle $\alpha_V = 6.615°$
- Length of vane pressure side $l_{PS} = 178 \;\; mm$
- Length of vane suction side $l_{PS} = 190 \;\; mm$
- Invariant diffuser channel divergence angle $2\theta = 9.037°$
- Diffuser channel length-width ratio $LWR = L/h_5 = 9.31$
- Diffuser channel area ratio $AR = h_6/h_5 = 2.47$
- Diffuser channel aspect ratio $AS = b/h_5 = 0.68$

III.3.2. Measurement planes:

The measurement planes are indispensable for comprehensively analysing the centrifugal compressor's performance, enabling precise control over its design, optimisation, and operational efficiency.

The different planesare shownin Figures III.3 and III.4:

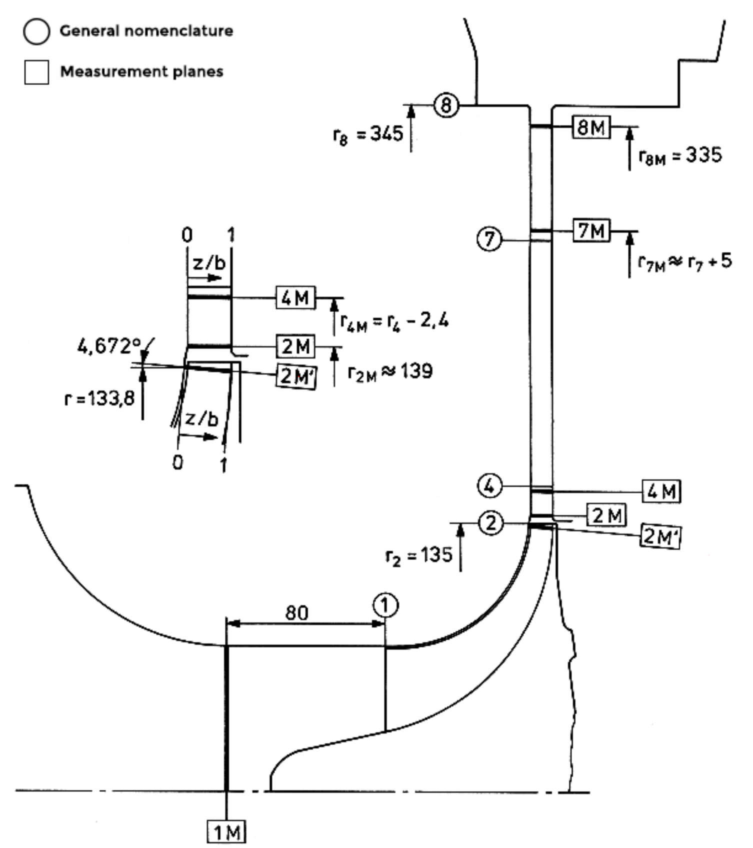

Figure III. 3 : Measurment planes in meridional view [1]

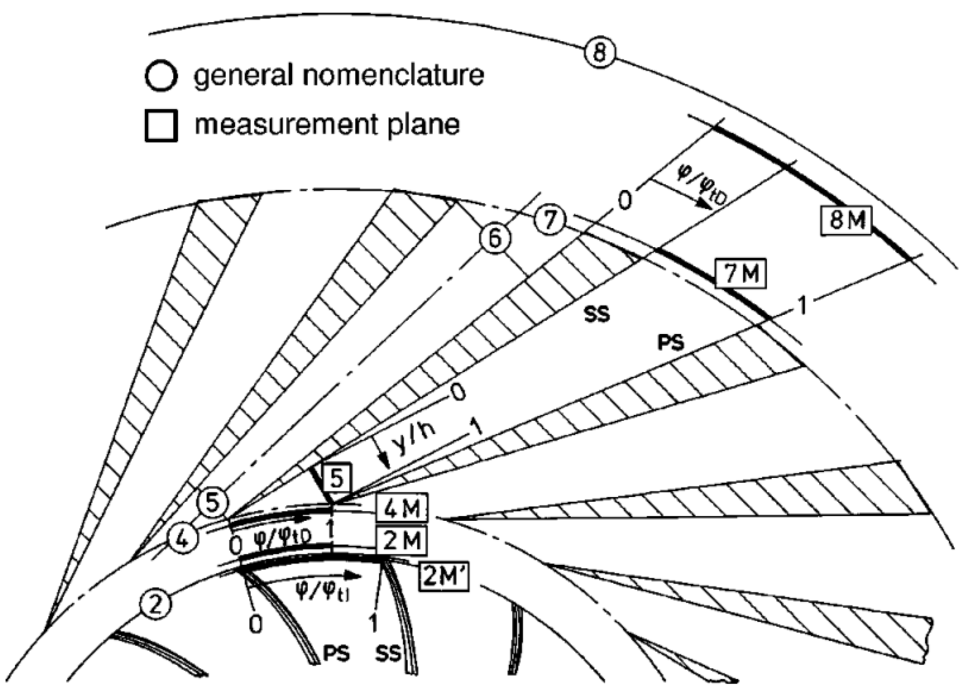

Figure III. 4 : Measurment planes in blade to blade view [1]

- **Inlet Flow Characterization (Plane 1M):**

It provides baseline data on the incoming fluid (Velocity, pressure, temperature, and flow rate), which can influence the performance of the entire compressor.

- **Pre-Impeller Flow Analysis (Planes 2M and 2M'):**
  Measuring the flow properties just before the impeller helps assess the uniformity and stability of the flow entering the impeller.
- **Impeller Exit Flow Analysis (Planes 4M and 4M'):**
  These planes helpanalyse energy transfer efficiency from the impeller to the fluid and identify losses or flow separations.
- **Diffuser Performance Evaluation (Plane 7M):**
  This plane provides information about the performance of the diffuser section, which is responsible for converting the kinetic energy of the fluid into pressure.
- **Compressor Exit Flow Analysis (Plane 8M):**
  The final measurement plane at the compressor outlet is essential for assessing the overall performance of the compressor. It helps determine if the compressor delivers the desired pressure and flow rate.

III.4. Software presentation:

We have mentioned before that we will use the ANSYS CFX solver for this study. This high-performance computational fluid dynamics (CFD) software tool provides robust solutions for complex fluid flow problems. Widely used across various industries, ANSYS CFX excels in simulating fluid dynamics and heat transfer behaviour within and around different geometries. It integrates seamlessly with the ANSYS Workbench environment, offering a comprehensive suite for pre-processing, solving, and post-processing tasks.

Alongside with ANSYS CFX, we will have two other ANSYS modules for geometry modelling and mesh generation, which are :

- **ANSYS BladeGen:**

AnsysBladeGen is a component of AnsysBladeModeler, a specialised and user-friendly tool designed for the rapid 3D design of rotating machinery components. BladeGen enables redesigning existing blades to meet new design goals or createnew designs. It allows for the interactive or file-based import of blade geometry. BladeGen supports sculpted or ruled element blades with linear or compound lean leading or trailing edges. Additionally, it offers features such as over/under-filing and the ability to specify leading and trailing edge shapes as a full radius, an ellipse ratio, or a simple cutoff[16].

- **ANSYS TurboGrid:**

  AnsysTurboGrid is a tool that enables designers and analysts of rotating machinery to create high-quality hexahedral meshes while preserving the integrity of the underlying geometry. These precise meshes are integral to the Ansys workflow, facilitating the solution of complex blade passage problems[16].

  The Figure III.5 below represents the simulation procedure organigram:

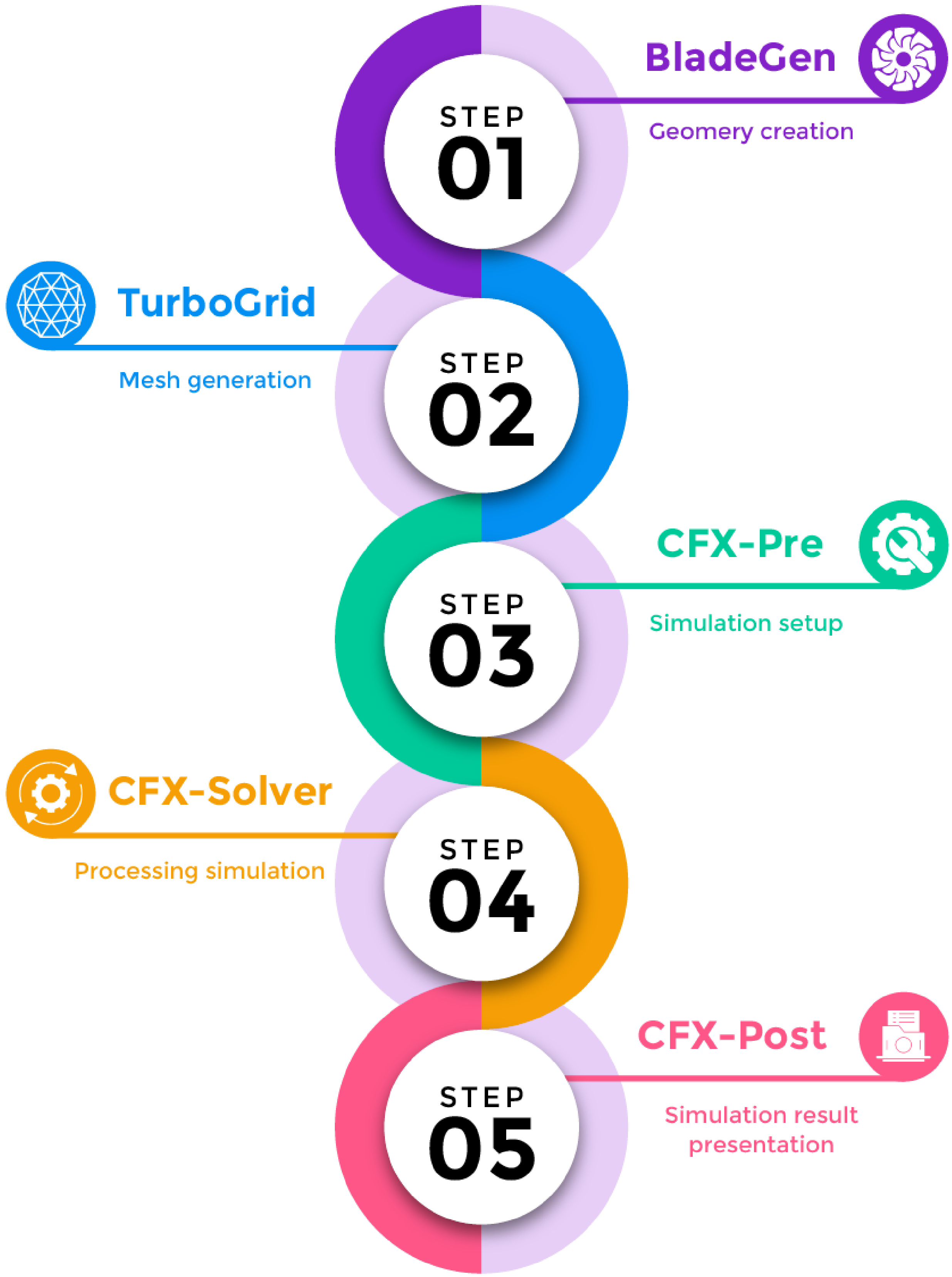

Figure III. 5 : Simulation procedure organigram

III.5. Simulation Procedure:

The centrifugal compressor with splitter bladesperforms better than a compressor without a splitter. Several researchers have investigated the impact of splitters, but in this research, we will study the effects of splitter blade length.

This simulationis divided into two parts:

- The first part focuses on mesh sensitivity and result validation to the experimental one, where we will simulate the flow through our centrifugal compressor in its original form (without splitter blades)
- In the second part, we will modify the original geometry by adding splitter blades. We will run different cases, varying the splitter blade's length each time.

III.5.1. Geometry creation:

To perform this simulation, we need to create our geometry. So, first, we will create the geometry of the centrifugal compressor without splitter blades.

BladeGen operates in two distinct modes: the Angle/Thickness (Ang/Thk) Mode and the Pressure Side/Suction Side (Prs/Sct) Mode. These modes provide the design environment for radial blades. Both modes utilise a set of Common Views, including a Meridional View and an Auxiliary View, positioned side by side at the top of the window. The Meridional View defines the blade in radial versus axial space, generating the streamlines required for all other views. The Auxiliary View displays a Blade-to-Blade View, 3D View, Meridional Contour View, and several graphs of various blade parameters, as shown in Figure III.6 And III.7.

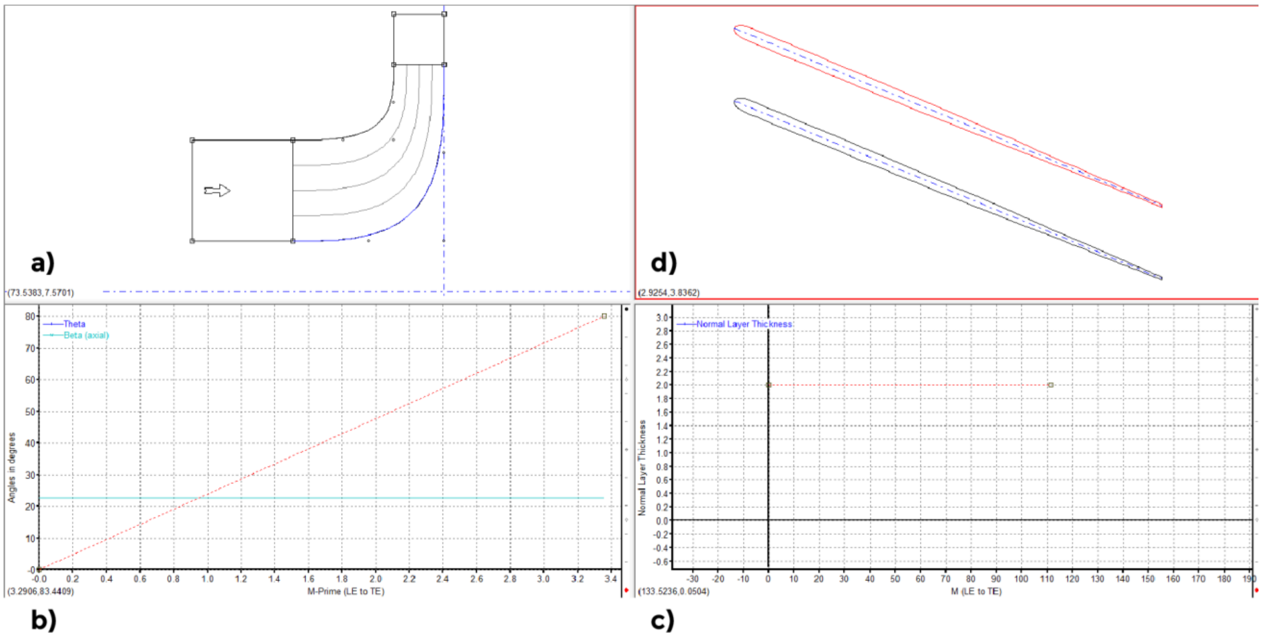

Figure III. 6: Impeller design with BladeGen

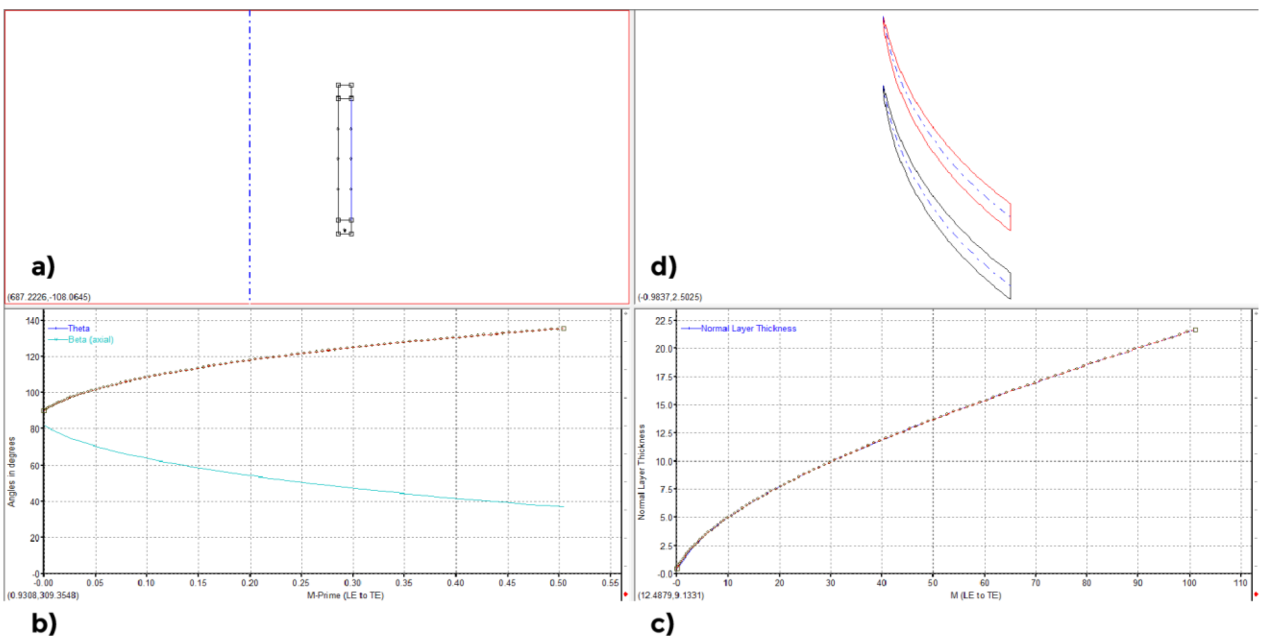

Figure III. 7 : Diffuser design with BladeGen

a) This window represents the initial step in creating the geometry. The meridian vane design follows a predefined model tailored for radial impellers. The surfaces are defined by two curves in the **(z;r)** plane, where "**z**" represents the axial direction and **"r"** represents the radial direction.

b) In the second window, we define the pitch angles β and the recovery angle Θ as functions of the meridian distance using a conformal transformation; we need to map the coordinates from the frame R(x,y,z) to a referenceframe $R(M',\theta)$.

c) This step Involves specifying the blade thickness based on the meridian distance.

d) This is the final step, where we create the geometric shape of our blades. We can also represent the overall model in 3D, as shown in figure III.8 And III.9.

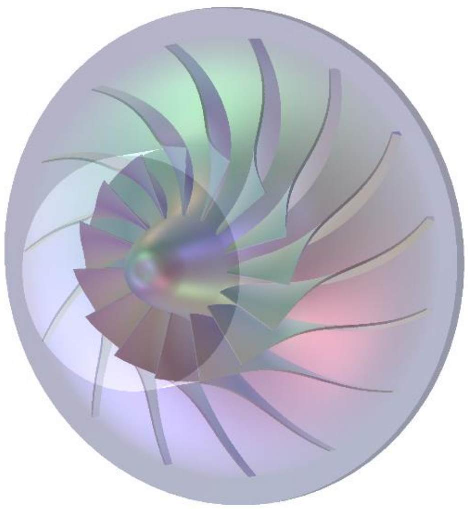

Figure III. 8 : 3D presentation for impeller

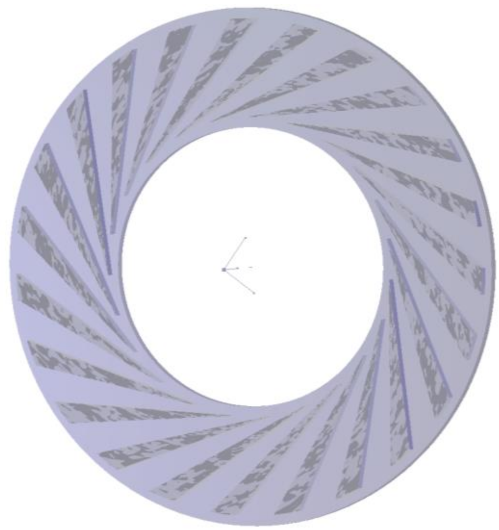

Figure III. 9 : 3D Presentation for diffuser

After creating the basic centrifugal compressor design, it is time to add splitter blades to our geometry. To do that, we need to specify two things: first, the relative circumferential position ratio. ξ and the length ratioof the splitter blade.

- **The relative circumferential position:**refers to the angular position of the splitter blade relative to the main blades; itcan be expressed by the equation(.2).
- **The length coefficient:**represents the ratio of the length of the splitter blade to the length of the main blade; its equation is given by(.1).

The two parameters are explained clearly in Figure III.10.

Additionally, the shape of the splitter blades is similar to that of the main blades.

$$\sigma = \frac{L_{2,shroud}}{L_{1,shroud}} = \frac{L_{2,hub}}{L_{1,hub}} \quad (.1)$$

$$\xi = \frac{\theta_2}{\theta_1} \quad (.2)$$

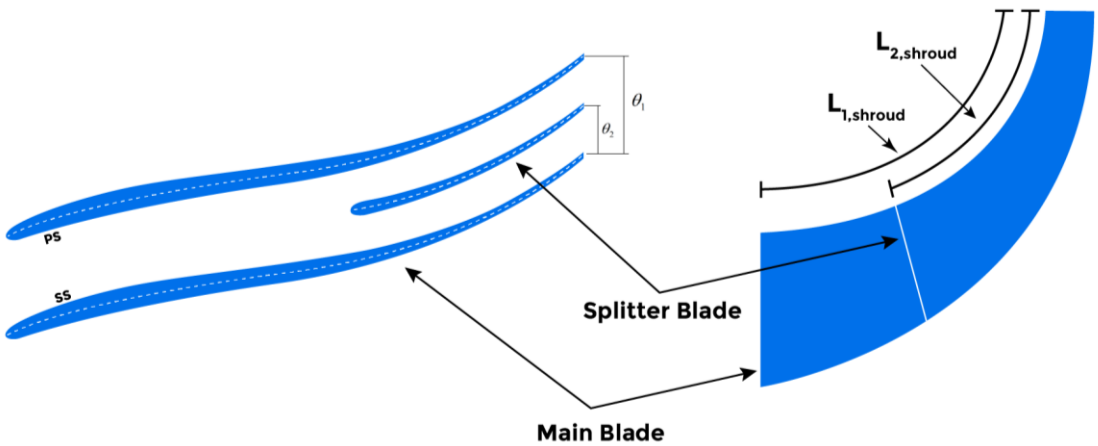

Figure III. 10 : Presentation of angular position and length of splitter blade

In this study, we examined the impact of splitter blade length on the performance of centrifugal compressors. While the circumferential position of 0.5 is chosen because it is a standard design choice,and we are focusing on the influence of splitter blade length.It's interesting to note that the optimal position may vary depending on specific design and performance requirements. To further optimise the design, I will conduct simulations across 6 cases, varying the splitter blade length from 40% to 90% of the main blade length as illustrated in Figure III.11. This extensive analysis aims to identify the most advantageous splitter blade length.

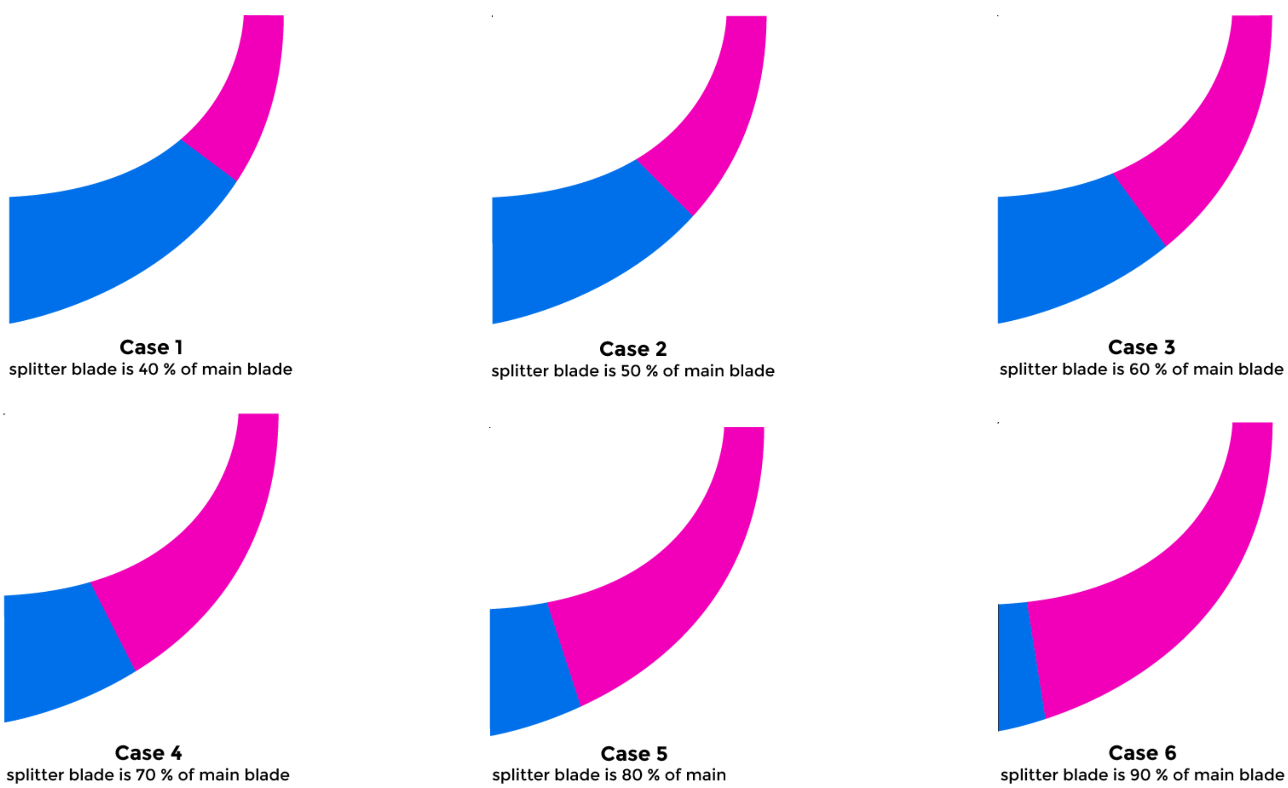

Figure III. 11: The diffrent simulation cases

III.5.2. Mesh generation:

In CFD, the physical domain is divided into small, discrete elements called a mesh. This allows the complex differential equations governing fluid flow to be approximated and solved numerically. A high-quality mesh captures the geometry accurately and ensures stable and accurate results.

It is essential to input specific parameters to initiate mesh generation in ANSYS TurboGrid. These parameters encompass the paths to the geometry files, which detail the hub, shroud, and blade designs, the chosen mesh topology, and the node distribution strategy. This information is encapsulated within a series of data structures termed 'CCL objects.' Once these CCL objects are accurately defined, a command can be executed within ANSYS TurboGrid to start the meshing process.

The generated mesh by AnsysTurboGridis shown in Figures III.12 and III.13

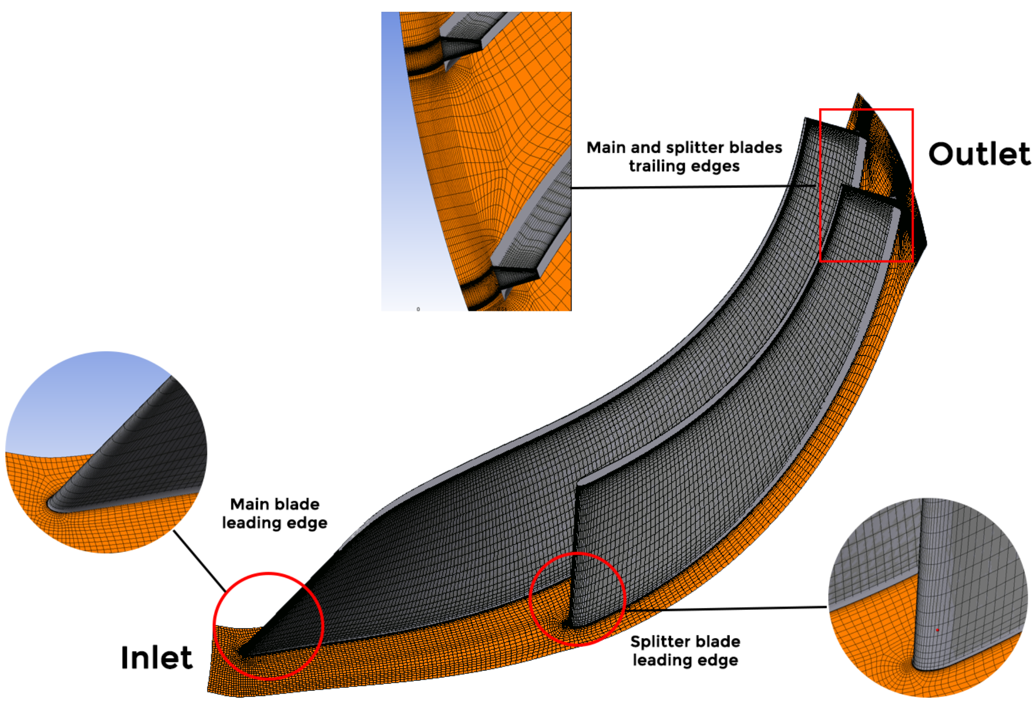

Figure III. 12 : Impeller mesh

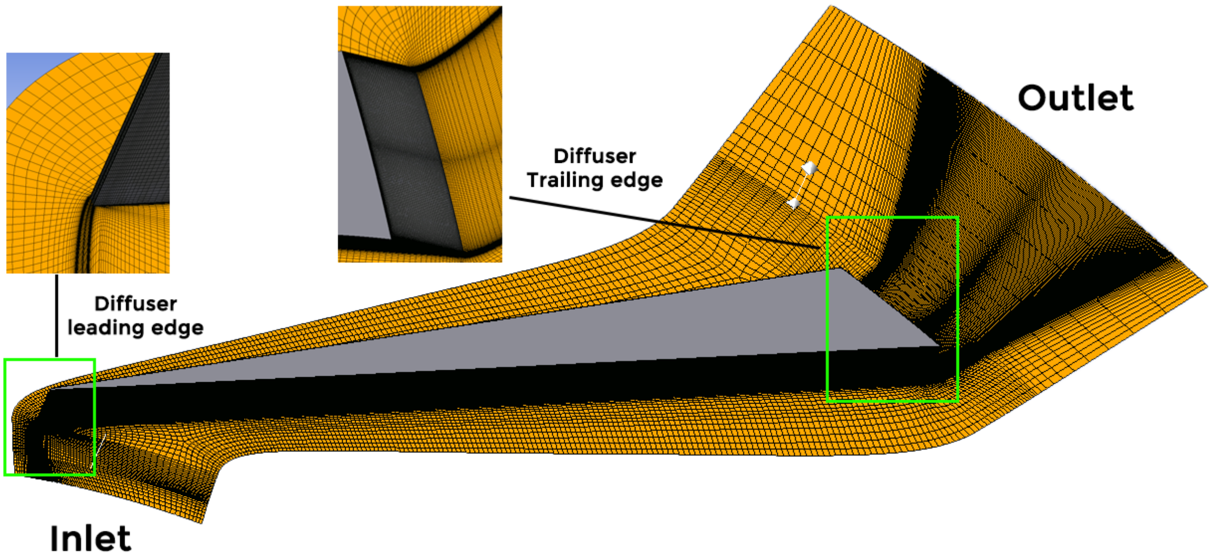

Figure III. 13 : Diffuser mesh

- **Mesh topology:**

  We used the ATM topology automatic setting toselect the appropriate topology based on the blade style (cut-off or rounded edges) and angle. In our case, the Single Splitter Method includes special topologies of the type H / J / C / L and the type 'O 'around the blade and the walls in the mesh creation see Figure III.14below:

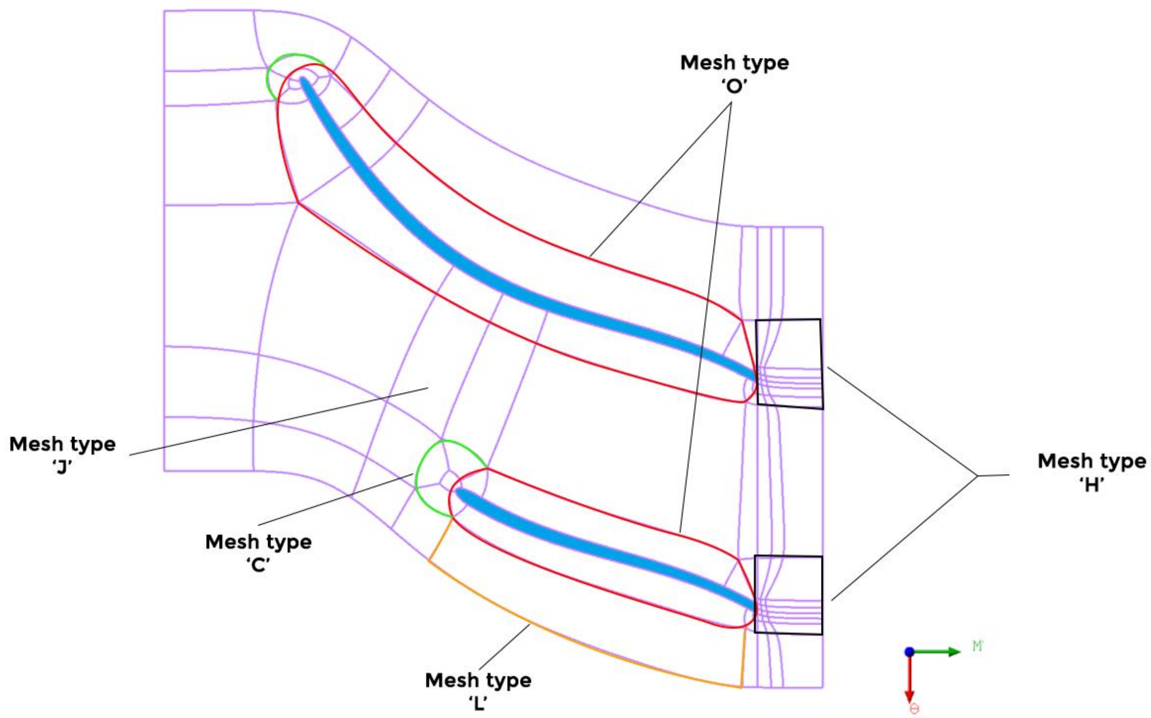

Figure III. 14 : Mesh typology

- **Mesh manipulation Data:**

  AnsysTurboGrid gives you a lot of parameters that help manipulate the mesh in a friendly user interface, as shown in Figure III.15 below:

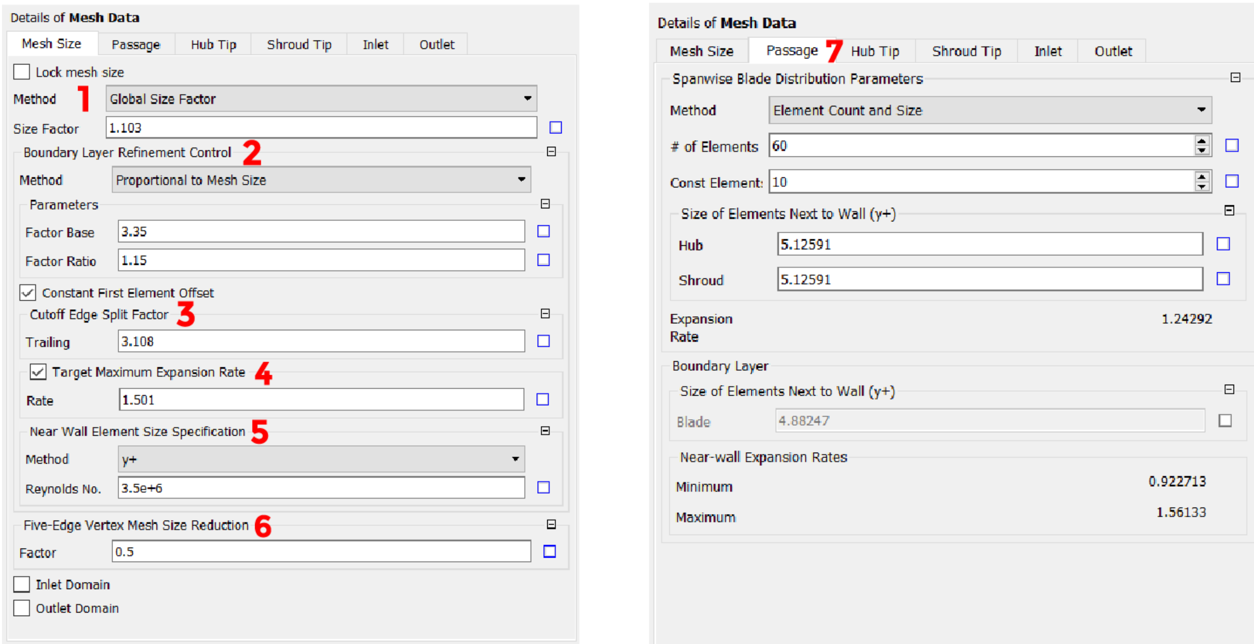

Figure III. 15 : Mesh controle parameters

- Global size factor:

AnsysTurboGrid aims to achieve the target node count by adjusting the number of elements along each topology block edge. After pressing Apply, you can view the number of elements by switching the method to Global Size Factor, which defines the overall mesh size. This increases the mesh's resolution.

When used with proportional refinement, this factor can scale the mesh size for a mesh refinement study.

- Boundary Layer Refinement Control:

The topology blocks along the blade's edges define the boundary layer region. The thickness of this boundary layer region changes around the blade profile.

The "Proportional to mesh size" option adjusts the number of elements across the boundary layer and along any cut-off edges based on the Factor Base and Factor Ratio values, ensuring consistent expansion rates even with changes to the Global Size Factor. Increasing these values adds more elements while decreasing them reduces the number of elements.

- Cutoff Edge Split Factor:

This setting is available when Constant First Element Offset is selected. It allows you to control the number of elements along each cut-off edge by specifying a factor for the leading and trailing edges.

- Target Maximum Expansion Rate:

This setting allows you to define a target maximum expansion rate. TurboGridensures that the expansion rate does not exceed the specified maximum at any location around the blade profile. Its approach varies based on the selected option under the Boundary Layer Refinement Control method.

- Near Wall Element Size Specification:

The Near Wall Element Size Specification setting determines how the spacing of nodes near the wall is specified on the Passage and Hub/Shroud Tip tabs. This spacing refers to the distance between a wall (such as a hub, shroud, or blade) and the first layer of nodes adjacent to the wall. In this setting, the Y plus method is selected.

- Five-Edge Vertex Mesh Size Reduction:

The Near Wall Element Size Specification setting determines how the spacing of nodes near the wall is specified on the Passage and Hub/Shroud Tip tabs. This spacing refers to the distance between a wall (such as a hub, shroud, or blade) and the first layer of nodes adjacent to the wall.

- Passage Tab:

The Spanwise Blade Distribution Parameters section manages the allocation of mesh elements along the blade's spanwise direction.

This was a brief presentation of these basic parameters, and all the settings are detailed in the AnsysTurboGrid user guide.

III.5.3. Mesh statistics:

The mesh quality for a turbomachine depends on the following conditions:

- Maximum face angle: This is the largest angle of all the faces touching the node, measuring distortion. Its value is 165 degrees.
- Minimum face angle: This is the smallest angle between two edges touching the node. Its value is 15 degrees.

- Connectivity number: This is the number of elements connected to a node, with a maximum value of 12 and a minimum value of 0.
- Element volume ratio: This is the ratio between the largest and smallest volumes associated with a node. This ratio is positive.
- Edge length ratio: This is the ratio of the distance of the longest edge to the shortest edge on the same face, with a maximum value of 10.
- Minimum volume: This is the positive volume of the mesh, which ensures that no negative volume exists in the fluid passage.

The Figure III.16 below are the mesh statistics and skewness parameters:

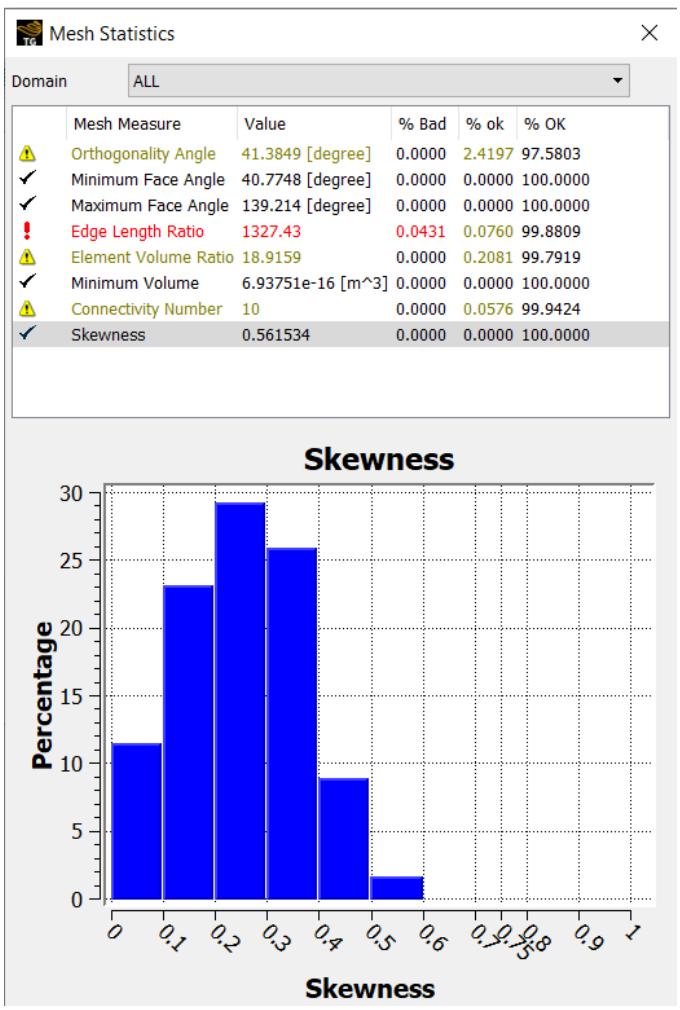

Mesh Statistics

Domain: ALL

Mesh Measure	Value	% Bad	% ok	% OK
Orthogonality Angle	41.3849 [degree]	0.0000	2.4197	97.5803
Minimum Face Angle	40.7748 [degree]	0.0000	0.0000	100.0000
Maximum Face Angle	139.214 [degree]	0.0000	0.0000	100.0000
Edge Length Ratio	1327.43	0.0431	0.0760	99.8809
Element Volume Ratio	18.9159	0.0000	0.2081	99.7919
Minimum Volume	6.93751e-16 [m^3]	0.0000	0.0000	100.0000
Connectivity Number	10	0.0000	0.0576	99.9424
Skewness	0.561534	0.0000	0.0000	100.0000

Figure III. 16: Mesh statistics

- **Skewness:**

  Refers to the distortion or non-uniformity of the elements comprising the mesh. There are two methods for determining skewness:

  - First, Equilateral Volume deviation:

$$\text{Skewness} = \frac{\text{optimal cell size - cell size}}{\text{optimal cell size}} \qquad (.3)$$

  Applies only to triangles and tetrahedrons.

  - Second,Normalized Angle deviation:

$$\text{Skewness}= \max\left[\frac{\theta_{\max}-\theta_e}{180-\theta_e}, \frac{\theta_e-\theta_{\min}}{\theta_e}\right] \qquad (.4)$$

  Where θ_e is the equiangular face/cell (60 for tets and tris, and 90 for quads and hexas)

Excellent	Very good	Good	Acceptable	Bad	Unacceptable
0-0.25	0.25-0.50	0.50-0.80	0.80-0.94	0.95-0.97	0.98-1.00

Figure III. 17: Skewness mesh metrics spectrum [16]

III.5.4. CFX Solver:

After the mesh has been generated, following the creation of the geometry, we will initiate the CFX simulation. This simulation consists of three primary steps: pre-processing, processing, and post-processing. In this part, we will discuss the first two steps, andin the next chapter, we will delve into post-processing and discuss the results in detail.

III.5.4.1. Pre-processing:

Ansys CFX-Pre has a special feature to handle turbomachine simulations called “TURBO mode.” After choosing the machine type, TURBO mode, with its simple interface, helps define each component by importing their mesh from TurboGrid and then identifying the basic parameters and physics definitions like boundary conditions (see Figure III.18) and solver parameters.

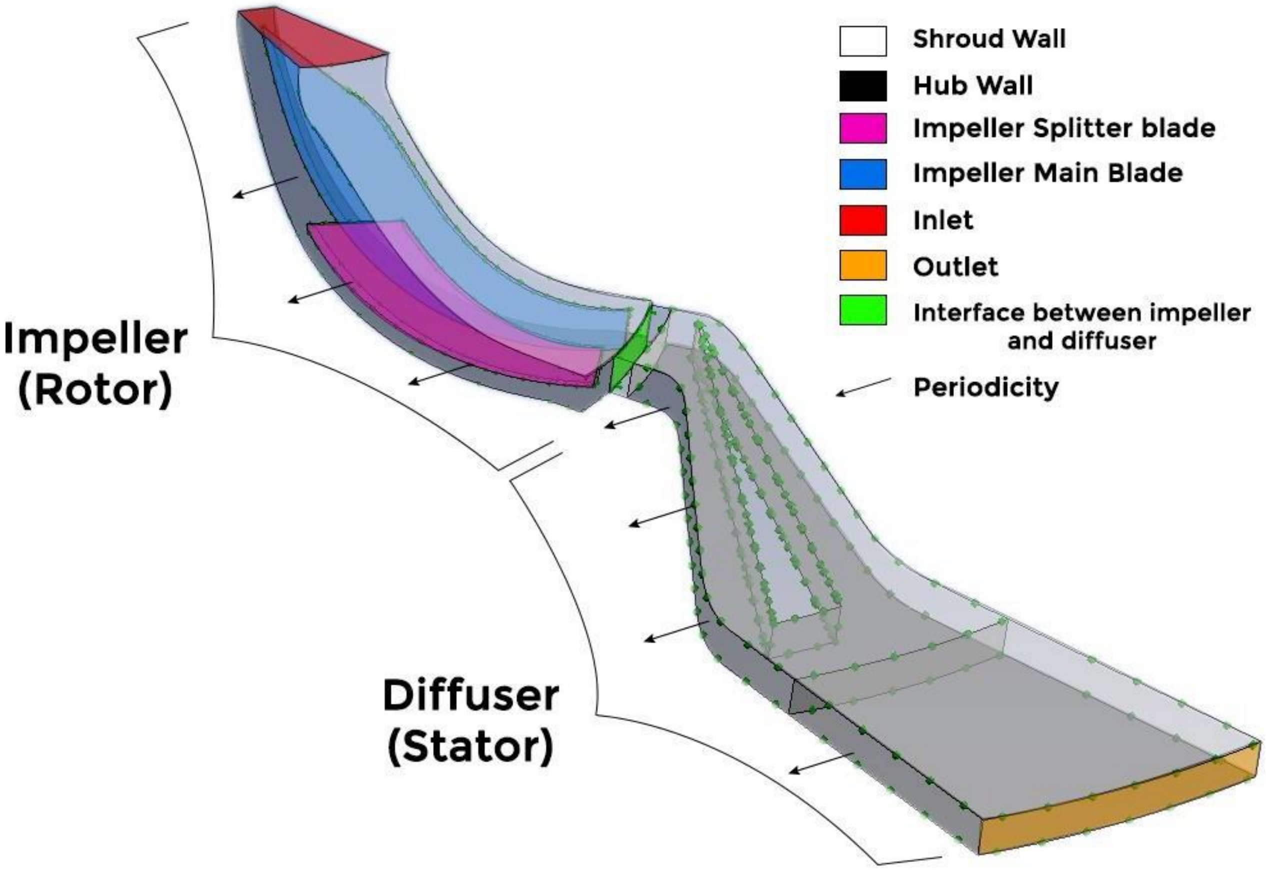

Figure III. 18 : Presentation of boundary conditions

The simulation configuration is summarised in the table below and the boundary conditions are presented in figure III.19 [1]:

Table III. 2: Simulation configuration

Basic parameters	Machine type	Centrifugal compressor
	Analysis type	Steady state
	Rotation speed	28541 rpm
	Wall configuration	Tip clearance at shroud
Physics Definition	Type of fluide	Air ideal gas
	Turbulence model	Shear stress transport (SST)
	Inlet condition	Total preassure
	Outlet condition	Static preassure
	interface	Stage (mixing-plane)
Solver control	Advection sheme	Upwind
	Max iteration	800
	Convergence crititia	(RMS) 10^{-4}

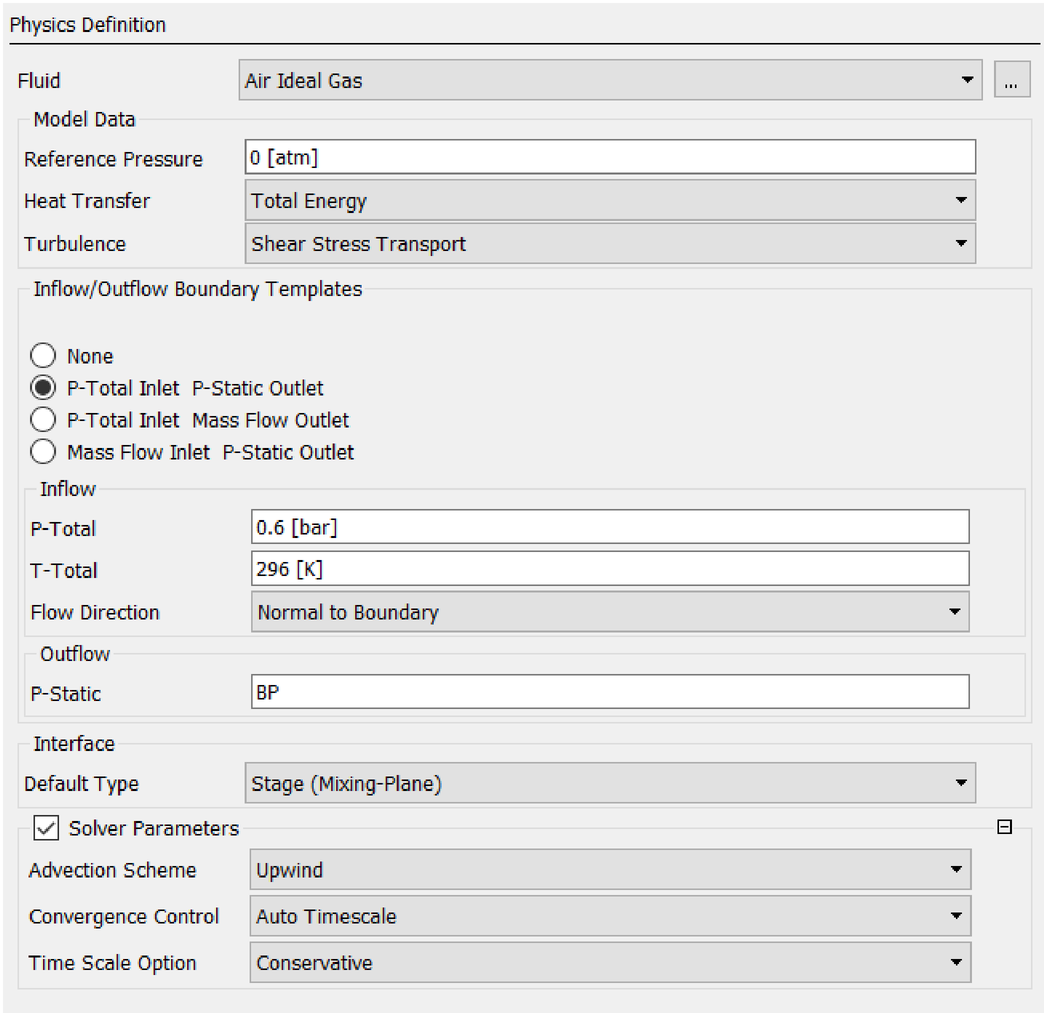

Figure III. 19: Simulartion physics definition

III.5.4.2. Processing:

In this phase, the CFX solver performs multiple iterations to obtain the results, minimizing the global residual error between consecutive iterations. The simulation time varies depending on the hardware being used.

In this study, we performed the simulation using two setups:

- Personal laptop Predator Helios 300 comes with intel core i7-10750H CPU, Nvidia RTX 2070 8 Go VRAM graphic card, and 16 Go RAM.
- The Institute of Aeronautics laboratory (numerical calculation laboratory)workstation has the following specs :
  Intel core i9-13900K CPU, Radeon RX7900X 24Go VRAM, and 128 Go RAM.

Figure III. 20:IASS laboratory workstation

Figure III. 21: Laptop Predator Helios 300

Chapter 04

Presentation and Discussion of Results

IV.1. Introduction:

In this final chapter, we present and discuss the results of the numerical simulations conducted using ANSYS CFX. The primary objective of these simulations is to analyse the influence of the splitter blade span oncentrifugal compressor performance. Key parameters such as velocity, pressure, temperature distributions, and compressor efficiency were examined in detail.

This chapter is divided into two main parts:

- Part one: Mesh sensitivity and result validation (impeller without splitter).
- Part two: Examining the performance of the impeller with different splitter blade spans (impeller with splitter).

IV.2. Mesh sensitivity and result validation:

Mesh sensitivity analysis helps us ensure the results are independent of the mesh size. By systematically refining the mesh and comparing the outcomes, we find that the finer the mesh, the more precise the result until we reach a specific mesh density. At this point,we can determine the optimal mesh configuration that balances computational cost and solution accuracy.

To validate our simulation model, we conducted a series of simulations on the impeller without splitter blades. We achieved good results using mesh 1 with 0.8 million elements and mesh 2 with 0.6 million elements. The results from these simulations were then compared with experimental data to assess the reliability and accuracy of our numerical approach (Figure IV.1).

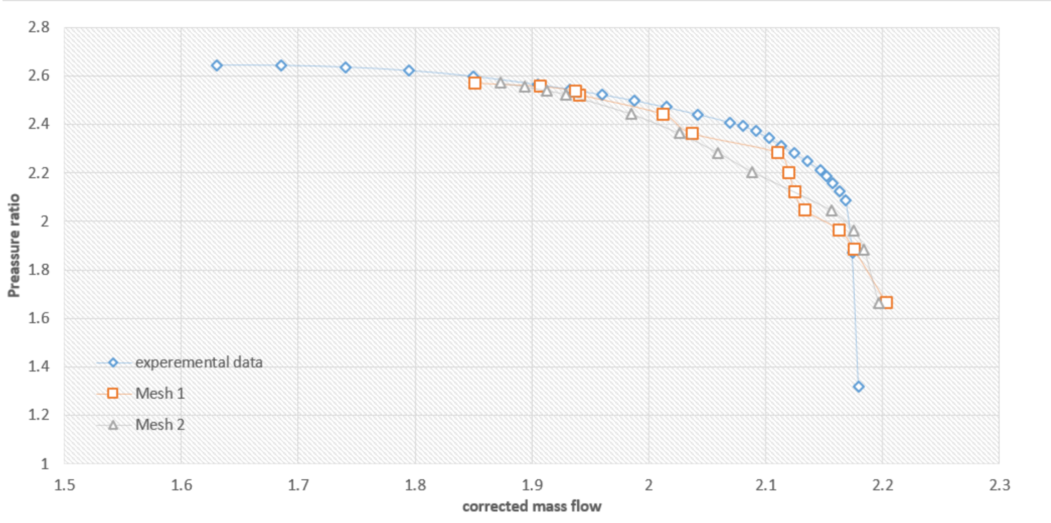

Figure IV. 1 : Mesh sensitivity

The Figure above is a graphical representation of the performance map of our centrifugal compressor as a function of the pressure ratio (P8M/P2M) and corrected mass flow. As it appears in the graph, the simulation results of both Mesh 1 and Mesh 2 are very close to experimental Data,

IV.2.1. y+ validation:

A critical aspect of mesh quality in turbulent flow simulations is the dimensionless wall distance, denoted as **y+**. Proper **y+** values ensure that the boundary layer is accurately resolved, which is essential for capturing the flow physics near the walls. To have good precision in the boundary layer while using the SST turbulence model, the y+ value has to be less than 5.The figures below, Fig IV-2 and IV-3 show that y+ is valid at the shroud and the hub of both the impeller and diffuser.

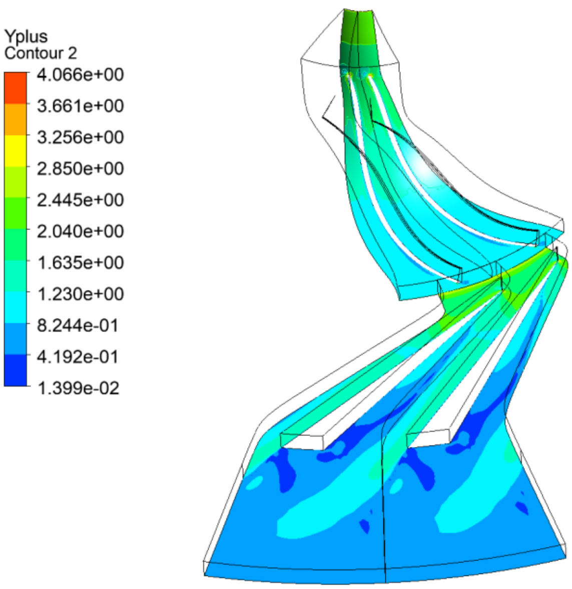

Figure IV. 2: y+ contour in the hub

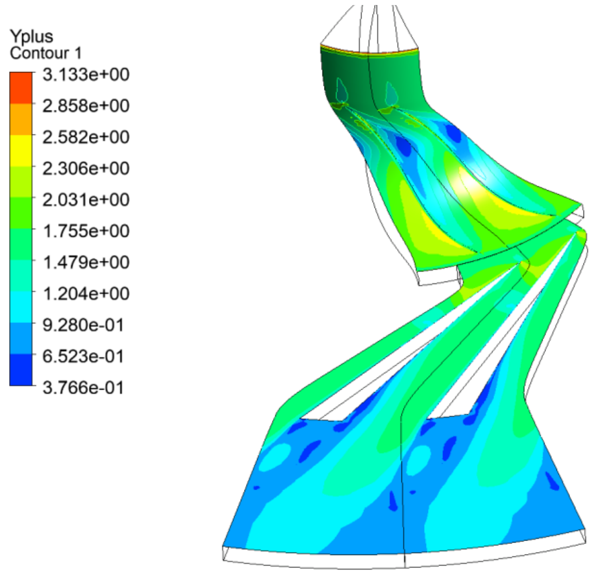

Figure IV. 3: y+ contour in the shroud

As shown below in Figure IV-4, which represents the y+ contour for the impeller and diffuser blades, the y+ value is respected on the suction and pressure sides of both the impeller and diffuser blades. However, it reaches its maximum value at the trailing edge of both blades becauseAnsysTurboGridcannot control the mesh as it should be at the trailing edge because of the cutoff type.

The simulation is unaffected by this small area since it is tiny relative to the blade.

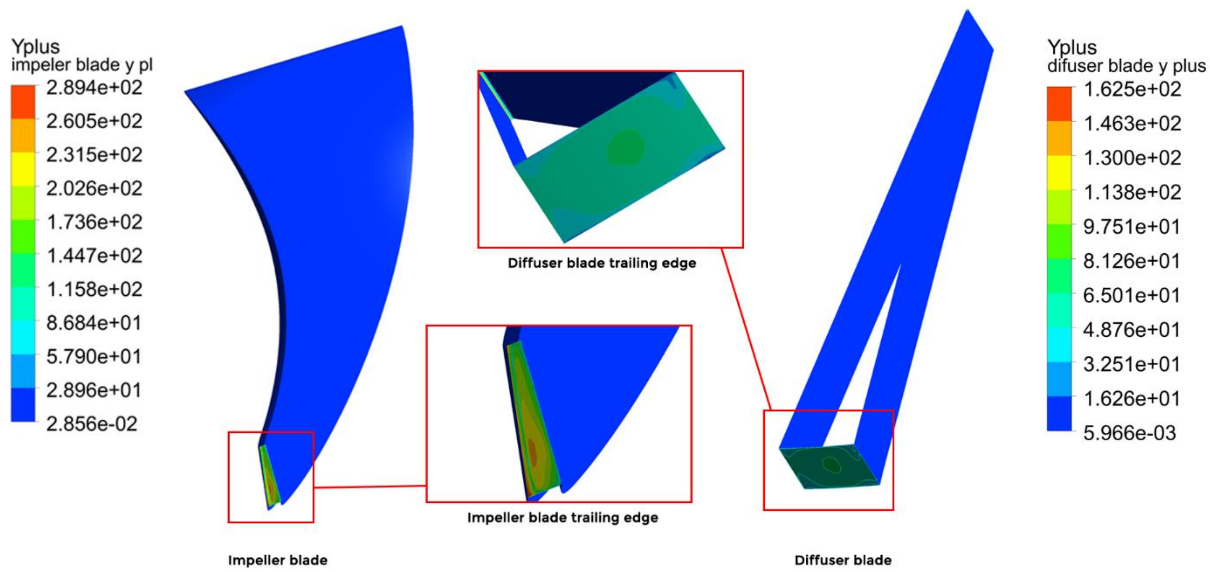

Figure IV. 4 :y+ contour of impeller and diffuser blades

IV.2.2. Result and discussion:

Using ANSYS CFX, we will present and analyse the key parameters influencing the centrifugal compressor's overall performance and flow characteristics.

Let's start with Figures IV-5 and IV-6 below, representing the distribution of static pressure in meridional and blade-to-blade planes.

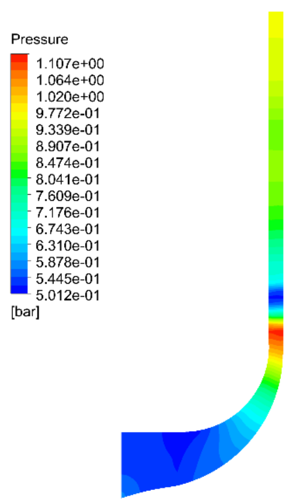

Figure IV. 5: Static pressure contour in meridional plane

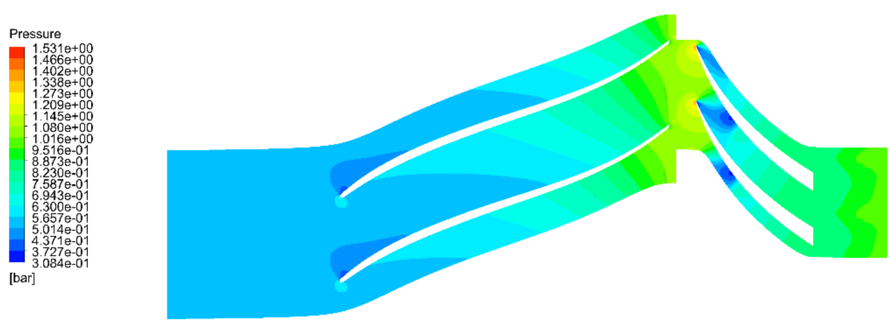

Figure IV. 6 : Static pressure contour in blade-to-blade plane

As noticed above, the static pressure increases through the impeller to the inlet of the diffuser due to the convergence of the section in the streamwise direction and of the rotating impeller.Suddenly, a pressure drop happens at the leading edge of the diffuser, and after that, pressure recovery is noticed until the outlet of the diffuser.

We can distinguish three phases in the pressure distribution chart by analysing the Mach number contour and the inlet-to-outlet pressure distribution chart (Figures IV-7 and IV-8, respectively).

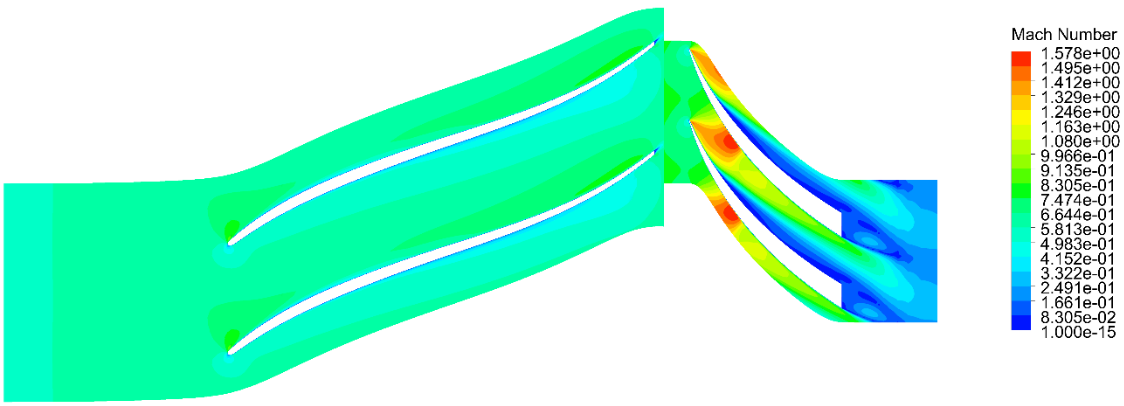

Figure IV. 7 : Mach number contour

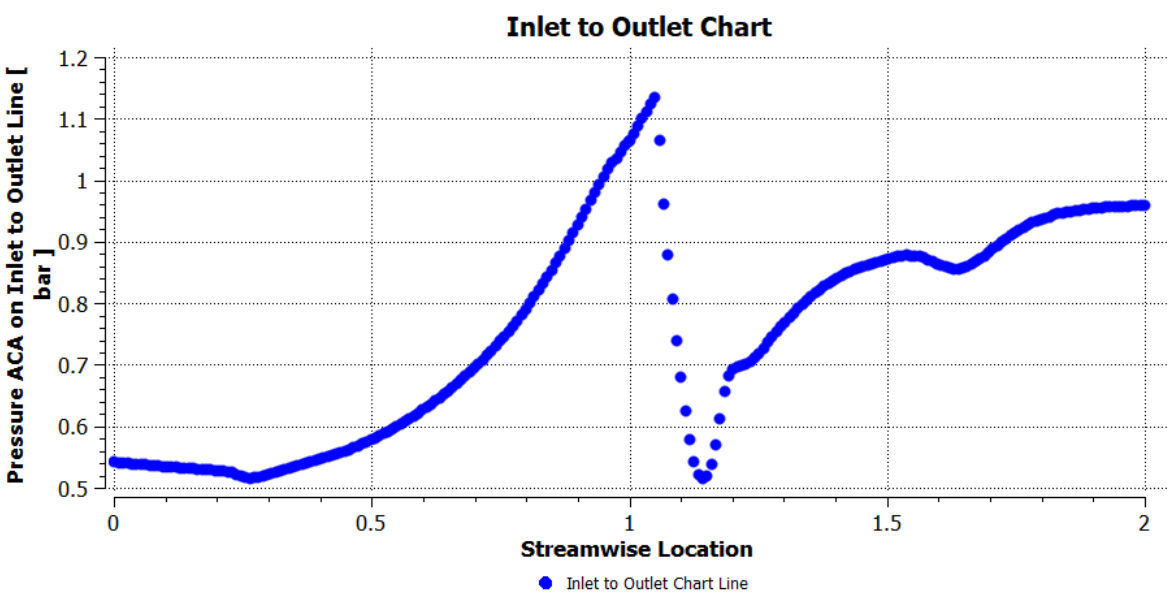

Figure IV. 8: inlet to outlet pressure distribution chart

The first phase starts with pressure increasing, then a sudden pressure drop in the second phase, and finally, a pressure recovery in the last phase. The Mach number contour plot illustrates the variation in Mach number across a centrifugal compressor stage. The Mach number is deficient at the inlet and increases gradually as the flow progresses through the impeller, indicating a significant flow acceleration. In the diffuser region, the Mach number decreases as the flow decelerates after Sharp gradients at the diffuser leading edge,suggestinga potential oblique shock wave that caused the sudden pressure drop because of the geometry of the diffuser and the simulation conditions.

In the Mach number magnitude, we can notice some high Mach number gradients on the trailing edge of both the impeller and diffuser blades and the suction side of the diffuser blade. To understand more about these areas, we will present the static entropy magnitude (Figure IV-9 and IV-10).

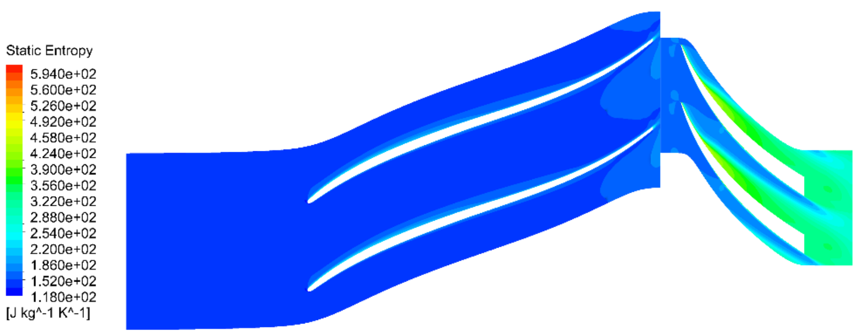

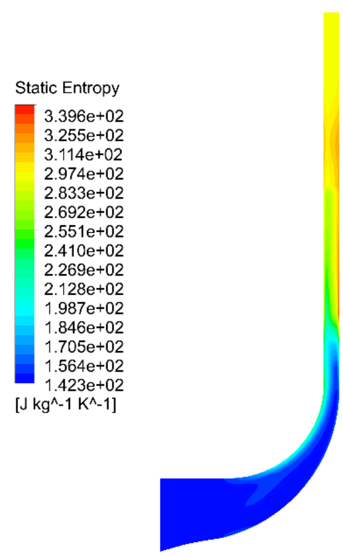

Figure IV. 9: Static entropy in blade-to-blade plane

Figure IV. 10: Static entropy in meridional plane

The static entropy magnitude helps identify regions of the flow where irreversible processes occur, such as losses due to friction, shock waves, and flow separation.High entropy generation indicates energy losses, so according to Figure IV-10, we have higher energy losses in The diffuser than in the impeller. We need to use the total pressure and absolute velocity contour plots separately for the impeller and diffuser to identify these losses.

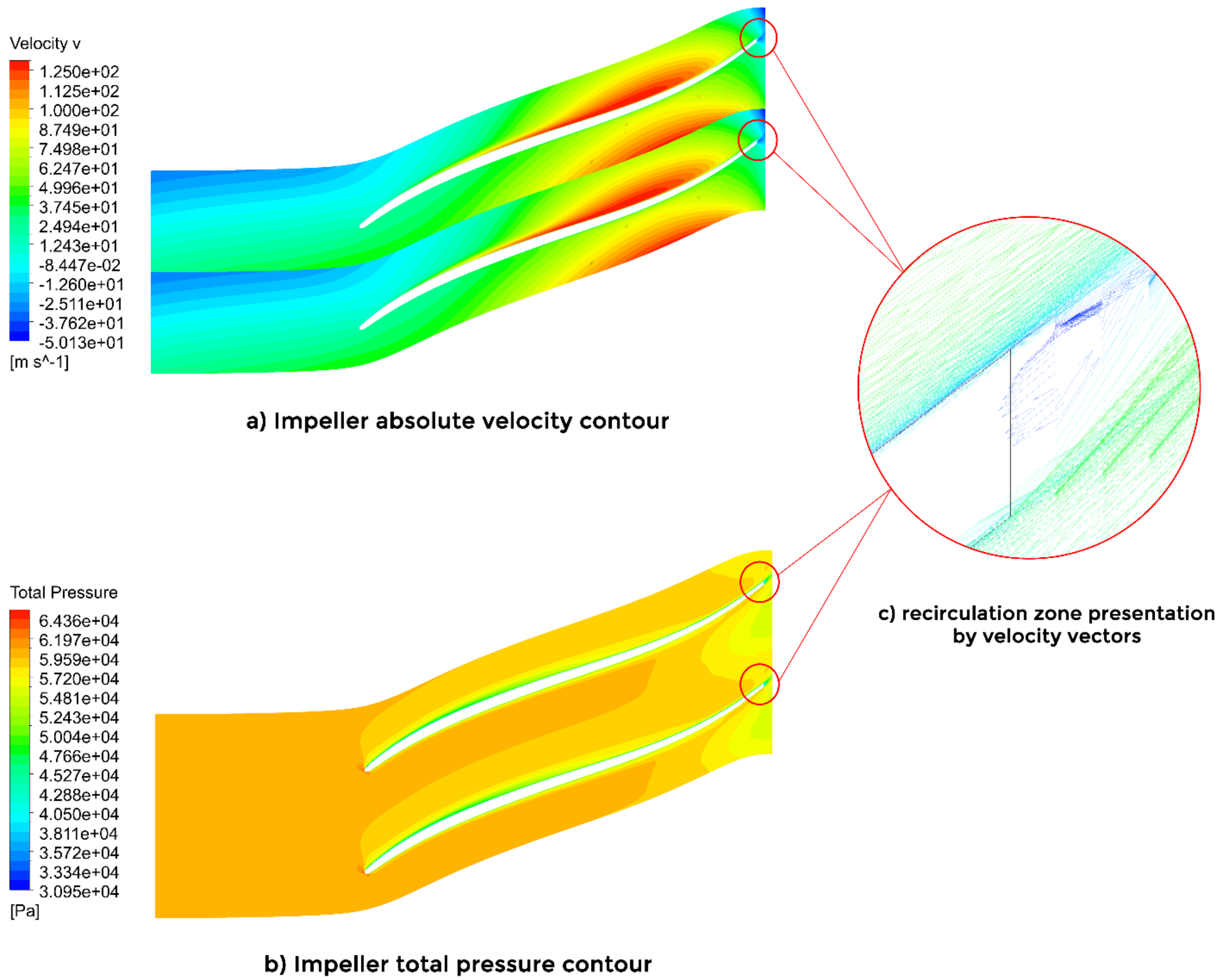

Figure IV. 11: impeller energy losses

Figure IV.11 (a) shows the impeller's absolute velocity, which indicates an acceleration of the flow through the impeller where energy is imparted to the fluid by the rotating blades. The areas highlighted by a circle where the absolute velocity drops abruptly at the trailing edge refer to the flow recirculation zone. Figure IV-11 (b) represents the total pressure distribution on the impeller; the uniform pressure distribution indicates smooth flow. However, areas with high-pressure drops (those highlighted by a circle) indicate energy loss regions caused by recirculation zones, as we mentioned earlier.

Figure IV-12 below represent the energy losses in the diffuser. As we can see, a vast absolute velocity deceleration area near the diffuser blade wall (a), with a remarkable total pressure drop (b) due to flow separation (highlighted in (b)), caused by the reverse flow from the trailing edgein which there is a recirculation zone (highlighted in (a)), this energy losses accrues because of the diffuser geometry and simulation conditions and chock wave creation.

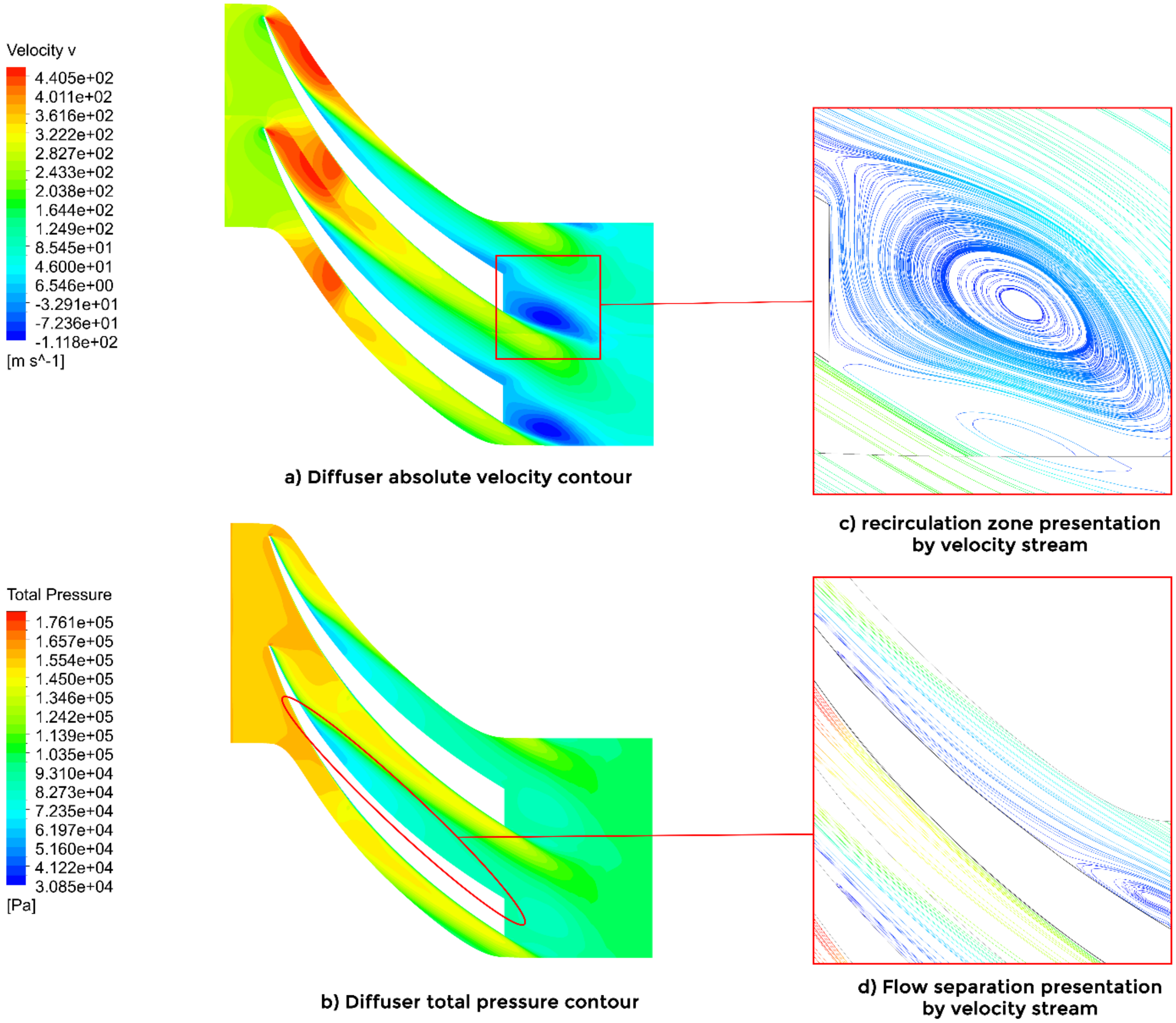

Figure IV. 12: Diffuser energy losses

- **Orthogonal planes:**

Jet-wake flow is caused by the secondary flow coming from the shroud tip leakage flow. These secondary flows disrupt the primary flow path and contribute to additional losses. It can be observed by the orthogonal plane in different impeller and diffuser sections.

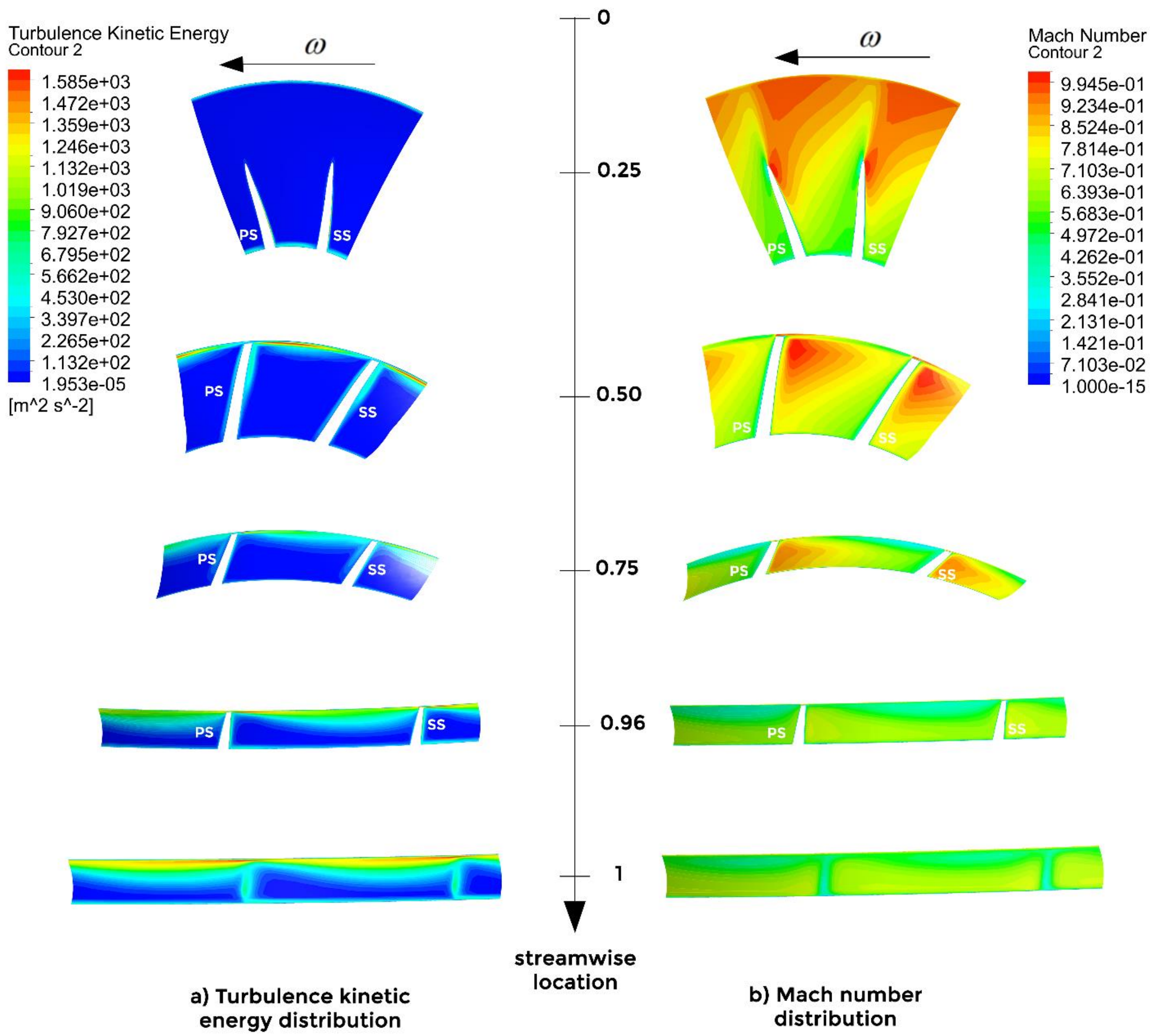

Figure IV. 13: Impeller orthogonal planes

Fig IV-13 represents the impeller orthogonal views; as we can see in the turbulence kinetic energy distribution in different sections of the impeller (Fig IV-13 (a)),turbulence develops on the shroud, where sharp gradients appeardue to the secondary flow from the tip clearance interfering with the primary flow.The turbulence intensity rises as we get close to the impeller outlet; on the other hand, we can see that a shock wave occurs at the blade's leading edge (Fig IV-13 (b)), and this is most likely caused by the blade’s angle of incidence, and as we get close the outlet the Mach number decreases because of the secondary flow from tip clearance. These gradients of Mach number plus the turbulence regions observed before.This indicates the existence of a jet-wake flow with velocity variation from the hub to the shroud, as shown in Fig IV-13 below, which represents the velocity variation from hub to shroud in different impeller sections.

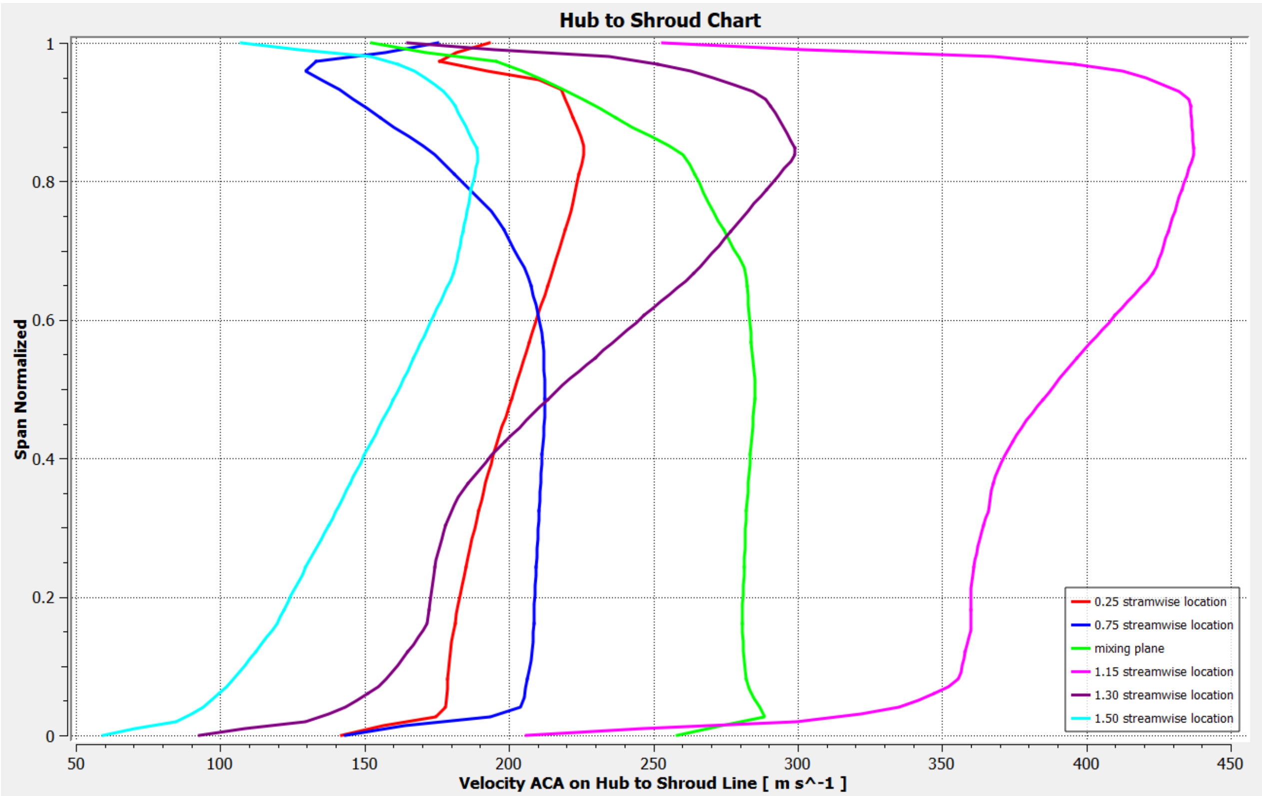

Figure IV. 14: Hub to Shroud velocity chart

The following figure represent TKE and Much number distribution at the diffuser:

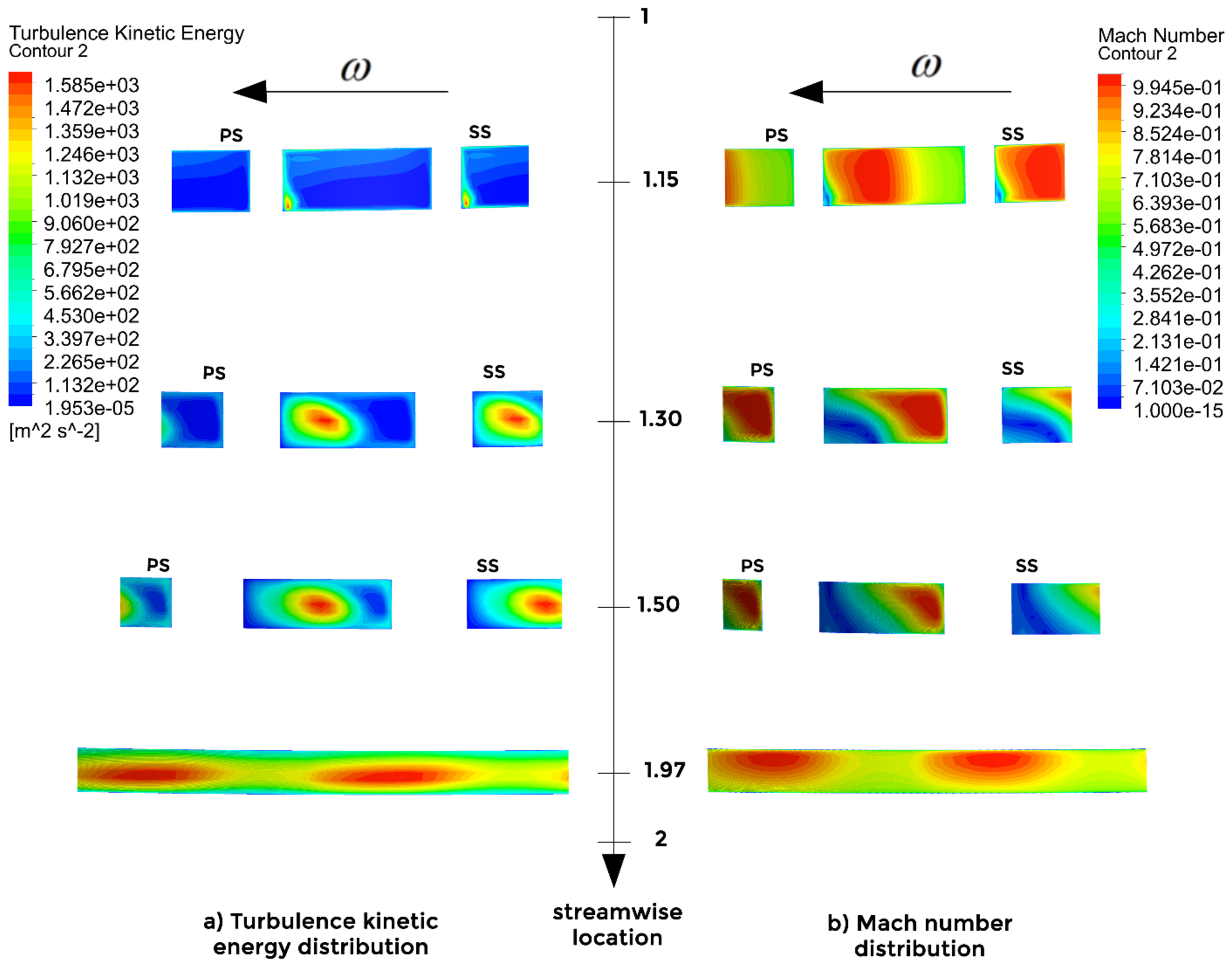

Figure IV. 15: Diffuser orthogonal planes

Fig IV-15 (a) represent turbulence kinetic energy (TKE) distribution of the diffuser in orthogonal planes. We see that low TKE values are observed close to the leading edge of the diffuser (location 1.15), indicating the beginning of turbulence generation, TKE values increase along the streamwise direction (1.30 to 1.50 location), with the highest values concentrated near the blade surfaces, especially on the suction side. That means the boundary layer interactions and potential flow separation are causing turbulence to increase. This turbulence can lead to higher energy dissipation and may affect overall efficiency.Towards the diffuser exit, high TKE regions are noticed, suggesting a substantial mixing and turbulent dissipation, which is essential for pressure recovery.

Fig IV-15 (b) represents the Mach number distribution. The flow decelerates along the suction side, with high-speed regions shrinking towards the exit. This indicates efficient energy transfer and pressure recovery in the diffuser.

Fig IV-16 represents the relative velocity distribution:

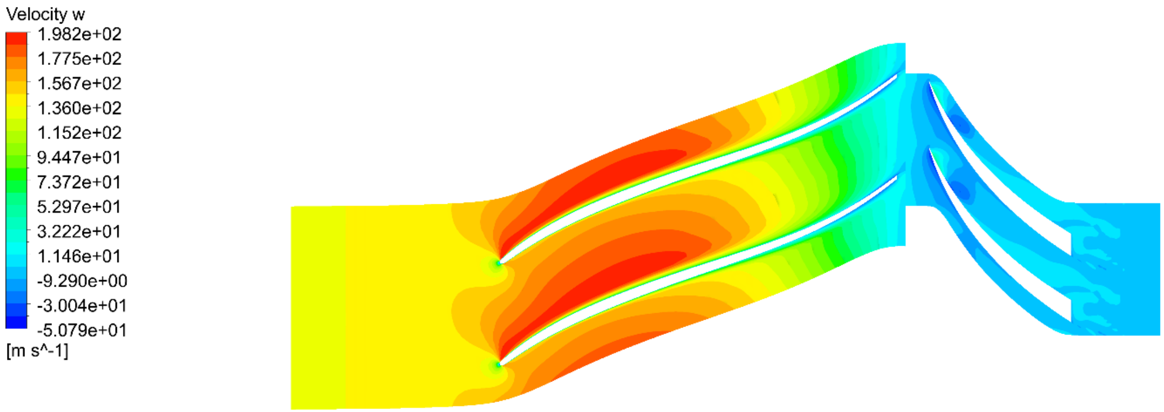

Figure IV. 16: Relative velocity contour

which can indicate the loading on different blade parts. High relative velocities near the leading edge and lower velocities near the trailing edge suggest effective energy transfer, as observed in the figure. Uneven blade loading can lead to vibration and mechanical stresses, influencing the compressor's durability.

IV.3. Splitter blade simulation analysis:

After validating the experimental results and analyzing the performance of the compressor without splitter blades, we will now see the influence of splitter blades on the flow dynamics and overall performance of the centrifugal compressor. The purpose of adding splitter blades is to enhance the flow conditions within the impeller, thereby improving the compressor's efficiency and performance. After performing several simulations for six cases varying in each splitter blade length,we will present key parameters, such as Mach number, pressure distribution, turbulence kinetic energy, and entropy generation, to highlight the differences and improvements brought by the splitter blades.

IV.3.1. The overall performance:

The figure below presentsthe performance of different splitter blade configurations compared to the experimental and numerical data without splitters.

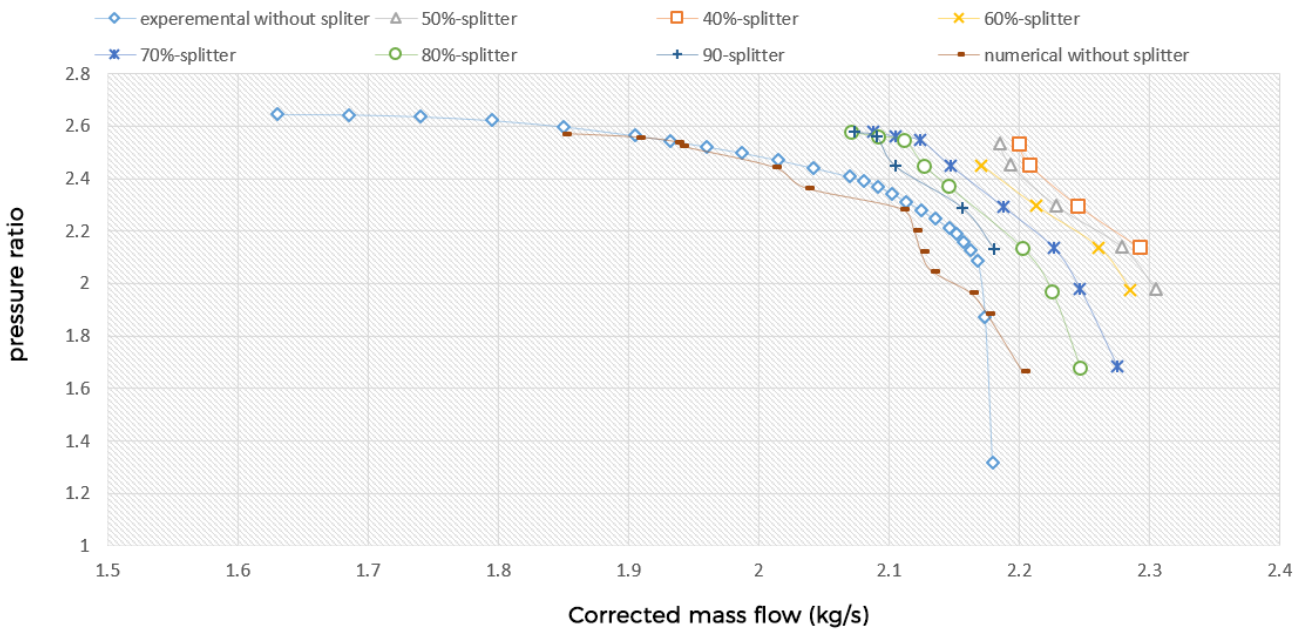

Figure IV. 17: Performance curves of different splitter blade cases

As we can see, all the splitter cases performed better than the baseline model (without splitter); the 40%, 50%, and 60% are similar, with the 40% case slightly higher. The more the splitter blade length increases, the closer the chart gets to the baseline. Still, in general, the splitter blades help maintain a higher pressure ratio at increased mass flow rates, also enhancing their functioning field and indicating their effectiveness in managing flow dynamics.

As a result, the 40%-splitter blade configuration stands out for maintaining a higher pressure ratio across a range of mass flows, particularly at higher flow rates.

For good performance analysis,we willcomprehensively compare the splitter blade configurations at a specific design point, which is a particular value of corrected mass flow typical across all configurations. Then, compare the key parameters extracted for the chosen design point as shown in the table below:

Table IV. 1: Comparison of Performance Parameters for Different Splitter Blade Configurations at a Corrected Mass Flow of 2.2 kg/s

		Pressure ratio	Temperature ratio	Efficiency (%)
Design point: $\dot{m}_{cor} = 2.2\ kg.s^{-1}$	Baseline (without splitter)	1.6677	1.3414	46.07
	40% splitter blade	2.5333	1.37563	80.97
	50% splitter blade	2.45247	1.37323	78.27
	60% splitter blade	2.29499	1.3691	72.57
	70% splitter blade	2.21416	1.3798	70.41
	80% splitter blade	2.13617	1.3665	66.06
	90% splitter blade	2.1316	1.3648	65.15

The table above presents the performance metrics of various splitter blade configurations compared to the baseline without a splitter. Including splitter blades significantly improves the pressure ratio and efficiency across all configurations compared to the baseline, as the higher pressure ratio observed in the 40% splitter blade configuration (2.5333)and an increase of 34.9% in efficiency compared to the baseline. As the splitter percentage increases beyond 50%, there is a gradual decline in the pressure ratio and efficiency, with the 90% splitter blade showing the lowest values.The temperature ratio shows slight variations among the configurations but generally increases with the inclusion of splitter blades.

The data clearly show that splitter blades positively influence the pressure ratio and efficiency of the centrifugal compressor. As a result, the 40% splitter blade configuration emerges as the optimal choice, providing the highest pressure ratio and efficiency.

IV.3.2. flow characteristics analysis:

As we saw earlier, the splitter blades have influenced the centrifugal compressor's performance. To understand how these modifications affect overall performance, we need to analyse the key parameters, such as Mach number, static pressure, turbulence kinetic energy … etc., for three splitter configurations (40%, 60%, and 90%).

The figure below represents the distribution of static pressure in three cases of splitter blades. We notice that static pressure increases through the impeller as we get closer to the outlet. In addition, there is a pressure drop in the leading edge of the splitter blade on the suction side, and its intensity increases as the splitter blade’s length increases due to the compressibility effect and the geometry Variation due to diminishing the section of the passage.

In the diffuser, we observe a smooth pressure recovery in the 40% splitter configuration, but in the two other cases, there is a pressure drop on the leading edge, most likely caused by an oblique shock wave.

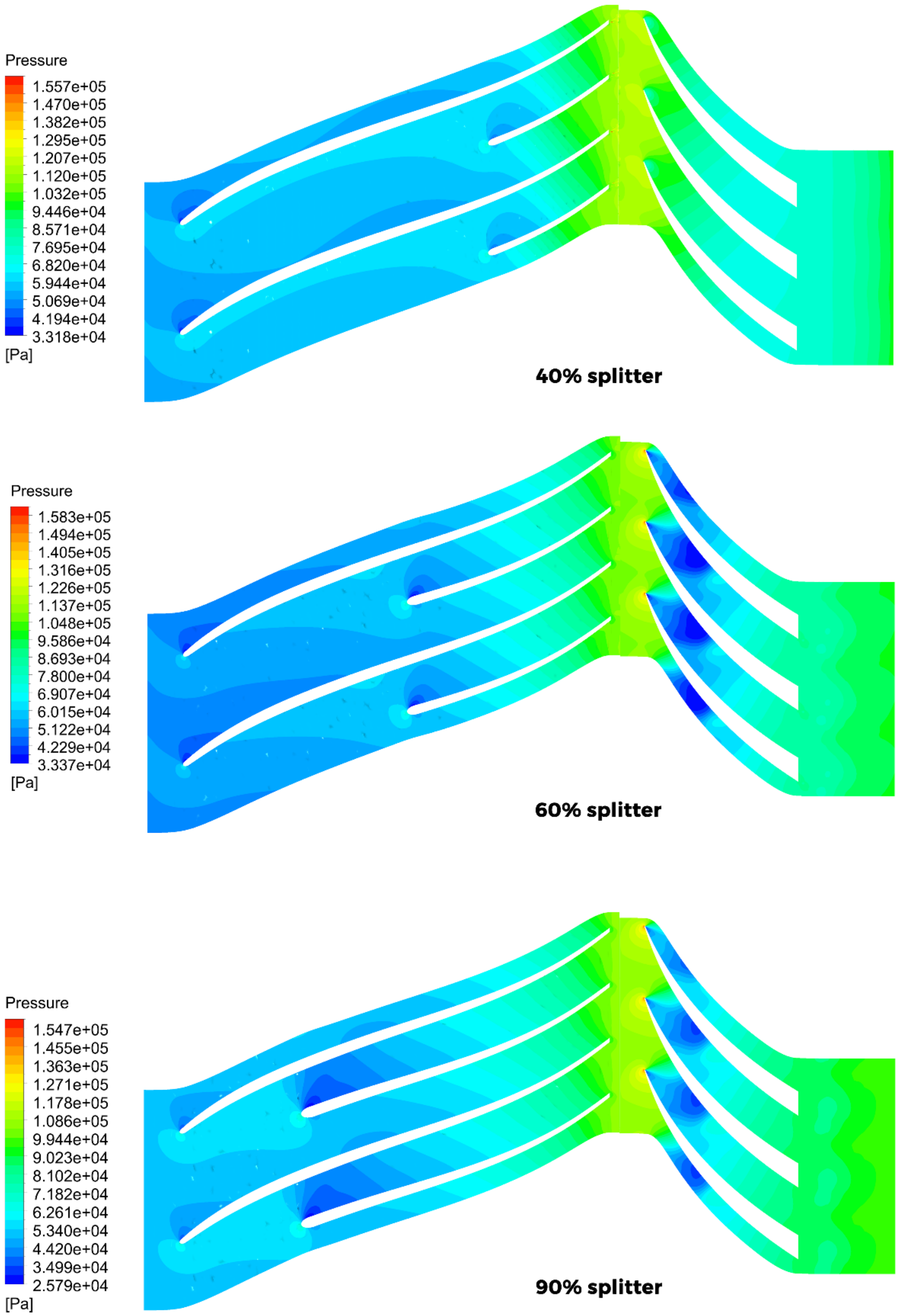

Figure IV. 18: Static pressure distribution

The following Figure represents the Mach number and static entropy for a 40% splitter configuration. We notice a high Mach number at the leading edge of both the main blade and splitter blade due to the angle of incidence and the geometry and the absence of shock wave at the leading edge of the diffuser. This is because of the short splitter blade passage andthe increase in the spanwise ratio between the diffuser and the impeller. This diminishes the cross-area between the impeller and diffuser and the primary flow that goes in a single diffuser passage. For the static entropy, we observe no areas for high energy loss as the baseline model, only some recirculation zones at the trailing edge of blades in the impeller and the diffuser due to the cutoff type. This configuration improves the overall performance compared to the baseline model.

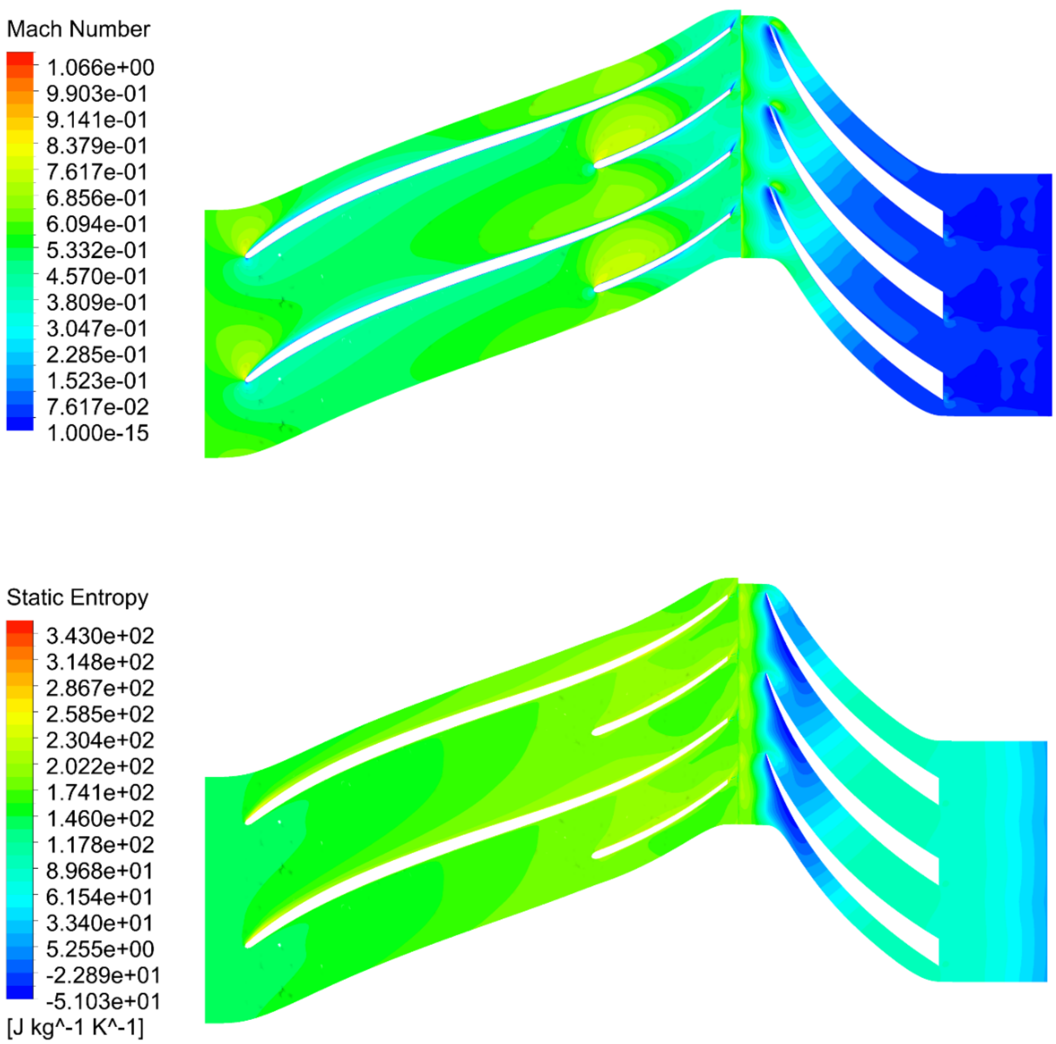

Figure IV. 19 : Mach number and static entropy distributions for 40% splitter impeller energy losses

The following Figure represents the Mach number and static entropy for a 40% splitter configuration. We notice a high Mach number at the leading edge of both the main blade and splitter blade as the previous case, but this time an oblique shock wave appeared at the leading edge of the diffuser. Because of the long passage between the splitter blade and the main blade leads the velocity to increase and eventually a shock wave will appear. What caused the pressure drop and the stall region in the diffuser. When analyzing the static entropy distribution, we notice a high energy loss region near the wall, indicating a potential flow separation and a recirculation zone at the diffuser's trailing edge, which causes a reduction in performance compared to the previous case.

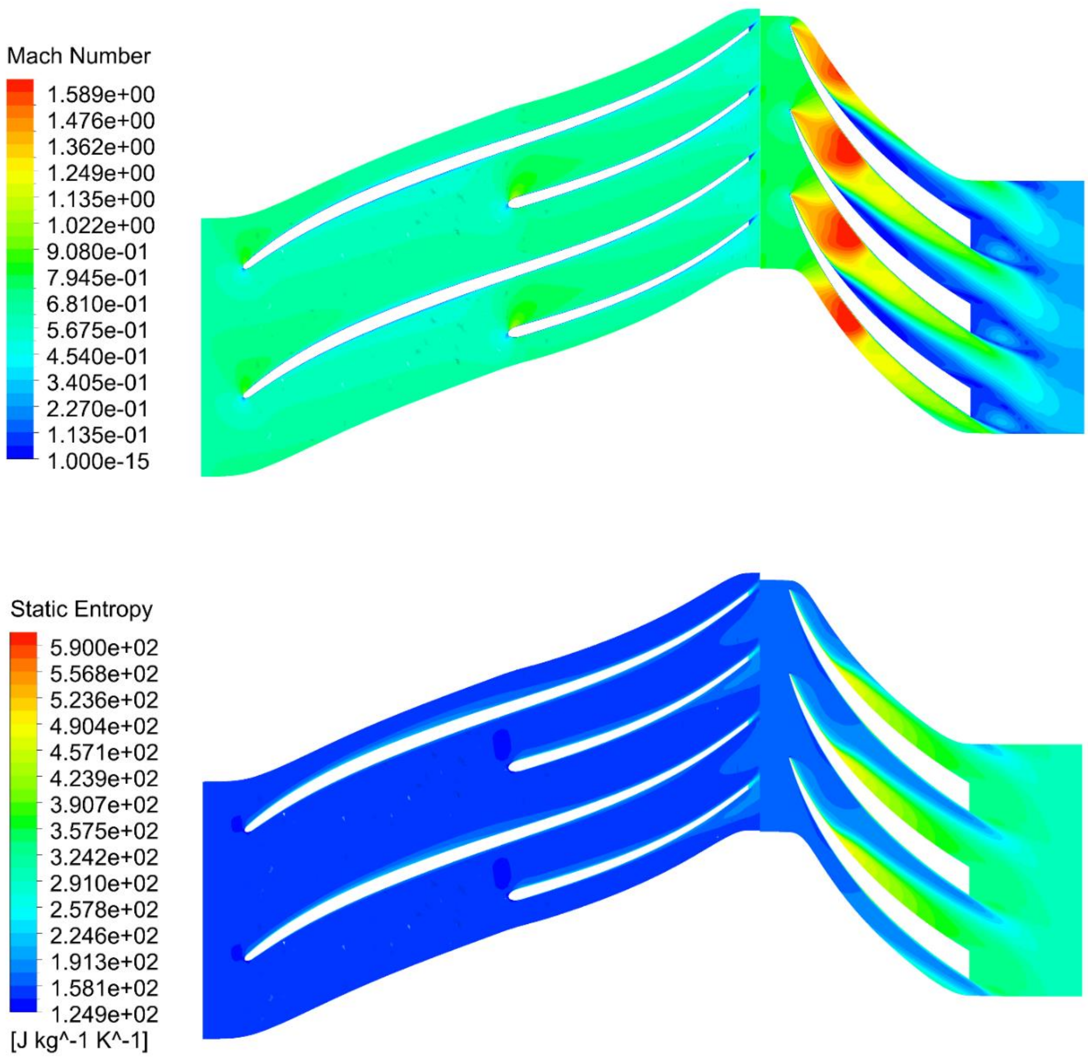

Figure IV. 20 : Mach number and static entropy distributions for 60% splitter configuration

In the last case of the 90% splitter configuration, the contours of Mach number and static entropy show the same phenomenon as the 60% splitter configuration. In this case, we observe an increase in energy losses caused by the flow separation in the diffuser and the recirculation zones in the diffuser trailing edge due to the geometry and the compressibility effect. There is also a remarkableincrease in the Mach number on the leading edge of the main and splitter blades due to the angle of incidence.

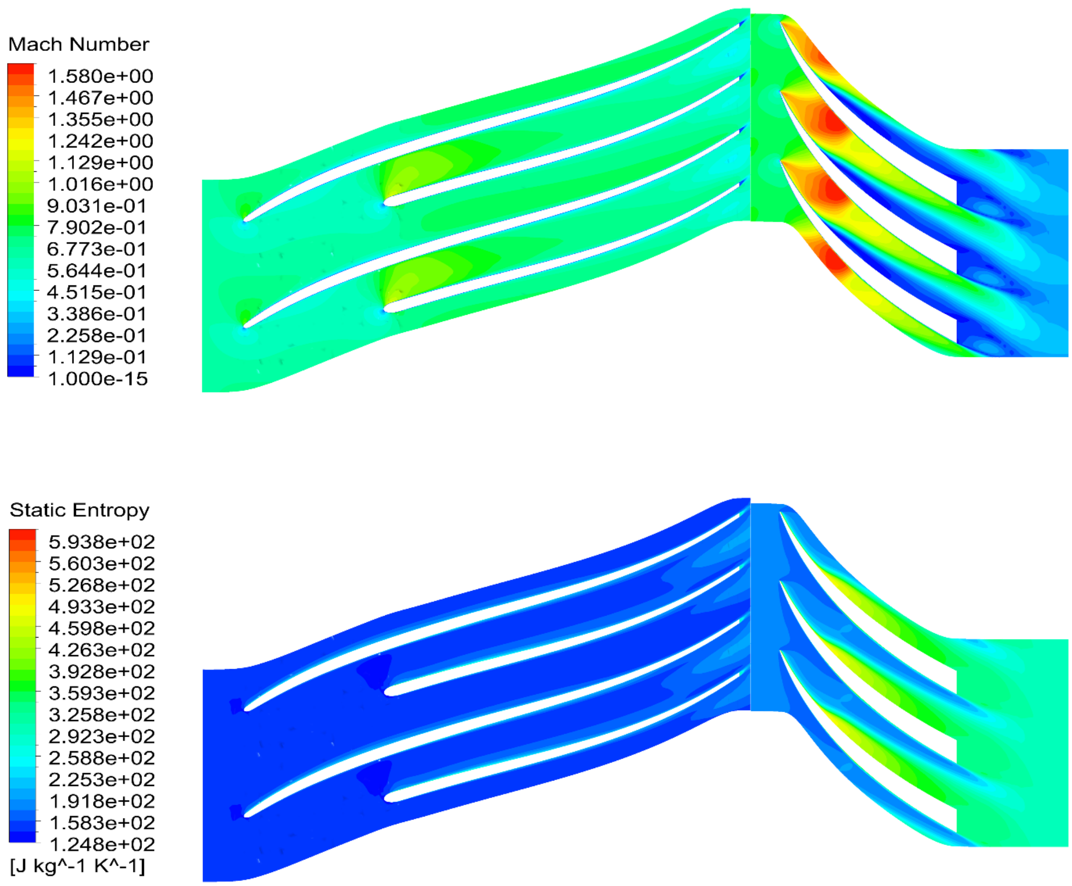

Figure IV. 21 : Mach number and static entropy distribution for 90% splitter configuration

IV.3.3. Orthogonal planes:

We will need to examine the orthogonal planes to analyze the flow characteristics in the impeller cross-section and the energy loss regions for the 40% splitter blade configuration. We created three orthogonal planes in three different positions. The figure below illustrates the different planes and their position:

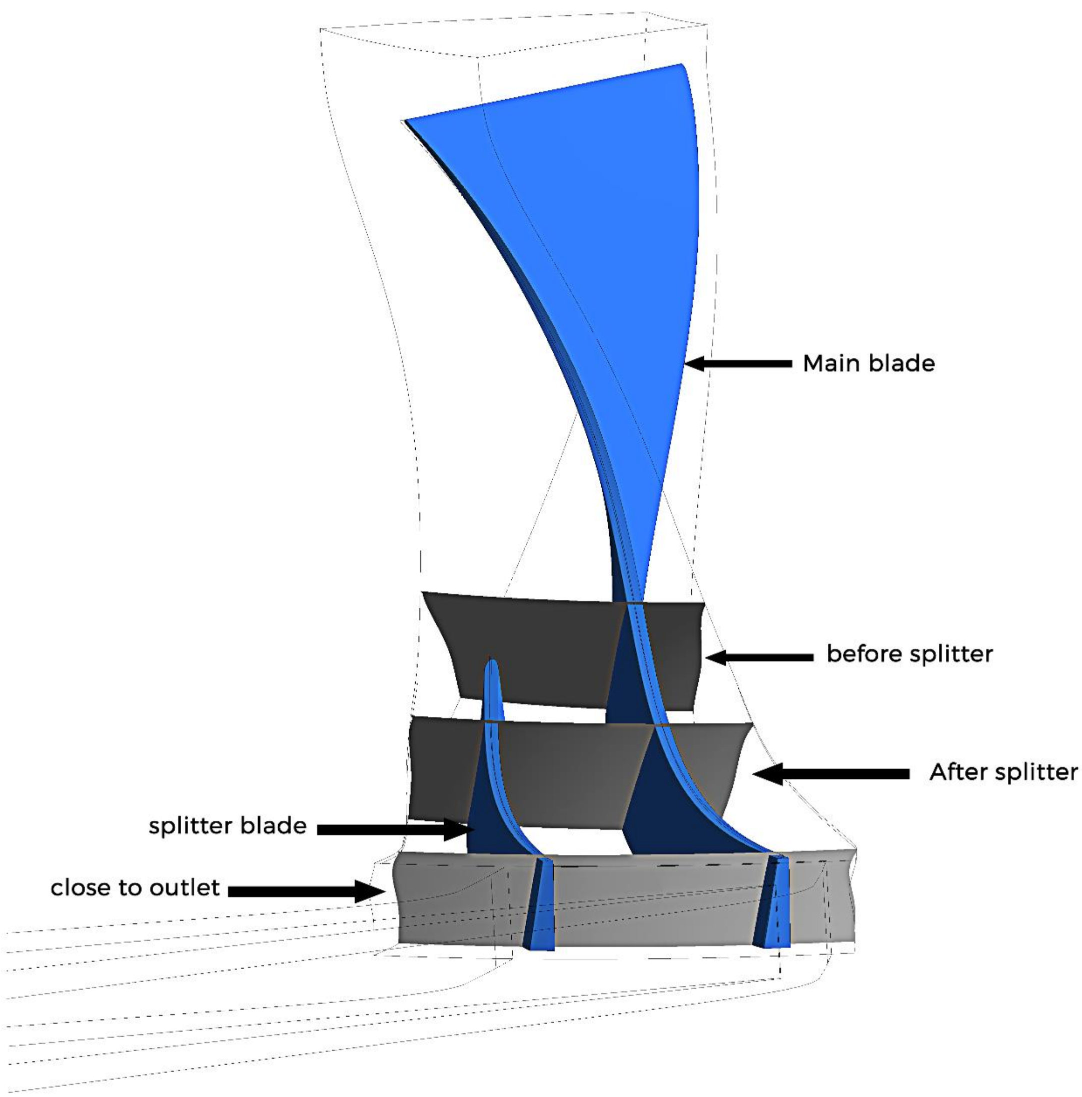

Figure IV. 22 : The position of the orthogonal planes

The following figures represent the turbulence kinetic energy and Mach number distributions in the orthogonal planes of the 40% splitter configuration:

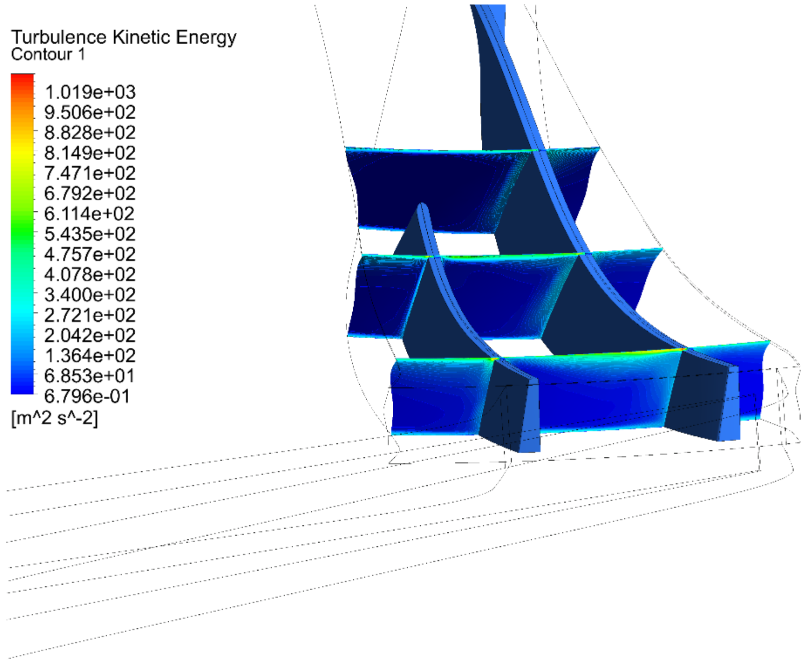

Figure IV. 23: Turbulence kinetic energy distribution

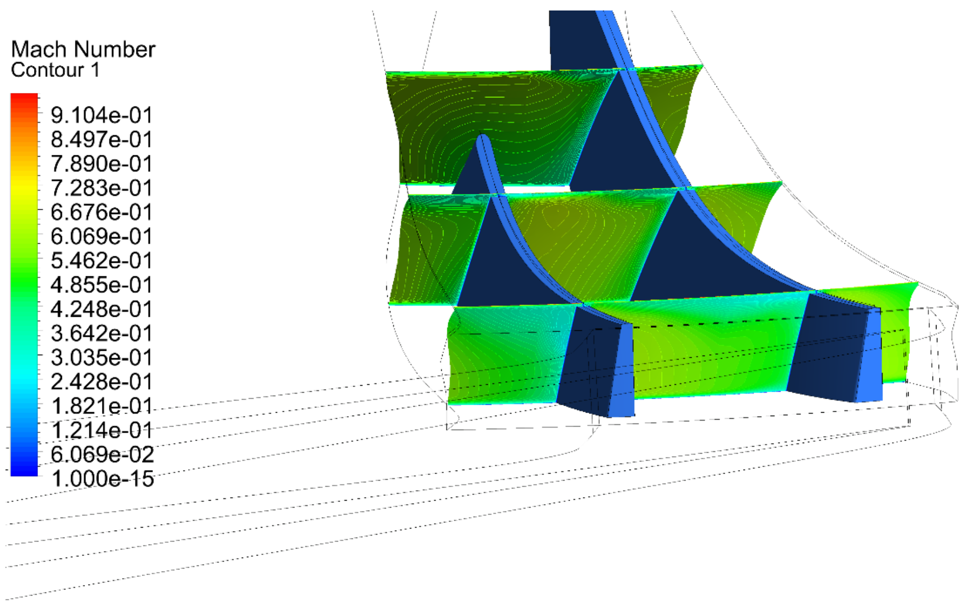

Figure IV. 24: Mach number distribution

The analysis of Turbulence Kinetic Energy (TKE) distribution for the 40% splitter blade configuration highlights critical regions of turbulence within the impeller. High TKE is observed at the inlet near the pressure side of the inlet, mid-span between the main and splitter blades near the shroud, and at the trailing edges, indicating strong turbulence due to flow separation, complex interactions, and vortex formations due to secondary flow from tip clearance at the shroud. Lower TKE is found near the hub and closer to the splitter blades, suggesting more stable flow conditions and reduced turbulence in these areas. The splitter blades help reduce turbulence by breaking down large vortices, improving flow uniformity. However, regions of high TKE still indicate energy losses and potential areas for performance improvement.

The Mach number distribution for the 40% splitter blade configuration reveals High Mach numbers at the leading edge and mid-span regions, indicating significant flow acceleration as the flow navigates through the narrow passages, while lower Mach numbers near the hub, shroud, and trailing edges suggest flow deceleration and potential wakes. These regions of changing Mach numbers highlight energy transfer and loss areas, particularly due to turbulence and secondary flows. The splitter blades effectively smooth the flow, reduce large-scale turbulence, and maintain a uniform velocity distribution, enhancing the aerodynamic performance of the impeller. This results in improved pressure ratio and efficiency.

General Conclusion:

In this study, we performed a Computational Fluid Dynamics (CFD) analysis to investigate the performance of Radiver centrifugal compressor with different splitter blade configurations. We started by considering key flow hypotheses, including the assumptions of steady-state flow, compressible fluid, three-dimensional, and turbulent flow, to simulate real-world conditions accurately.

Our first focus was on mesh sensitivity analysis to ensure the accuracy and reliability of the CFD simulations. We tested various mesh densities and found that a finer mesh significantly improves the precision of the results, capturing intricate flow details without excessively increasing computational costs. The optimal mesh was selected based on a balance between computational efficiency and result accuracy. Without forgetting the y+ validation.

Next, we examined the impact of various splitter blade configurations (40%, 50%, 60%, 70%, 80%, and 90%) on the performance parameters of the compressor. By comparing the pressure ratio, temperature ratio, and efficiency at a corrected mass flow of 2.2 kg/s, we identified significant differences in performance. The 40% splitter blade configuration emerged as the optimal design, showing the highestpressure ratioand an increase inefficiency by 34.9% and. This configuration effectively reduced turbulence kinetic energy, especially in the mid-span regions between the main and splitter blades, leading to lower energy losses and improved flow uniformity.

For future work, improving this study could involve exploring more advanced turbulence models or transient simulations to capture dynamic flow phenomena more accurately. Additionally, investigating the impact of three-dimensional blade geometries or variable blade angles could provide further insights into enhancing compressor performance. Another promising area is the application of optimisation algorithms to automatically refine splitter blade designs for maximum efficiency and minimal energy losses under various operating conditions. These advancements could significantly improve centrifugal compressor performance, making them more efficient and reliable for industrial applications.

Bibliography

[1] Ziegler, K.U., Gallus, H.E., Niehuis, R. (2002a), "A Study on Impeller-Diffuser Interaction: Part I - Influence on the Performance", ASME GT-2002-30381.

[2] Ziegler, K.U., Gallus, H.E., Niehuis, R. (2002b), "A Study on Impeller-Diffusor Interaction: Part II - Detailed Flow Analysis", ASME GT-2002-30382.

[3] Sharma, N.Y., & Karanth, K.V. (2009). Numerical Analysis of a Centrifugal Fan for Improved Performance using Splitter Vanes.

[4] Layth H. Jawad1, S. Abdullah, R. Zulkifli, and W.M.F.W. Mahmood. (2013). "Numerical Investigation on the Effect of Impeller Trimming on the Performance of a Modified Compressor"

[5] A. Malik, S. R. Qureshi, Q. Zheng and N. Ikram. (2018). "Aerodynamic analysis of splitter blade location on centrifugal compressor performance,"

[6] Khalafallah, M.G., Saleh, H.S., Ali, S.M. et al. CFD investigation of flow through a centrifugal compressor diffuser with splitter blades. J. Eng. Appl. Sci. 68, 43 (2021).

[7] Kiryll Kabalyk, Władysław Kryłłowicz. (2016). "Numerical modeling of the performance of a centrifugal compressor impeller with low inlet flow coefficient"

[8] Malik A., Zheng Q., Zaidi A.A., Fawzy H. (2018). Performance enhancement of centrifugal compressor with addition of splitter blade close to pressure surface.

[9] S.A. MoussaviTorshizi, A. HajilouyBenisi and M. Durali. (2016). Multilevel optimization of the splitter blade pro.

[10] Ou, J., Jin, D. &Gui, X. (2022). Numerical Investigation of the Load Distribution between the Main Blade and the Splitter Blade in a High-Loading Centrifugal Compressor.

[11] Omidi, M., Liu, Y., Mohtaram, S. et al. (2022). Investigating on performance parameters and flow field of centrifugal compressor based on the splitter blade leading edge's location effect.

[12] Guillaume Dufour. Contributions a la modelisationet au calcul des ecoulementsdans les compresseurs centrifuges: application a la conception par lois de similitude. PhD thesis, 2006

[13] Dean, R., &Senoo, Y. (1960). Closure to "Discussions of 'Rotating Wakes in Vaneless Diffusers'" (1960, ASME J. Basic Eng., 82, pp. 570–572). Journal of Basic Engineering, 82, 573-574.

[14] David C. Wilcox. (1993)." Turbulence Modeling for CFD".

[15] Ansys CFX-solver theory guide, 2023.

[16] Ansys Workbench users guide, 2023.

[17] Simscale documentation (2024). (https://www.simscale.com/docs/).

[18] Florian R Menter. (1994)."Two-equation eddy-viscosity turbulence models for engineering applications." AIAA journal, 32(8):1598-1605.

[19] RadostinaPetrova. (2012). "FINITE VOLUME METHOD – POWERFUL MEANS OF ENGINEERING DESIGN".

[20] Erik Dick (2015). "Fundamentals of Turbomachines".